Chapter 4

VOLTAGE STABILITY INDICES

Performance indices to predict proximity to voltage collapse problems are of great interest for researchers and technical staff in power systems operation, as these indices could be used on-line or off-line to help operators determine how close the system is to collapse [1, 2]. The objective of these indices is to define a scalar magnitude that can be monitored as system parameters change. These indices should have a "predictable" shape and be "smooth," so that acceptable predictions may be made; furthermore, their computation should be fast, particularly for on-line system monitoring. This chapter concentrates on describing and comparing some of the indices proposed and used throughout the world. However, before presenting a detailed description of these indices, it is important to briefly review some basic concepts introduced in Chapter 2, as well as the related mathematical terminology, to establish a general theoretical framework for these indices.

4.1 REVIEW OF BASIC CONCEPTS

The typical quasi-steady-state description of a power system applicable to voltage stability analysis is given by the differential-algebraic equations

$$\begin{aligned} \dot{x} &= f(x, y, \lambda) \\ 0 &= g(x, y, \lambda) \end{aligned} \tag{4.1}$$

where x corresponds to the system state variables, and y represents the "algebraic" variables. The variable λ stands for a parameter or a set of parameters that "slowly" change in time, so that the system moves from one equilibrium point to another until reaching the collapse point. Another way of representing this system is by defining $z = [x\ y]^T$, so that equations (4.1) can be rewritten as

$$\begin{bmatrix} \dot{x} \\ 0 \end{bmatrix} = F(z, \lambda)$$

If one assumes that the Jacobian $D_y g(\cdot)$ in (4.1) is nonsingular along some system trajectories of interest, these equations can be reduced, at least locally, to

$$\dot{x} = f(x, y^{-1}(x, \lambda), \lambda) = s(x, \lambda)$$

This reduction requires that $D_y g(\cdot)$ is locally nonsingular along these trajectories. Cases where this does not apply are discussed in more detail in Section 2.11.

An equilibrium point (z_o, λ_o) of (4.1), is defined by $F(z_o, \lambda_o) = 0$. Hence, based on the nonsingularity assumption of the algebraic equations, an equilibrium point (z_*, λ_*) where $D_z F(z_*, \lambda_*)$ is singular, is mathematically known as a "singular" bifurcation point [3]. This equilibrium point in power systems has been directly associated with voltage collapse problems, as thoroughly discussed in Chapter 2. Thus, in power systems, one is usually interested in determining the singularity of the Jacobian associated with the system dynamic equations. Different models of the system elements, particularly generators and loads, affect the location of these collapse points [4, 5]. Furthermore, changing various parameters in the system can produce different types of bifurcating phenomena [6].

For the purpose of this chapter, the popular load-flow or power flow model is used, where the variations of constant active and reactive powers are assumed to be the main parameter driving the system to a singularity. Although this simple system model is certainly not adequate to thoroughly study the voltage collapse phenomenon, for certain particular dynamic models, the power flow equations yield adequate results, as singularities in the related power flow Jacobians can be associated with actual singular bifurcations of the corresponding dynamical system [3]. Moreover, regardless of the direct relations between singularities of the power flow Jacobians and the actual bifurcations of the full dynamical system, it is always of interest to determine the system conditions where the power flow problem is not solvable, as most operating decisions nowadays are made on-line based on power flow solutions. Thus, various utilities throughout the world currently using the indices discussed in this chapter, base some of their operating decisions related to voltage collapse problems mostly on a power flow system model. Nevertheless, without any loss of generality, most of the methodologies described in this document can be directly and readily applied to any system model; brief comments on whether the different techniques presented here are applicable or not to system models other than the power flow based model are given throughout this chapter.

The power flow model used here to obtain and compare different voltage stability indices, is represented by the typical load-flow vector nonlinear equations defining the active and reactive power mismatches at the system buses, i.e.,

$$\left[\begin{array}{c} \Delta P(u, \lambda) \\ \Delta Q(u, \lambda) \end{array} \right] = \mathcal{F}(u, \lambda) = 0 \tag{4.2}$$

where $\mathcal{F}(u, \lambda)$ is a subset of $F(z, \lambda)$, with u typically representing V and δ, i.e., the phasor bus voltages. However, given the processing power and numerical techniques currently available, (4.2) can also be used to compute other system variables besides voltages and angles, so that system controls and its limits may be readily handled by swapping variables in u without the need for changing the structure and number of the equations used in the computational process. For example, generation reactive power injections Q can be part of u by including the reactive power mismatch equations at PV buses in (4.2), so that when a Q-limit is reached, or released, the corresponding

bus voltage magnitude V is swapped for Q in u, or vice versa; automatic transformer taps or any other control variables can be handled in a similar fashion. Observe that $\mathcal{F}(u, \lambda)$, and u for that matter, could be modified to include more detailed models of certain system devices such as generators (inclunding AVRs and other controls) and loads, or other devices such as HVDC links and FACTS, making the power flow equations more adequate for computing the equilibrium points of the full system model represented by the nonlinear function $F(z, \lambda)$ [7].

The λ variable typically represents a scalar parameter or loading factor used to simulate the system load changes that drive the system to collapse in the following way:

$$\begin{aligned} P_L &= P_{L_P}(1 + k_P\lambda) + P_{L_I}\left(\frac{V}{V_0}\right)(1 + k_{V_P}\lambda) + P_{L_Z}\left(\frac{V}{V_0}\right)^2(1 + k_{Z_P}\lambda) \\ Q_L &= Q_{L_Q}(1 + k_Q\lambda) + Q_{L_I}\left(\frac{V}{V_0}\right)(1 + k_{V_Q}\lambda) + Q_{L_Z}\left(\frac{V}{V_0}\right)^2(1 + k_{Z_Q}\lambda) \end{aligned}$$

Here P_L and Q_L represent the load at bus L, and P_{L_P}, P_{L_I}, P_{L_Z}, k_P, k_{V_P}, k_{Z_P}, Q_{L_Q}, Q_{L_I}, Q_{L_Z}, k_Q, k_{V_Q}, k_{Z_Q}, and V_0 are all pre-defined constants that determine the composition of the ZIP load (constant impedance-current-power load) [5]. The results shown in this report were obtained for constant power changes only, i.e.,

$$\begin{aligned} P_L &= P_{L_P}(1 + k_P\lambda) \\ Q_L &= Q_{L_Q}(1 + k_Q\lambda) \end{aligned} \tag{4.3}$$

Hence, λ represents in this case a net MVA change in the total system load.

4.2 SAMPLE SYSTEM

All voltage stability indices presented in this report are used to study the same sample system, so that direct comparisons can be made and useful conclusions can be drawn. The sample system used here is the 32 bus system utilized in CIGRE's report [2], due to the readily available data and results, and especially for its particular voltage stability characteristics. This system, depicted in Figure 4.2-1, has 32 buses, 5 areas, 9 generators, 25 lines, 15 transformers (7 ULTCs), and was originally created to study the voltage collapse of the northern part of Belgium in 1982. Any active load changes are picked up "equally" by generators N15 and N16 (slack buses), representing the "external" system; bus N15 is the angle reference bus and its voltage is controlled by the corresponding generator; generators M1, M2, and N10 control their terminal voltages (PV buses), with no Q-limits, whereas the rest of the generators deliver constant power (PQ buses); there is no area flow control.

The following is the power flow data for the initial solution point in IEEE Common Format [8]:

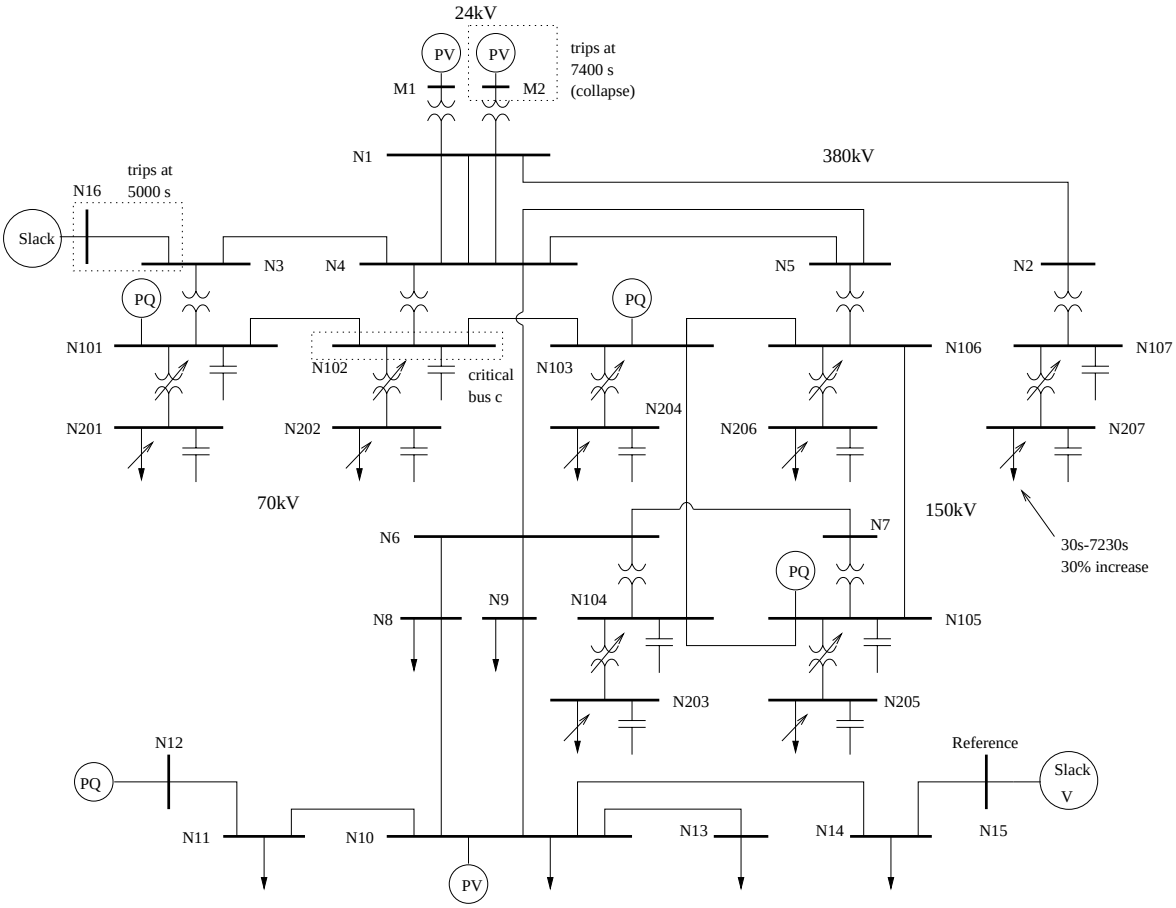

Figure 4.2-1. Sample system [2].

```
C        1         2         3         4         5         6         7         8         9         0         1         2         3
C 345678901234567890123456789012345678901234567890123456789012345678901234567890123456789012345678901234567890123456789012345678901234567890
TAPE
                                100.00        CIGRE TF 38-02-11 TEST SYSTEM
BUS DATA FOLLOWS                    32 ITEMS
   1 N201     70.   1  7  0 1.0425 -9.697 298.7000 164.8000 0.000000 0.00000 70.0000 1.0425 0.00000 0.00000 0.00000 .450000     0
   2 N202     70.   1  7  0 1.0236 -11.37 300.9000 167.4000 0.000000 0.00000 70.0000 1.0236 0.00000 0.00000 0.00000 .450000     0
   3 N203     70.   1  7  0 1.0247 -9.986 301.2000 167.7000 0.000000 0.00000 70.0000 1.0247 0.00000 0.00000 0.00000 .450000     0
   4 N204     70.   1  7  0 1.0134 -11.31 301.0000 167.5000 0.000000 0.00000 70.0000 1.0134 0.00000 0.00000 0.00000 .450000     0
   5 N205     70.   1  7  0 1.0332 -9.757 296.8000 162.5000 0.000000 0.00000 70.0000 1.0332 0.00000 0.00000 0.00000 .450000     0
   6 N206     70.   1  7  0 1.0256 -10.13 301.3000 167.9000 0.000000 0.00000 70.0000 1.0256 0.00000 0.00000 0.00000 .450000     0
   7 N207     70.   1  7  0 1.0254 -11.69 301.2000 167.7000 0.000000 0.00000 70.0000 1.0254 0.00000 0.00000 0.00000 .450000     0
   8 N101    150.   1 15  0 1.0547 -5.761 0.000000 0.000000 176.7000 30.2000 150.000 1.0547 999999. -99999. 0.00000 .750000     0
   9 N102    150.   1 15  0 1.0285 -7.190 0.000000 0.000000 0.000000 0.00000 150.000 1.0285 0.00000 0.00000 0.00000 .750000     0
  10 N103    150.   1 15  0 1.0193 -7.052 0.000000 0.000000 150.8000 19.7000 150.000 1.0193 999999. -99999. 0.00000 0.00000     0
  11 N104    150.   1 15  0 1.0296 -5.811 0.000000 0.000000 0.000000 0.00000 150.000 1.0296 0.00000 0.00000 0.00000 .750000     0
  12 N105    150.   1 15  0 1.0552 -5.852 0.000000 0.000000 176.7000 28.3000 150.000 1.0552 999999. -99999. 0.00000 .750000     0
  13 N106    150.   1 15  0 1.0305 -5.957 0.000000 0.000000 0.000000 0.00000 150.000 1.0305 0.00000 0.00000 0.00000 0.00000     0
  14 N107    150.   1 15  0 1.0303 -7.521 0.000000 0.000000 0.000000 0.00000 150.000 1.0303 0.00000 0.00000 0.00000 .750000     0
  15 M1       24.   1 40  2 1.0000 4.1614 47.90000 39.90000 849.9000 306.769 24.0000 1.0000 999999. -99999. 0.00000 0.00000     0
  16 M2       24.   1 40  2 1.0000 1.5591 53.90000 44.90000 499.9000 236.230 24.0000 1.0000 999999. -99999. 0.00000 0.00000     0
  17 N1      380.   1 40  0 1.0502 -.1696 0.000000 0.000000 0.000000 0.00000 380.000 1.0502 0.00000 0.00000 0.00000 0.00000     0
  18 N10     380.   1 40  2 1.0840 2.5467 579.9000 99.90000 2800.000 483.564 380.000 1.0840 999999. -99999. 0.00000 0.00000     0
  19 N11     380.   1 40  0 1.0881 .80207 97.90000 31.90000 0.000000 0.00000 380.000 1.0881 0.00000 0.00000 0.00000 0.00000     0
  20 N13     380.   1 40  0 1.0593 -.3546 599.9000 199.9000 0.000000 0.00000 380.000 1.0593 0.00000 0.00000 0.00000 0.00000     0
  21 N14     380.   1 40  0 1.0814 .80455 299.9000 74.90000 0.000000 0.00000 380.000 1.0814 0.00000 0.00000 0.00000 0.00000     0
  22 N16     380.   1 40  2 1.0400 -1.680 0.000000 0.000000 -2.27072 -12.576 380.000 1.0400 999999. -99999. 0.00000 0.00000     0
  23 N2      380.   1 40  0 1.0485 -.3844 0.000000 0.000000 0.000000 0.00000 380.000 1.0485 0.00000 0.00000 0.00000 0.00000     0
  24 N3      380.   1 40  0 1.0398 -1.663 0.000000 0.000000 0.000000 0.00000 380.000 1.0398 0.00000 0.00000 0.00000 0.00000     0
  25 N4      380.   1 40  0 1.0442 -.9636 0.000000 0.000000 0.000000 0.00000 380.000 1.0442 0.00000 0.00000 0.00000 0.00000     0
  26 N5      380.   1 40  0 1.0400 -1.428 0.000000 0.000000 0.000000 0.00000 380.000 1.0400 0.00000 0.00000 0.00000 0.00000     0
  27 N6      380.   1 40  0 1.0443 -1.550 0.000000 0.000000 0.000000 0.00000 380.000 1.0443 0.00000 0.00000 0.00000 0.00000     0
  28 N7      380.   1 40  0 1.0303 -2.044 0.000000 0.000000 0.000000 0.00000 380.000 1.0303 0.00000 0.00000 0.00000 0.00000     0
  29 N8      380.   1 40  0 1.0552 -.6752 236.9000 77.90000 0.000000 0.00000 380.000 1.0552 0.00000 0.00000 0.00000 0.00000     0
  30 N9      380.   1 40  0 1.0554 -.6351 222.9000 72.90000 0.000000 0.00000 380.000 1.0554 0.00000 0.00000 0.00000 0.00000     0
  31 N12     380.   1 90  0 1.0977 -1.306 318.9000 -99.9000 0.000000 0.00000 380.000 1.0977 0.00000 0.00000 0.00000 0.00000     0
  32 N15     380.   2 94  3 1.0920 0.0000 0.000000 0.000000 -66.3707 39.6181 380.000 1.0920 999999. -99999. 0.00000 0.00000     0
-999
BRANCH DATA FOLLOWS                 40 ITEMS
   1    8  1  7 1 2 .00060000 .02500000 0.0000000                    1 0  1.0200 0.00000 .90000 1.1000 0.0000 1.0425 1.0425
   2    9  1  7 1 2 .00060000 .02500000 0.0000000                    2 0  1.0300 0.00000 .90000 1.1000 0.0000 1.0236 1.0236
   3   11  1  7 1 2 .00060000 .02500000 0.0000000                    3 0  1.0300 0.00000 .90000 1.1000 0.0000 1.0247 1.0247
   4   10  1  7 1 2 .00060000 .02500000 0.0000000                    4 0  1.0300 0.00000 .90000 1.1000 0.0000 1.0134 1.0134
   5   12  1  7 1 2 .00060000 .02500000 0.0000000                    5 0  1.0100 0.00000 .90000 1.1000 0.0000 1.0332 1.0332
   6   13  1  7 1 2 .00060000 .02500000 0.0000000                    6 0  1.0300 0.00000 .90000 1.1000 0.0000 1.0256 1.0256
   7   14  1  7 1 2 .00060000 .02500000 0.0000000                    7 0  1.0300 0.00000 .90000 1.1000 0.0000 1.0254 1.0254
   8   24  1 15 1 1 .00050000 .04350000 0.0000000                    0 0  1.0420 0.00000 0.0000 0.0000 0.0000 0.0000 0.0000
   9   25  1 15 1 1 .00080000 .04720000 0.0000000                    0 0  1.0527 0.00000 0.0000 0.0000 0.0000 0.0000 0.0000
  11   27  1 15 1 1 .00030000 .02200000 0.0000000                    0 0  .99000 0.00000 0.0000 0.0000 0.0000 0.0000 0.0000
  12   28  1 15 1 1 .00050000 .04350000 0.0000000                    0 0  1.1113 0.00000 0.0000 0.0000 0.0000 0.0000 0.0000
  13   26  1 15 1 1 .00030000 .02230000 0.0000000                    0 0  1.0207 0.00000 0.0000 0.0000 0.0000 0.0000 0.0000
  14   23  1 15 1 1 .00060000 .04370000 0.0000000                    0 0  1.0207 0.00000 0.0000 0.0000 0.0000 0.0000 0.0000
  15   17  1 40 1 1 .00020000 .01070000 0.0000000                    0 0  .93000 0.00000 0.0000 0.0000 0.0000 0.0000 0.0000
  16   17  1 40 1 1 .00010000 .00760000 0.0000000                    0 0  .94000 0.00000 0.0000 0.0000 0.0000 0.0000 0.0000
   8    9  1 15 1 0 .01700000 .06320000 .02300000                    0 0
   9   10  1 15 1 0 .00100000 .01140000 .00400000                    0 0
  10   11  1 15 1 0 .00620000 .03000000 .01000000                    0 0
  10   13  1 15 1 0 .00550000 .02500000 .00800000                    0 0
  11   12  1 15 1 0 .00620000 .03000000 .01000000                    0 0
  12   13  1 15 1 0 .00800000 .04300000 .01400000                    0 0
  17   23  1 40 1 0 .00010000 .00140000 .03240000                    0 0
  17   25  1 40 1 0 .00050000 .00460000 .11340000                    0 0
  17   25  1 40 2 0 .00050000 .00520000 .12820000                    0 0
  17   25  1 40 3 0 .00050000 .00520000 .12820000                    0 0
  18   19  1 40 1 0 .00080000 .00840000 .19720000                    0 0
  18   20  1 40 1 0 .00100000 .01000000 .23620000                    0 0
  18   21  1 40 1 0 .00090000 .00970000 .23140000                    0 0
  18   29  1 40 1 0 .00150000 .01600000 .40000000                    0 0
  18   30  1 40 1 0 .00150000 .01600000 .40000000                    0 0
  19   31  1 40 1 0 .00130000 .01330000 .27100000                    0 0
  21   32  2 40 1 0 .00220000 .02310000 .28860000                    0 0
  22   24  1 40 1 0 .00130000 .01330000 .27100000                    0 0
  24   25  1 40 1 0 .00070000 .00770000 .18960000                    0 0
  25   26  1 40 1 0 .00050000 .00490000 .10900000                    0 0
  25   26  1 40 2 0 .00050000 .00490000 .10900000                    0 0
  25   27  1 40 1 0 .00080000 .00710000 .17280000                    0 0
  27   28  1 40 1 0 .00080000 .00710000 .17280000                    0 0
  27   29  1 40 1 0 .00100000 .01000000 .24400000                    0 0
  27   30  1 40 1 0 .00090000 .00990000 .24420000                    0 0
-999
LOSS ZONES FOLLOW                   0 ITEMS
-99
INTERCHANGE DATA FOLLOWS            2 ITEMS
-9
TIE LINES FOLLOW                    1 ITEMS
-999
END OF DATA
```

The series of events that drive the system to collapse are as follows:

1. At 30 s, the P and Q powers in buses N201 through N207 (load buses with ULTCs) start increasing steadily at a rate of 30 % in 2 hours (7200 s). P and Q are assumed to change in the same proportion as their initial values, i.e., in (4.3), P_{L_P} and Q_{L_Q} are equal to the corresponding initial values, whereas $k_P = k_Q = 1$. All other load buses remain unchanged.

2. Line N3-N16 is tripped off at 5000 s. The system is assumed to transiently recover from this "large" contingency.

3. At 7230 s, the load stops increasing.

4. Finally, machine M2 trips off at 7400 s, precipitating the system voltage collapse.

It is interesting to highlight the fact that in the CIGRE report where the test system is originally described and studied [2], the ULTCs were actually blocked to better represent the operation of the real system, where the taps are controlled by operators. In the studies presented here, however, these taps were assumed to change automatically to better illustrate the effect of control limits on the different indices. In spite of the different treatment of the ULTCs, these taps and their corresponding limits do not make a significant difference on the maximum loading margins of the test system, as demonstrated by the close agreement between the results presented here and those reported in [2].

4.3 INDICES

Several indices are described in detail in this section. All indices are defined based on the original work that first proposed them, and the corresponding algorithm is explained and applied to the sample system. Advantages and disadvantages of the different indices are also discussed in view of practical applications.

A comprehensive comparison of all indices discussed in this section can be found in Section 4.5.

4.3.1 Sensitivity Factors

Sensitivity factors are well known indices used in several utilities throughout the world to detect voltage stability problems and to device corrective measures [1, 2]. These indices were first used to predict voltage control problems in generator QV curves, and they may be defined as

$$VSF_i = \max_i \left\{ \frac{\mathrm{d}V_i}{\mathrm{d}Q_i} \right\}$$

where VSF stands for Voltage Sensitivity Factor. As generator "i" approaches the "bottom" of its QV curve, the value of VSF_i becomes large and eventually changes sign, indicating an "unstable" voltage control condition.

Based on this concept, more general, system wide indices have been proposed. Thus, the following SF (Sensitivity Factor) index may be defined for a system represented by equations $F(z, \lambda)$ in (4.1):

$$SF = \left\| \frac{\mathrm{d}z}{\mathrm{d}\lambda} \right\|$$

When SF becomes large the system turns "insecure" and eventually collapses, due to all entries $\mathrm{d}z_i/\mathrm{d}\lambda \to \pm\infty$ when the system approaches a maximum value of the parameter λ ($\Delta\lambda \to 0$). As λ typically represents load changes, the collapse point associated with a maximum value of λ is usually referred to as the maximum loadability or loading point. If only system voltages V are monitored, an equivalent VSF may be defined as

$$VSF = \left\| \frac{\mathrm{d}V}{\mathrm{d}\lambda} \right\|$$

Although by definition all norms are "equivalent," the L_∞-norm $||\cdot||_\infty$ typically yields the best results, since the maximum entry on the vector $\mathrm{d}z/\mathrm{d}\lambda$ can be used to pinpoint the system areas directly associated with the collapse problem, as explained in Section 4.3.5.2 below.

The application of these indices to the sample system is depicted in Figures 4.3-1 and 4.3-2, which were obtained by solving a series of power flows at different load levels. Three different cases are jointly shown in these figures; namely, the effect of increasing the load in the original full system and in the system with generators N16 (line N16-N3) and M2 tripped off. Thus, the following observations can be made regarding these plots and the data used to generate them:

- The full system collapses at a total load level of 6050 MVA (this value represents the MVA sum of all system loads), whereas for the system without generator N16, the collapse occurs at a loading level of 5876 MVA. When generator M2 is removed as well, the loading level at which collapse occurs is reduced to 5520 MVA. As expected, the more generators removed from the system, the less the loading margin to collapse.

- Both sensitivity factors behave in a similar manner, i.e., as the system approaches the collapse point, the indices increase significantly, appearing somewhat insensitive to loading changes except when very close to collapse. If the inverse is used, however, these indices have a more "predictable" shape, especially for the VSF index, which appears to be "quadratic" *after the first large step change*, i.e.,

$$\begin{aligned} \lambda &= -a\,(1/VSF)^2 + \lambda_* \\ \Rightarrow \quad \Delta\lambda &= a\,(1/VSF)^2 \end{aligned} \tag{4.4}$$

  where a and λ_*, the maximum parameter value at the bifurcation or collapse point, can be estimated from a couple of points in the VSF curve, before the system collapses. For example, for the full system, the points (5440 MVA, 2)

and (5850 MVA, 1) in Figure 4.3-2(b) yield $a \approx 137$ and $\lambda_* \approx 5990$ MVA. Hence, based on (4.4), an index value can be transformed into a load margin to collapse $\Delta\lambda$ in MVA at any given point; this is typical in many indices as shown in this report, allowing for some predictions of proximity to collapse.

Observe that when the index exhibits large changes due to system control limits, as is the case for tap limits in the sample system's VSF, it is not feasible to make adequate predictions of loading margins. These sharp changes are characterisitc of several other indices as well, especially when applied to large systems where Q-limits or any other device limits are considered. On the other hand, these sharp index changes have certain advantages as discussed below, since they allow to rate the relative importance of the different limits on system loadability, so that operators may take certain corrective actions early in the loading process.

It is important to highlight the fact that the quadratic shape of these sensitivity factors *is not always observed*, especially in large systems, where these indices tend to be less sensitive to parameter changes than in the sample system studied here.

- ULTC limits produce sharp changes on SF and VSF, which is also the case for any other voltage support device reaching its limits. This is more evident in the VSF index, where the desired quadratic shape is severely affected by the ULTC limits of transformer N103-N204, which is the first to hit its maximum limit. Hence, predictions of distance to collapse made using the VSF index are somewhat suspect. On the other hand, this sharp change indicates early in the loading process the need for voltage support at bus N204, which is part of the system "critical area" as explained below.

- The L_∞-norm used to compute these indices indicates that buses N204 (N103) and N202 (N102), in the "northern" part of the system, form the critical area for all three cases studied here, i.e., corrective measures in these buses, such as load shedding or additional voltage support, would be the most effective way to avert system loss by increasing the distance to collapse.

Figure 4.3-3 depicts the changes in the VSF index versus time, as it would appear on an operator's console, showing the effect of the different contingencies on the system proximity to collapse. First, at about 4200 s, the ULTC of transformer N103-N204 hits its maximum limit, creating a sharp change in the index. After that, other ULTCs reach limits; however, no other single transformer has such a large effect on VSF. Next, at 5000 s, generator N16 is removed from the network, producing an approximate 200 MVA reduction in the maximum loading margin. The load stops increasing at 7230 s, when the system has about 180 MVA additional capacity before collapse. Finally, M2 is tripped off at 7400 s, producing the collapse of the system, as the load at that point has already exceeded the maximum loading margin of the network without N16 and M2.

Although this "post-mortem" analysis is useful to determine the causes of collapse in this system, from the operator point of view, who is monitoring this index as the

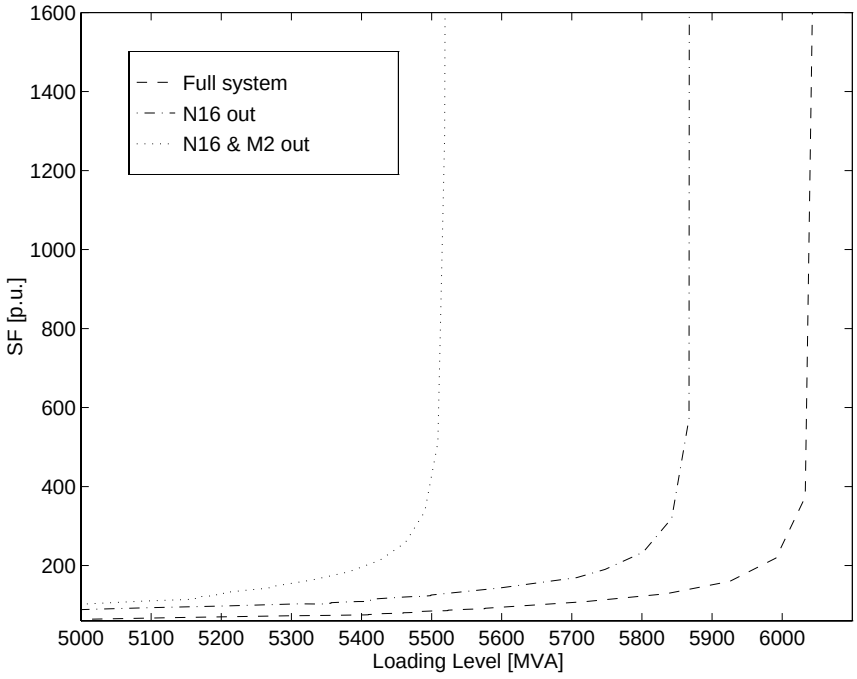

(a)

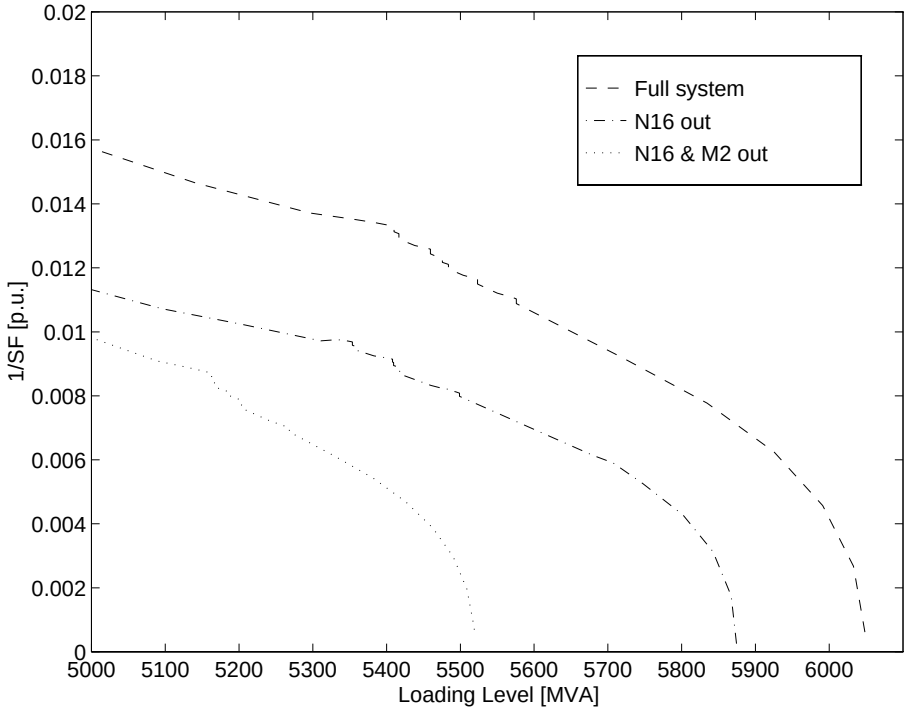

(b)

Figure 4.3-1. (a) Sensitivity factor and (b) its inverse.

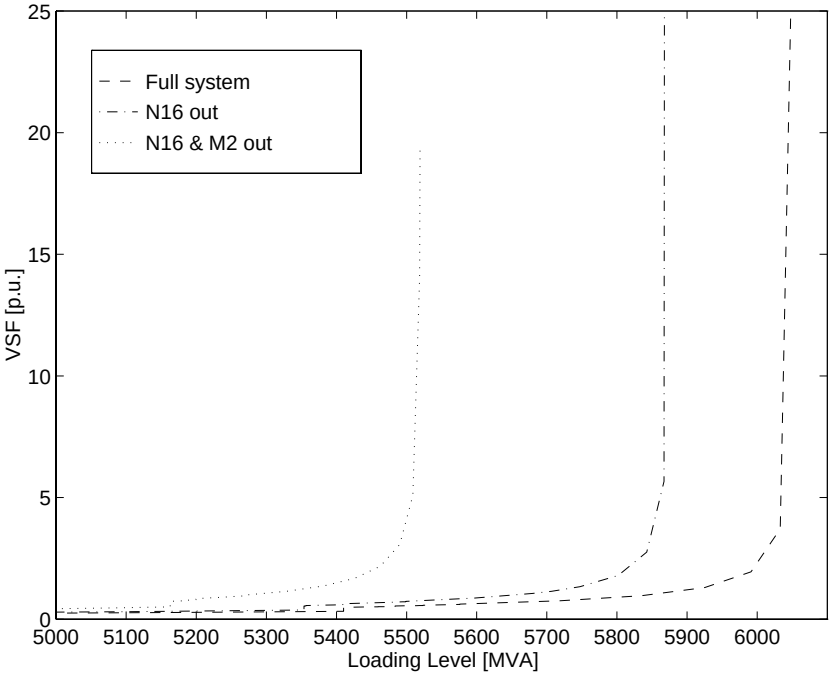

(a)

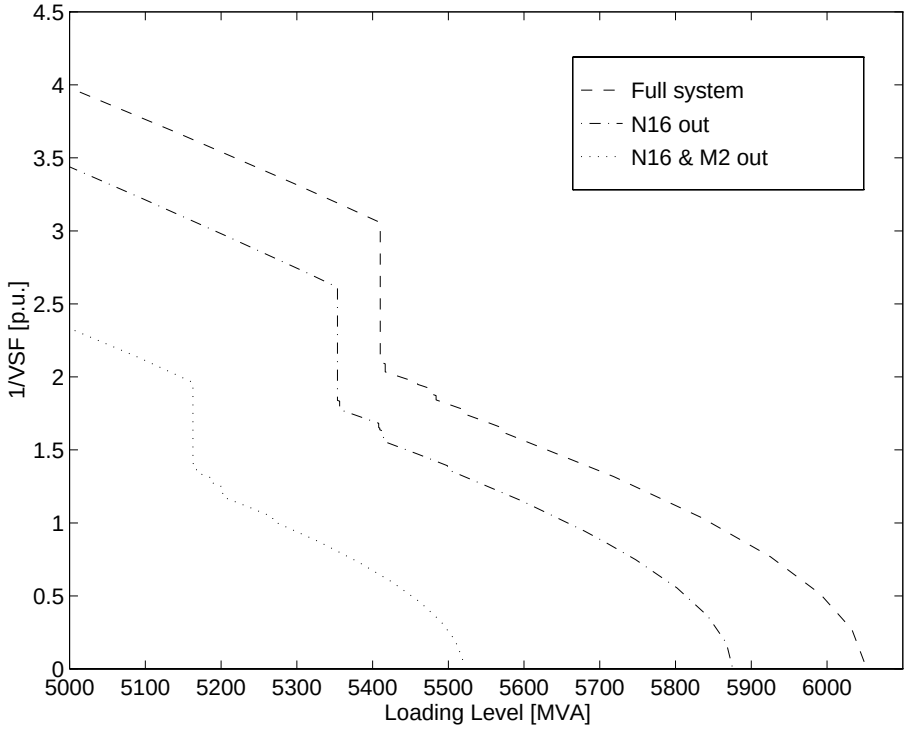

(b)

Figure 4.3-2. (a) Voltage sensitivity factor and (b) its inverse.

system is changing and has limited capability to study contingencies ahead of time to determine their effect on the network, the following information can be obtained on-line from the index, which applies as well to most of the other indices discussed in this report:

- Load margins to collapse can be readily estimated as the system load is changing from every two index values by applying (4.4); these estimates have to be revised after any sharp change on the index value. Based on these estimates, a threshold value of the index could be defined, based on historical data and off-line stability and contingency studies, so that this value may be used as a warning signal for the operator to take major and immediate corrective actions, such as load shedding, to prevent system collapse. For the sample system, based on the post-mortem collapse analysis, it appears that a threshold value of $1/VSF \approx 2$ would be appropriate, as the system is still "operable" even if M2 is removed; the later assumes that the system would be transiently stable for such contingency.

- If an L_∞-norm is used, the index also generates some information regarding "critical" buses in the system for a given operating condition. However, this information is only significant when "close" to the collapse point, as the critical areas tend to change as the system approaches collapse; this is particularly true in large systems (this is discussed in more detail in subsequent sections).

- Sharp reductions in the index value indicate a reduction on load margin to collapse. Hence, corrective actions may be devised to increase distance to collapse based on the system critical areas and the system changes directly associated with the sharp index changes. For example, the first large change in VSF indicates a need for additional voltage support or load shedding at bus N204.

The SF and VSF indices are rather inexpensive to compute and, in "small" systems, they allow for some predictions of proximity to collapse. However, for large systems, this is not always the case, as these indices, particularly the SF, are not very sensitive to system parameter variations. Also, unless an infinity norm is used, these indices do not generate much additional information to help pinpoint the system areas that are more strongly associated with the collapse problem, so that corrective measures can be devised. Finally, based on the definitions of these indices, it is clear that they can be applied to any system model besides a power flow based model.

4.3.2 Singular Values and Eigenvalues

This section describes two well known proximity indices associated with singular value and eigenvalue decomposition. As these two indices require somewhat similar computations and produce rather similar results, they are jointly discussed in this report.

Although the results presented here were obtained for a power flow based model, these indices can be applied to other system models as well. However, the meaning of the eigenvalues and singular values on which these indices are based changes significantly with the system model used. For example, for most system dynamic models,

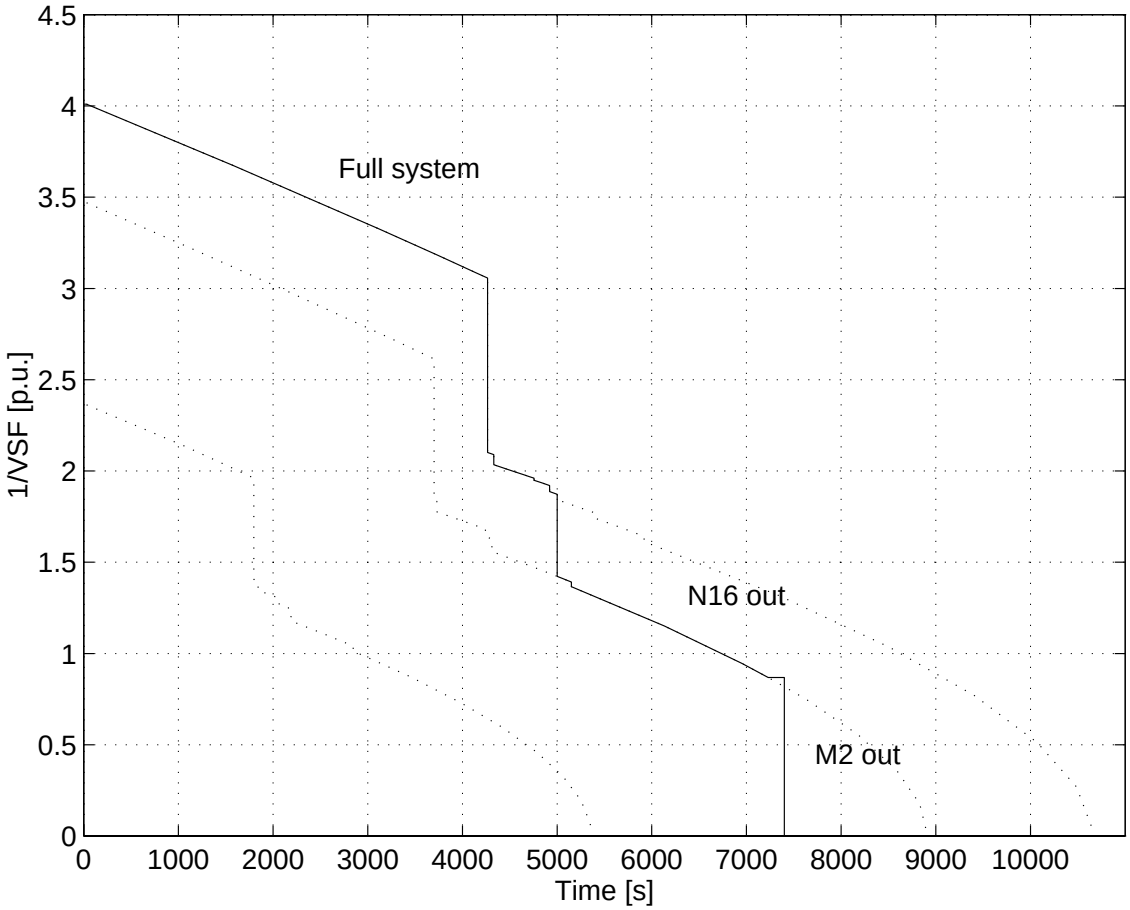

Figure 4.3-3. Voltage sensitivity factor inverse versus time.

the values obtained from a power flow model do not have any significant meaning in terms of the underlying system dynamics at equilibrium points, other than at the bifurcation or collapse point [3, 9].

4.3.2.1 Singular Values

Singular values have been employed in power systems because of the useful orthonormal decomposition of the Jacobian matrices. For the real $n \times n$ square Jacobian matrix $J = D_z F(z_0, \lambda_0)$ at the equilibrium point (z_0, λ_0) of (4.1), one has that

$$J = R\Sigma S^T = \sum_{i=1}^{n} r_i \sigma_i s_i^T$$

where the singular vectors r_i and s_i are the i^{th} columns of the unitary matrices R and S, and Σ is a diagonal matrix of positive real singular values σ_i, such that $\sigma_1 \geq \sigma_2 \geq \cdots \geq \sigma_n$. The diagonal entries of Σ^2 correspond to the eigenvalues of matrix JJ^T.

This singular value decomposition is typically used to determine the rank of a matrix, which is equal to the number of non zero singular values of J. Hence, its application to voltage collapse analysis focuses on monitoring the smallest singular value up to the point when it becomes zero at the collapse point [10].

In general, the Jacobian J contains the first derivatives of the reactive power mismatch equations $Q(z, \lambda)$ with respect to the voltage magnitude $V \in z$. Hence, linearizing the steady state equations $F(z, \lambda) = 0$ at an equilibrium point (z_0, λ_0),

$$\begin{aligned} \Delta F(z,\lambda) &= J\,\Delta z \qquad (4.5)\\ \Rightarrow \quad \begin{bmatrix} \Delta \hat{F}(\hat{z}, V, \lambda) \\ \Delta Q(\hat{z}, V, \lambda) \end{bmatrix} &= \begin{bmatrix} \frac{\partial \hat{F}}{\partial \hat{z}}(z_0,\lambda_0) & \frac{\partial \hat{F}}{\partial V}(z_0,\lambda_0) \\ \frac{\partial Q}{\partial \hat{z}}(z_0,\lambda_0) & \frac{\partial Q}{\partial V}(z_0,\lambda_0) \end{bmatrix} \begin{bmatrix} \Delta \hat{z} \\ \Delta V \end{bmatrix} \\ &= \begin{bmatrix} J_1 & J_2 \\ J_3 & J_4 \end{bmatrix} \begin{bmatrix} \Delta \hat{z} \\ \Delta V \end{bmatrix} \end{aligned}$$

For the typical power flow model, $\hat{F}(z, \lambda)$ represents the active power mismatches $P(z, \lambda)$, and $\hat{z}$ represents the bus voltage angles δ. One can rewrite (4.6), at equilibrium points other than the collapse point, as

$$\begin{bmatrix} \Delta \hat{z} \\ \Delta V \end{bmatrix} = \sum_{i=1}^{n} \sigma_i^{-1} s_i r_i^T \begin{bmatrix} \Delta \hat{F}(\hat{z}, V, \lambda) \\ \Delta Q(\hat{z}, V, \lambda) \end{bmatrix} \qquad (4.6)$$

Notice that the minimum singular value is a relative measure of how close the system is to the voltage collapse or singular point. Furthermore, near this collapse point, since σ_n is close to zero, equation (4.6) can be rewritten as

$$\begin{bmatrix} \Delta \hat{z} \\ \Delta V \end{bmatrix} \approx \sigma_n^{-1} s_n r_n^T \begin{bmatrix} \Delta \hat{F}(\hat{z}, V, \lambda) \\ \Delta Q(\hat{z}, V, \lambda) \end{bmatrix}$$

Hence, the associated left and right singular vectors r_n and s_n, respectively, contain important information. The maximum entries in s_n indicate the most sensitive voltage magnitudes (critical buses), and the maximum entries in r_n correspond to the most sensitive direction for changes of power injections.

Assuming that $\Delta\hat{F}(\hat{z}, V, \lambda) = 0$, which in the standard power flow model corresponds to only considering reactive power injections changes, equation (4.6) yields the following:

$$\begin{aligned} \Delta Q(\hat{z}, V, \lambda) &= (J_4 - J_3 J_1^{-1} J_2)\Delta V \\ &= J_{QV}\Delta V \end{aligned} \tag{4.7}$$

In general, at the collapse point one has that J_1 is nonsingular, even though J is singular; there is no definite proof of the latter statement, but in practice that seems to be the case in all examples discussed in the literature. Thus, J_{QV} is assumed well defined in (4.7), becoming singular at the collapse point since

$$\det J_{QV} = \frac{\det J}{\det J_1}$$

The singular values of this reduced matrix can then be used to determine proximity to voltage collapse. Furthermore, these singular values show "better" profiles than the ones of J, as observed in Figures 4.3-4 for the sample system, and demonstrated in [10].

It is interesting to highlight the fact that sub-matrix J_3 is quasi-symmetric, for small values of transmission system resistances. Therefore, one expects a similar attribute for J_{QV}, making the singular values and eigenvalues for this matrix practically identical [11], as symmetric matrices have similar singular value and eigenvalue decomposition.

4.3.2.2 Eigenvalue Decomposition

Eigenvalues, as singular values, are also often used to determine proximity to the voltage collapse point [1, 2]. The eigenvalue decomposition for the Jacobian matrix J, assuming that is diagonalizable (semi-simple), can be written as

$$J = W\Lambda U^T = \sum_{i=1}^{n} w_i \mu_i v_i^T$$

where W represents a complex matrix of left eigenvectors w_i, U corresponds to the complex matrix of right eigenvectors v_i, and Λ is a diagonal matrix of complex eigenvalues μ_i.

For the J_{QV} matrix defined in (4.7), this decomposition may be applied directly [12], as this matrix is quasi-symmetric and, therefore, diagonalizable. Furthermore, due to its quasi-symmetric structure, one expects to obtain a set of only real eigenvalues and eigenvectors, very similar in value to the corresponding singular values and singular vectors. Thus, for J_{QV}, the eigenvectors associated with the eigenvalue closest to zero have the same interpretation as the singular vectors near the collapse

point, i.e., the maximum entries in the right eigenvector correspond to the critical buses (most sensitive voltages) in the system, and the maximum entries in the left eigenvector pinpoints the most sensitive direction for changes of power injections [12, 13, 14].

Both minimum singular value and eigenvalue profiles of the full Jacobian J for the test system, which are basically identical, are shown in Figure 4.3-4(a). Observe the highly nonlinear behavior of these indices in all cases, i.e., they are rather insensitive to changes on the loading factor λ. It is interesting to highlight the fact that the Jacobian J does not become singular until very close to the collapse point; for this reason, standard power flows can be used to obtain solution points rather close to the point of collapse, as it has been the experience in many utilities [1].

When applied to the reduced Jacobian J_{QV}, these indices produce very similar results to the ones obtained for the VSF, as shown in Figures 4.3-4(b) and 4.3-5. These indices also present a quadratic profile when close to the bifurcation [15], but seem more sensitive to ULTC limits. Hence, similar comments and observations apply to these results as in the VSF case. It is important to highlight the fact that the quadratic behavior shown here is not always observed in larger systems [11].

The maximum entries in the corresponding eigenvectors and singular vectors once again point to buses N204 (N103) and N202 (N102) as critical buses of the system. However, in general, this information can only be obtained when close to collapse [11], as is the case here for the full Jacobian J.

Comparing the singular value and eigenvalue based indices to the sensitivity factors, somewhat similar information can be obtained, since all of these indices present similar profiles with respect to parameter changes, and the vector derivatives ("tangent" vectors) used in the sensitivity factors can also be used to pinpoint critical areas in the system, in the same way as what is done with singular vectors and right eigenvectors at a singularity point (the tangent vectors converge to the right eigenvectors at a singularity point [3]). However, singular values and eigenvalues present higher computational costs than in the case of the sensitivity factors.

4.3.3 Second Order Performance Index

Indices based on first order information (linearizations), such as singular values and eigenvalues and several other indices presented in this document, may be inadequate to predict proximity to collapse as these exhibit large discontinuities in the presence of system control limits like generator capability or transformer tap limits, as previously discussed. However, it is possible to calculate a "second order" index that exploits additional information embedded in these indices to overcome their weak points [15].

Simulations performed in several systems, including the test system used in this report, show that the maximum singular value of the full Jacobian inverse J^{-1} (i.e., the inverse of the minimum singular value of J), defined here as σ_{max}, can be approximated with respect to the load variations, represented here by the parameter λ, by the function

$$\sigma_{max}(\lambda) = (b - d\,\lambda)^{1/c}$$

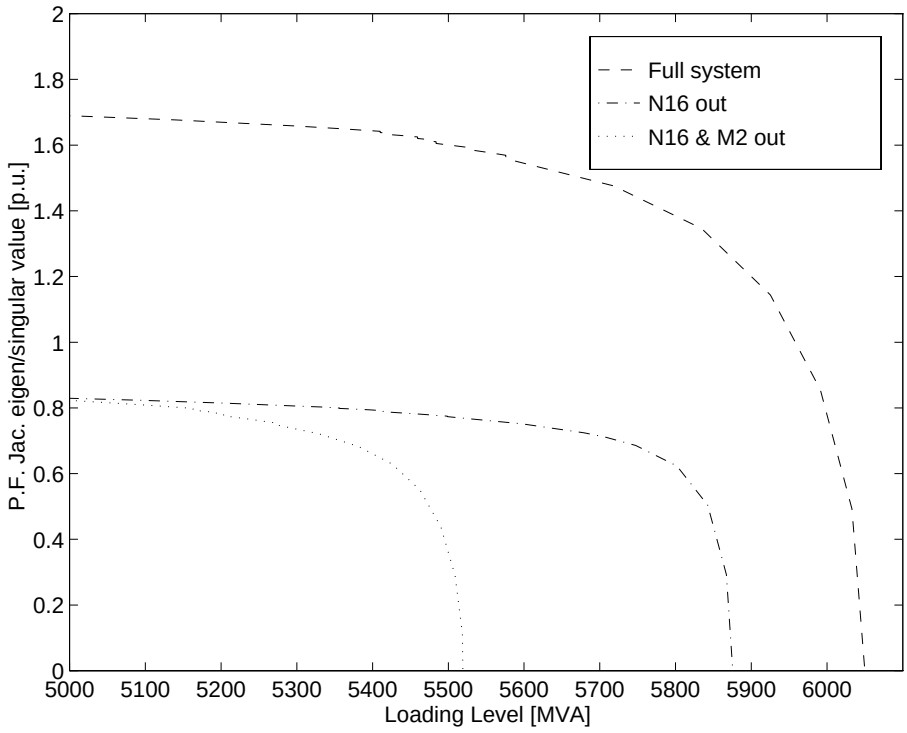

(a)

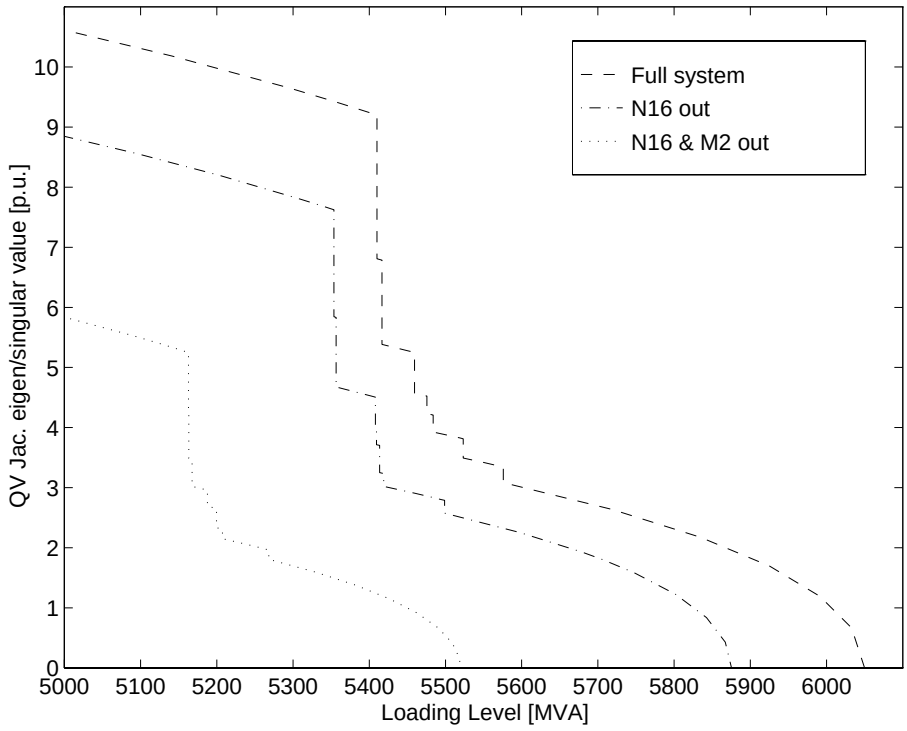

(b)

Figure 4.3-4. Minimum eigenvalues and singular values for (a) full J and (b) reduced power flow J_{QV} Jacobians.

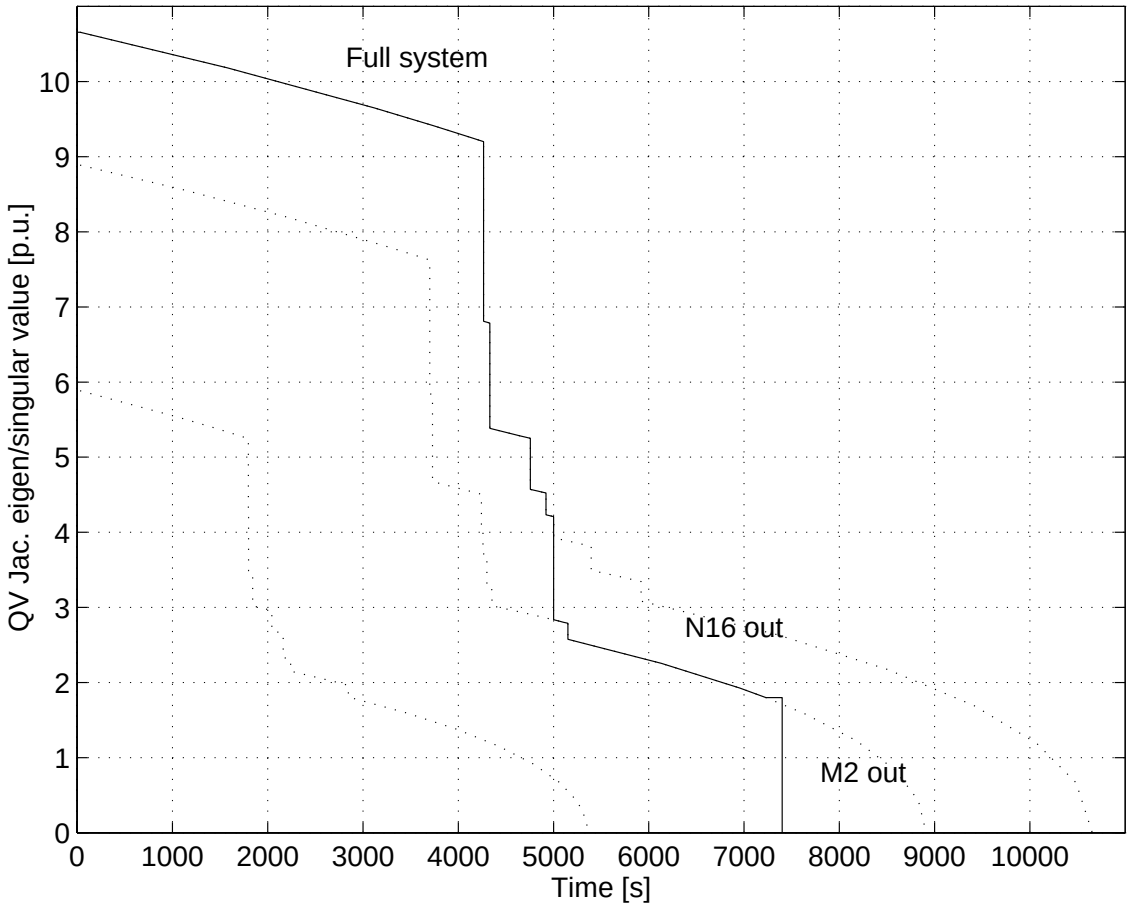

Figure 4.3-5. Minimum eigenvalue/singular value for J_{QV} versus time.

with suitable values of the scalar positive constants b, c and d, as illustrated in Figure 4.3-4. These types of functions have the characteristic that the ratio

$$\frac{\sigma_{max}(\lambda)}{\mathrm{d}\sigma_{\max}/\mathrm{d}\lambda} = c\,\lambda - \frac{bc}{d} \tag{4.8}$$

is linear with respect to the varying parameter λ. Thus, the following index is proposed

$$\iota = \frac{1}{\iota_o}\,\frac{\sigma_{max}(\lambda)}{\mathrm{d}\sigma_{\max}/\mathrm{d}\lambda} \tag{4.9}$$

where ι_o is the value of (4.8) at the starting loading point, to properly normalize the index ι. At the collapse point, $\iota = 0$, since the denominator tends to infinite as the Jacobian becomes singular. Based on the linear trend of ι, appropriate predictions can be made of the distance to the voltage collapse point.

Generator capability limits or other operating limits, and the consequent jump in the value of σ_{max}, could compromise the expected linearity of ι. However, a sudden change in σ_{max} due to device limits is somewhat compensated by the corresponding high value of the derivative $\mathrm{d}\sigma_{max}/\mathrm{d}\lambda$. Thus, experimental results show that ι approaches zero following a quasi linear pattern even in the presence of large discontinuities in σ_{max} due to device limits [15].

For power flow models, the derivative of the denominator in (4.9) can be calculated following the procedure proposed in [16, 17]. Thus, the power flow Jacobian matrix J_{PF}, which may be defined at a solution point (u_o, λ_o) of (4.2) as $J_{PF} = D_u\mathcal{F}|_o$, can be decomposed as follows:

$$J_{PF} = R\Sigma S^T$$

where R and S are orthonormal matrices, and Σ is a diagonal matrix whose elements σ are the singular values of J_{PF}. The idea is then to determine the influence of system parameters p, particularly real and reactive loads, on the minimum singular value σ_{min} of J_{PF} (which yields the maximum singular value $\sigma_{max} = 1/\sigma_{min}$ of J_{PF}^{-1}). This vector parameter p is usually a function of the scalar parameter λ, e.g., loading changes can be related back to the desired parameter λ by observing from (4.3) that

$$p = k\,\lambda \tag{4.10}$$

where k represents a loading "direction." Hence, a new Jacobian at a new solution point $u_1 = u_o + \Delta u$, where Δu represents a "small" change in the solution u_o due to a change Δp in the initial system loading p_o, can be approximated by

$$D_u\mathcal{F}|_1 \approx J_{PF} + \underbrace{D_u^2\mathcal{F}|_o}_{H}\,\Delta u$$

where H is a three-dimensional Hessian array of the power flow equations. If Δp represents a vector of real and reactive power injection changes in all system buses, based on the power flow equations $\mathcal{F}(u, p) = 0$,

$$D_u\mathcal{F}|_o\mathrm{d}u + D_p\mathcal{F}|_o\mathrm{d}p = 0$$

where $D_p\mathcal{F}$ results in the identity matrix; hence,

$$\Delta u = -J_{PF}^{-1}\Delta p$$

The change in the i^{th} singular value of J_{PF} may then be approximated by [16]

$$\Delta\sigma_i \;\approx\; R_i^T H\; J_{PF}^{-1}\Delta p\; S_i$$

where R_i and S_i are the i^{th} columns of matrices R and S, respectively. In particular, for the minimum singular value

$$\Delta\sigma_{min} \approx c^T\Delta p \tag{4.11}$$

where [17]

$$c^T = -R_1^T\left(H\; J_{PF}^{-1}S_1\right) \tag{4.12}$$

The change $\Delta\sigma_{max}$ can be computed based on a binomial series expansion, i.e.,

$$\begin{aligned}\sigma_{max}+\Delta\sigma_{max} &= \frac{1}{\sigma_{min}+\Delta\sigma_{min}}\\ &\approx \frac{1}{\sigma_{min}}\left(1-\frac{\Delta\sigma_{min}}{\sigma_{min}}\right)\end{aligned}$$

assuming that $\Delta\sigma_{min}/\sigma_{min}$ is "small." Thus, as $\sigma_{max} = 1/\sigma_{min}$, it follows that

$$\begin{aligned}\Delta\sigma_{max} &\approx \left(\sigma_{max}^2 c^T\right)\Delta p\\ &= c_{max}^T\Delta p\end{aligned} \tag{4.13}$$

From (4.10), (4.11), and (4.13),

$$\frac{\mathrm{d}\sigma_{max}}{\mathrm{d}\lambda} \approx c_{max}^T k \tag{4.14}$$

where the vector $c_{max} = \sigma_{max}^2 c$ is computed using (4.12). Using the loading and generation pattern k suggested in [18], (4.14) takes the following form:

$$\frac{\mathrm{d}\sigma_{max}}{\mathrm{d}\lambda} \approx \sum_{j\in N_L}\left(c_{Pmax_j} + c_{Qmax_j}\tan\varphi_j\right)\eta_j - \sum_{j\in N_G} c_{Pmax_j}\rho_j$$

where N_G and N_L are the set of generators and load buses, respectively; c_{Pmax_j} and c_{Qmax_j} are the entries in c_{max} related to the real and reactive power injections; η_j is the share of the total network load at bus j, and $\tan\varphi_j$ is the corresponding power factor; and ρ_j is the participation factor of generator j on the total generated power.

Computational efficiency of the technique presented here is discussed in [15, 17]. The following CPU times corresponding to different calculations on a Digital Alpha 233/255 workstation for the Italian system (approximately 650 buses) can be used to illustrate the costs associated with the computation of the index ι: 1.17s to compute 7 singular values σ and associated singular vectors of the power flow Jacobian

J_{PF}; 0.43s to factorize the Jacobian J_{PF}; 0.63s to compute the Hessian H. Notice that the computed singular values and vectors can also be used to evaluate certain control actions, which is a useful feature of this index as well as other indices based on eigenvalue and singular value calculations. Nevertheless, when compared to other indices, this index is definitely more expensive to compute, as several matrix and vector manipulations and products are required, besides the computation of the minimum singular value; tests on larger systems would allow for a better comparison of the computational burden of this technique with respect to other methodologies presented in this section. Another drawback of this index is that it is based on a particular power flow model; however, it seems feasible to extend the technique to encompass other system models by removing certain modeling assumptions on the derivation process.

The results of applying this technique to the test system are depicted in Figure 4.3-6. The index results in all cases have been normalized with respect to the initial value ι_o for the full system. Notice the smooth and linear behavior of the index in this case, allowing for good predictions of proximity to collapse.

4.3.4 Voltage Instability Proximity Index (VIPI)

Power flow equations typically present multiple solutions, with one of these solutions corresponding to an "operable" point of a power system [19]. It is known that the number of existing solutions decreases as an operating point approaches the collapse point, and only a pair of solutions remain near the collapse point and then coalesces on it. The VIPI index, as defined in [20], is used to predict proximity to voltage collapse using this solution pair. This index is defined based on the rectangular coordinate representation of the power flow equations as follows:

$$y_s = y(x) = (Ax)x + Bx + c \tag{4.15}$$

where x is the voltage vector in rectangular coordinates; y_s represents the node injection vector; and $y(x)$ is a quadratic function of x (A is a three-dimensional constant Hessian, B is a constant square matrix, and c is a constant vector). Denoting the high voltage (operable) solution and low voltage solution as x_1 and x_2, respectively, two vectors a and b can be defined as follows:

$$\begin{aligned} a &= (x_1 + x_2)/2 \\ b &= (x_1 - x_2)/2 \end{aligned} \tag{4.16}$$

At the collapse point, $x_1 = x_2$, i.e., $b = 0$.

From the quadratic nature of (4.15), the following relationships are identical [20, 21]:

$$y_s = y(a) + \tilde{y}(b) \tag{4.17}$$

$$J(a)b = 0 \tag{4.18}$$

where function $\tilde{y}(\cdot)$ is defined as $y(\cdot)$ with the slack node voltage set to zero, and $J(a) = \partial y(x)/\partial x|_{x=a}$ is the power flow Jacobian evaluated at $x = a$. Equation (4.18)

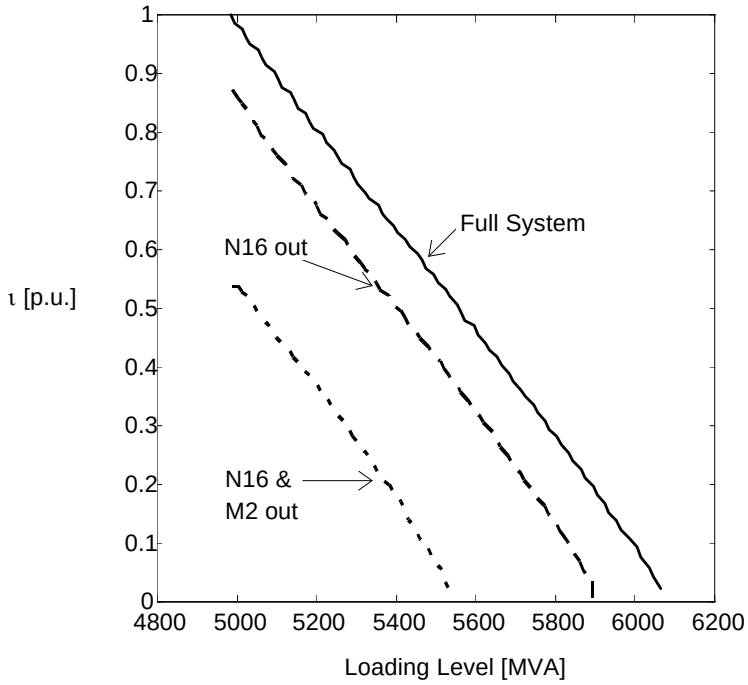
1
0.9
0.8
0.7
0.6
0.5
0.4
0.3
0.2
0.1
0
ι [p.u.]
Full System
N16 out
N16 &
M2 out
4800
5000
5200
5400
5600
5800
6000
6200
Loading Level [MVA]

(a)

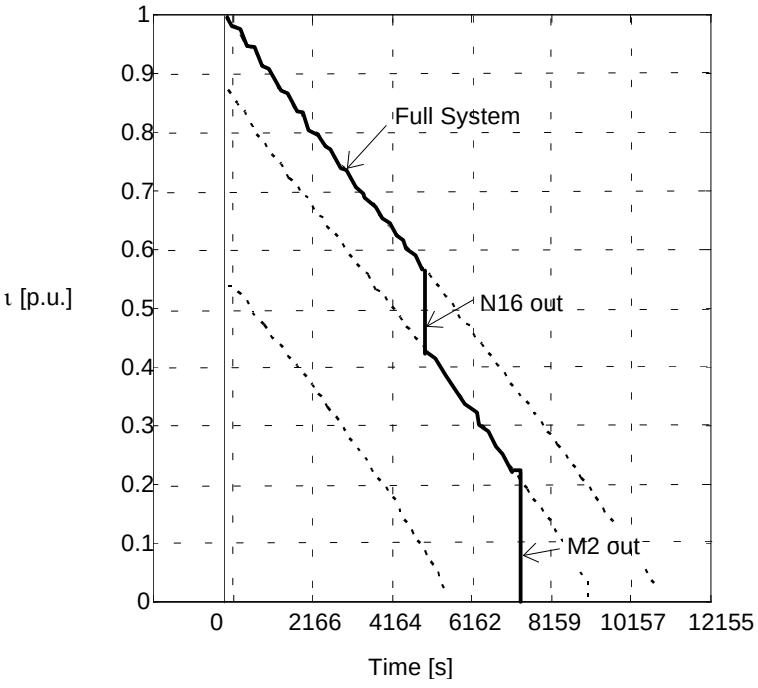
1
0.9
0.8
0.7
0.6
0.5
0.4
0.3
0.2
0.1
0
ι [p.u.]
Full System
N16 out
M2 out
0
2166
4164
6162
8159
10157
12155
Time [s]

(b)

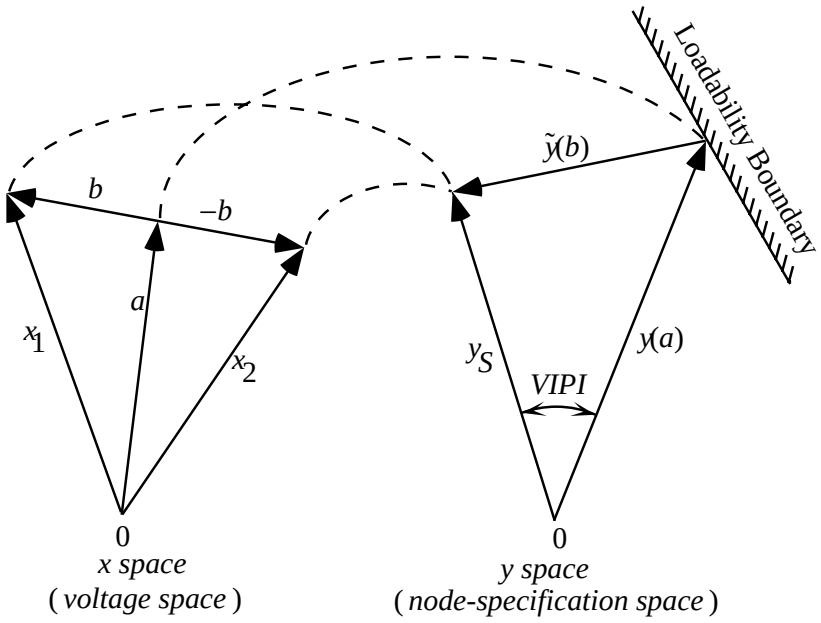

Figure 4.3-7. VIPI indices.

implies that det $J(a) = 0$, and, therefore, $x = a$ is a point on the loadability boundary (a set of voltage collapse points); thus, $y(a)$ represents the node injection vector at the collapse point a. The VIPI index is then defined as the angle between the vectors y_s and $y(a)$, i.e.,

$$VIPI = \cos^{-1}\left(\frac{y_s^{\mathrm{T}} y(a)}{\|y_s\|\|y(a)\|}\right)$$

This definition is graphically explained in Figure 4.3-7.

Taps are dealt with as pre-specified parameters in the definition of the power flow equations (4.15). This implies that the low voltage solution x_2 has to be computed with the taps fixed at the same values as those obtained for the corresponding operating solution x_1. Based on this treatment, the VIPI has the advantage of not presenting large discontinuities during the loading process due to tap limits. A similar procedure is followed to avoid discontinuous behavior due to Q-limits of generators [22]; thus,

1. First, obtain the high voltage solution x_1 and compute the reactive power output of generators at all PV buses.

2. Second, redefine power flow equations (4.15) by fixing the reactive power generated at all PV buses at the value obtained for x_1, and freeing the corresponding bus voltages, i.e., transform all PV buses into PQ buses. Compute the low voltage solution x_2 using these new equations.

The application of the VIPI index to the sample system is depicted in Figures 4.3-8 and 4.3-9. This system has extra singular points on the low voltage side of the solutions, as shown in Figure 4.3-10, which were obtained by fixing all taps at

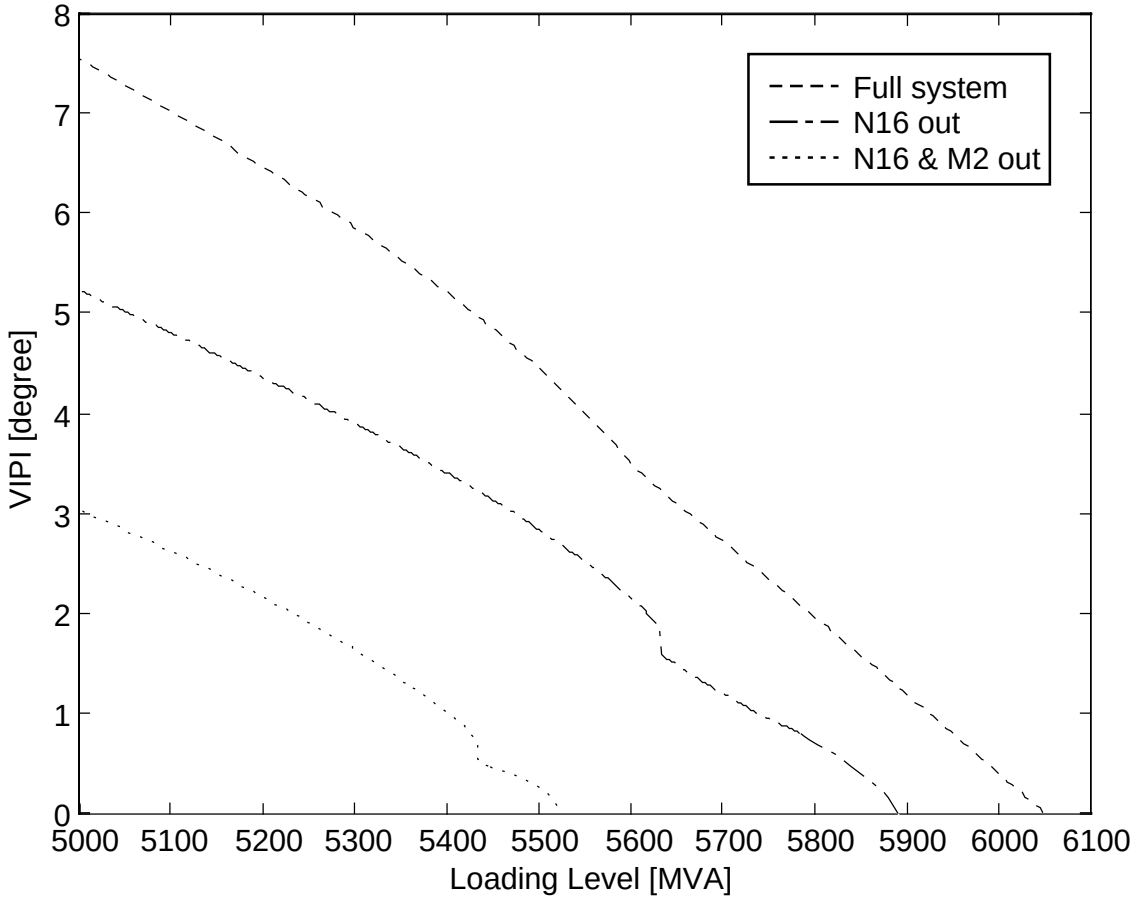

Figure 4.3-8. Voltage instability proximity index (VIPI).

the values computed for the corresponding high voltage solutions. Observe the rapid changes in the index near the low voltage singularities.

Since the VIPI index is defined as the angle difference of two node injection vectors, a disadvantage of this index is that its units are expressed in "degrees," and this information cannot be directly associated with any actual variables in the power system model. Another limitation of this index is that it is based on a particular power flow based model, and it does not appear to be directly applicable to other system models without modifications.

An issue requiring some care is the computation of suitable low voltage solutions. Even though various methods to compute low voltage solutions have been proposed recently, difficulties still exist in the identification of the target solution, particularly for lightly loaded systems. A possible strategy is to identify the target low voltage solution prior to on-line computations, where computational burden is not a major issue. Thus, once an x_2 is obtained off-line, this solution can be used as an initial value in the subsequent on-line computations of other low voltage solutions by means of continuation methods or power flows with optimal multipliers. After the target low voltage solution is identified, this index may be computed efficiently, so that it can be used in practical voltage control applications [23].

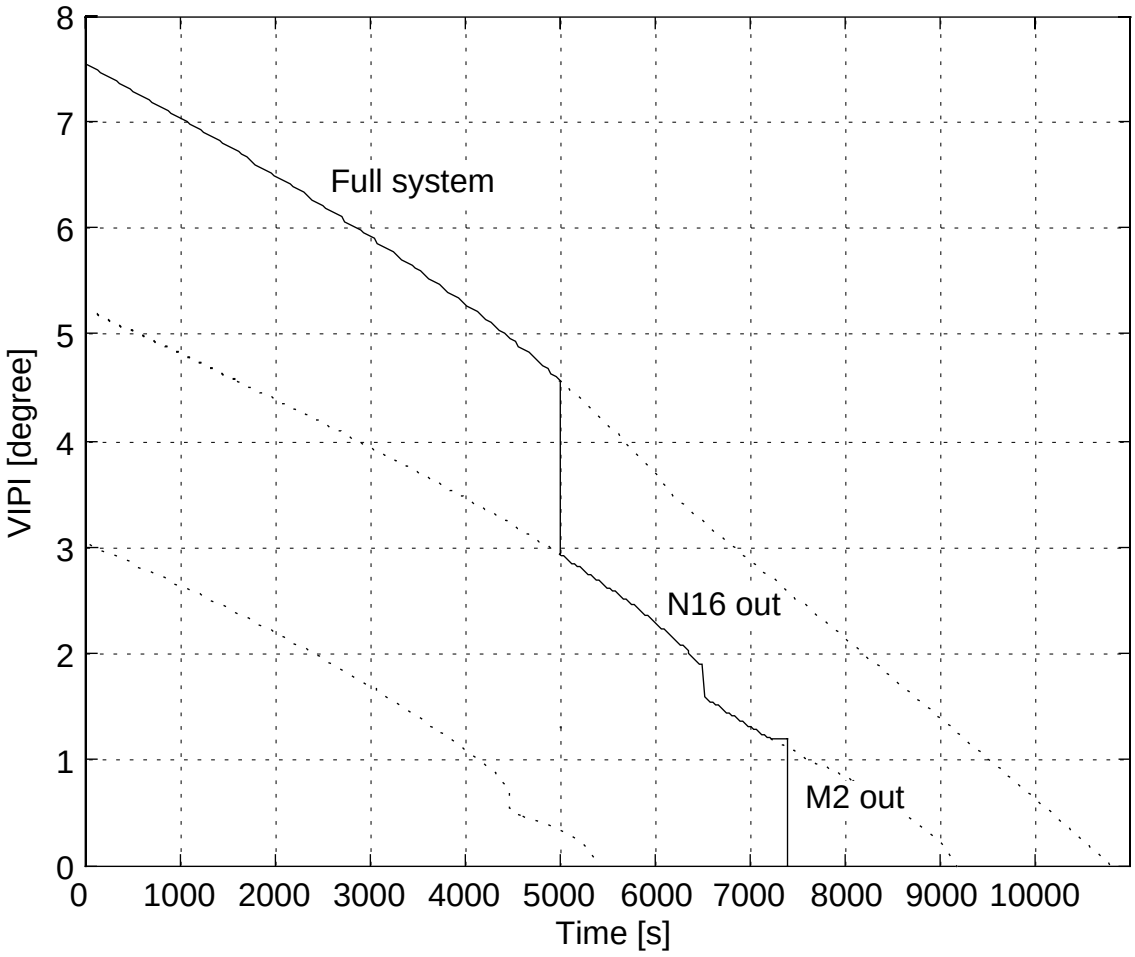

Figure 4.3-9. VIPI versus time.

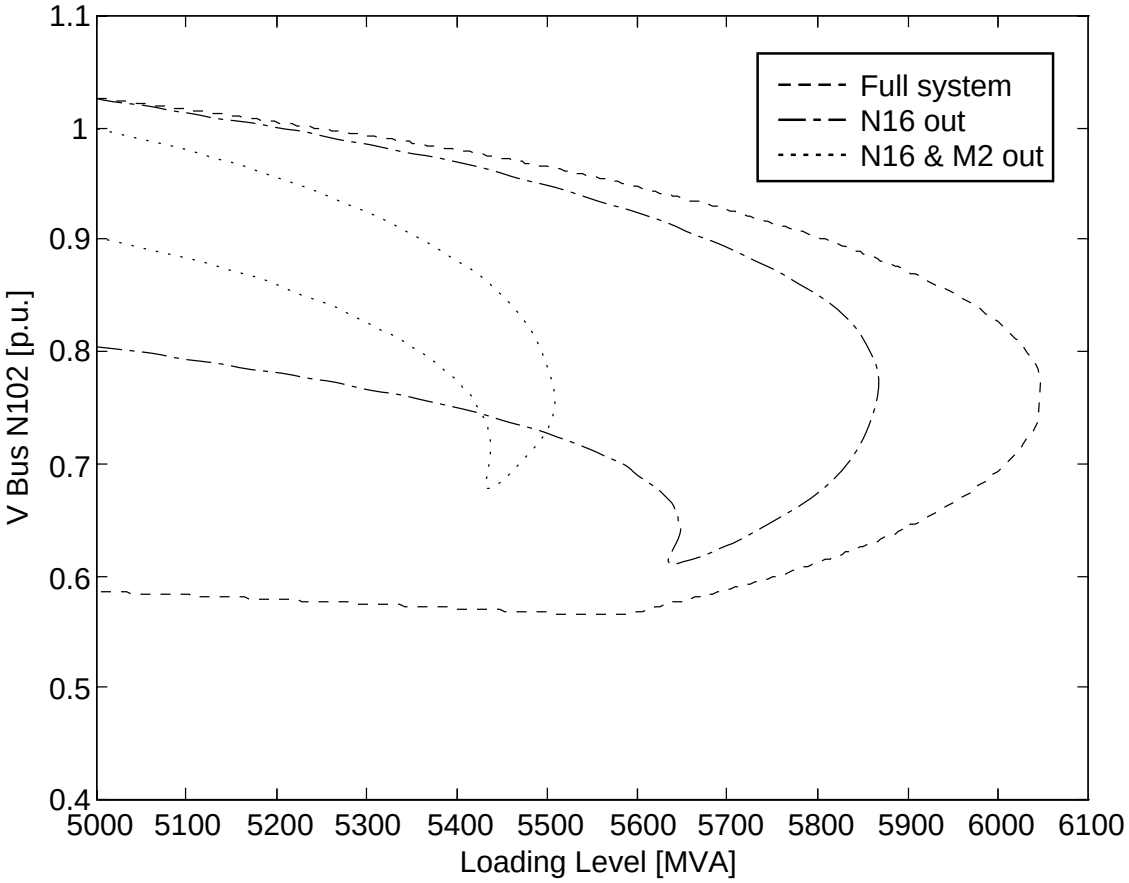

Figure 4.3-10. Complete voltage profiles for Bus N102.

4.3.5 Loading Margin

For a particular operating point, the amount of additional load in a specific pattern of load increase that would cause a voltage collapse is called the loading margin to voltage collapse. Loading margin is the most basic and widely accepted index of voltage collapse. Every paper on voltage collapse indices uses loading margin as the horizontal scale when the performance of the index is graphed.

If system load is chosen to be the parameter which varies, then a system PV curve can be drawn; in this case, the loading margin to voltage collapse is the change in loading between the operating point and the nose of the curve.

There are several choices in defining the loading margin. The change in loading can be measured either by the sum of the absolute changes in load powers or by the square root of the sum of squares of the changes in load powers. Often loads are assumed to have constant power factor and in that case the change in loading can be measured by the changes in real power only. Another useful choice for constant power factor loads is to measure the change in loading by the sum of absolute changes in load powers, which is the technique used in this report. A version of a loading margin measures the amount of power transferred between two areas when studying the transfer capability between areas. It is straightforward to generalize the idea of loading margin to the margin of some other parameter that is varied until the system reaches voltage collapse. For example, if the loads were temperature dependent, then one could define a "temperature margin" to voltage collapse.

The advantages of the loading margin as a voltage collapse index are:

- The loading margin is straightforward, well accepted and easily understood.
- The loading margin is not based on a particular system model; it only requires a static power system model. It can be used with dynamic system models, but it does not depend on the details of the dynamics [24]. It is especially useful that the load dynamics need not be known.
- The loading margin is an accurate index that takes full account of the power system nonlinearity and limits such as reactive power control limits encountered as the loading is increased. Limits are not directly reflected as sudden changes on the loading margin.
- Once the loading margin is computed, it is easy and quick to compute its sensitivity with respect to any power system parameters or controls [14, 25, 26, 27].
- The loading margin accounts for the pattern of load increase. This can be viewed as a disadvantage as well; see below.

It is important to emphasize the fact that device limits are not directly reflected as changes on the loading margin profile, since these limits are already accounted for in the computations. Hence, as opposed to other indices, estimates of distance to collapse based on this index are exact. On the other hand, operators cannot

use changes on the index to directly evaluate the relative effect of device limits on the loading margin and, thus, devise some early corrective measures. Nevertheless, using the techniques described in [14, 25, 26, 27], the effect of different limits on the loadability margin can be readily evaluated with some additional computations.

The disadvantages of the loading margin as a voltage collapse index are:

- The loading margin requires computation at points away from the current operating point and, hence, are computationally more expensive than indices only using information at the operating point. The computational costs are the most serious disadvantage of the loading margin.

- The loading margin requires the assumption of a direction of load increase. Sometimes this information is not readily available.

There are two ways to alleviate the dependence of the loading margin on an assumed pattern of load increase. One way is to compute the sensitivity of the loading margin to the assumed pattern of load increase or to recompute the loading margin with different patterns of load increase. Another way is to make further computations to find a worst case pattern of load increase giving a minimum value of loading margin [28, 29]; a technique to estimate this minimum margin is discussed in Section 4.3.6.

The loading margin can in principle be calculated by starting at the current operating point, making small increments in loading and recomputing load flows at each increment until the nose of the PV curve is reached. The loading margin is then the total increment in loading. In practice, elaborations of this idea, such as continuation or direct methods, are used; these computational methods are explained in the following sections.

4.3.5.1 Direct Methods

Direct methods, also known in power system applications as Point of Collapse methods [30], were originally developed to compute singular bifurcation points of nonlinear systems [31]. The method consist in solving equations

$$\begin{aligned} F(z,\lambda) &= 0 \\ D_z F(z,\lambda)^T w &= 0 \\ ||w||_\infty &= 1 \end{aligned} \tag{4.19}$$

for z, λ, and w, to directly obtain the collapse point (z_*, λ_*) [32, 33, 34]. Nonsingular equations (4.19) correspond to the system steady state equations, the singularity conditions at the collapse point, and the nonzero left eigenvector requirement, for any system model, which is an advantage of this method as it is not based on a particular model. Other equations with the right eigenvector and/or different nonzero eigenvector requirement may be used; however, equation (4.19) presents the best numerical characteristics for large systems [33].

This method allows to directly determine the loading margin to collapse $\Delta\lambda = \lambda_* - \lambda$ at any operating point defined by λ. For the sample system, this loading margin has a completely linear and smooth behavior as depicted in Figure 4.3-11, which

allows to make very accurate predictions of proximity to collapse. The linear profile is independent of limits on control variables or system size, since for a given operating conditions and load direction, the value of λ_* can be directly computed from (4.19) with all control variables and related limits considered. Any major contingencies, such as generator or line tripping, are depicted as a reduction in the available system power, which has a clear meaning in an operating environment. Thus, this index allows for a simple definition of the threshold value that would trigger corrective measures. Observe, however, that the effect of devices hitting limits as the system approaches collapse are not directly reflected as changes on the index profile; to determine the importance of the different control limits on the loading margin, additional computations must be carried out [14, 25].

An obvious disadvantage with this technique is the high computational cost, as the number of equations increases two fold with respect to the system steady state equations, requiring good initial conditions, particularly for w. The latter creates convergence problems when the system is far from the collapse point, since the system eigenvalues and eigenvectors change significantly as the system approaches collapse; this is especially true when device limits are encountered along the solution path.

Another disadvantage of the direct method is that it can only determine a collapse point associated with system singularities (bifurcations). Voltage collapses related to control limits, particularly generators reaching reactive power limits [33, 35, 36], cannot be detected using this technique, yielding wrong answers in this case [33].

Similar equations to (4.19) may be obtained by representing the problem as an optimization problem, as initially proposed in [37]. Thus, the collapse problem may be stated as

$$\begin{array}{ll} \text{Min.} & \lambda \\ \text{s.t.} & F(z,\lambda) = 0 \end{array} \tag{4.20}$$

This problem may be solved using the Lagrangian

$$\mathcal{L}(z,\lambda,w) = \lambda + w^T * F(z,\lambda)$$

where w corresponds to the Lagrangian multipliers. Hence, necessary conditions to obtain a solution of (4.20)) are

$$\begin{aligned} D_w\mathcal{L} &= F(z,\lambda) = 0 \\ D_z\mathcal{L} &= D_z F(z,\lambda)^T w = 0 \\ \frac{\partial \mathcal{L}}{\partial \lambda} &= w^T \frac{\partial F}{\partial \lambda}(z,\lambda) + 1 = 0 \end{aligned} \tag{4.21}$$

These equations are basically the same as (4.19), with the exception of the third one, which is another way of guaranteeing a nonzero w (it also corresponds to one of the transversality conditions of a saddle-node bifurcation [3]).

Stating the collapse problem as an optimization problem allows for the use of several well known optimization techniques to compute the collapse point, as discussed in [38]. One particular technique that is especially appealing due to its limit handling capabilities is Interior Point Methods, which has been successfully applied to the computation of the collapse point [39, 40].

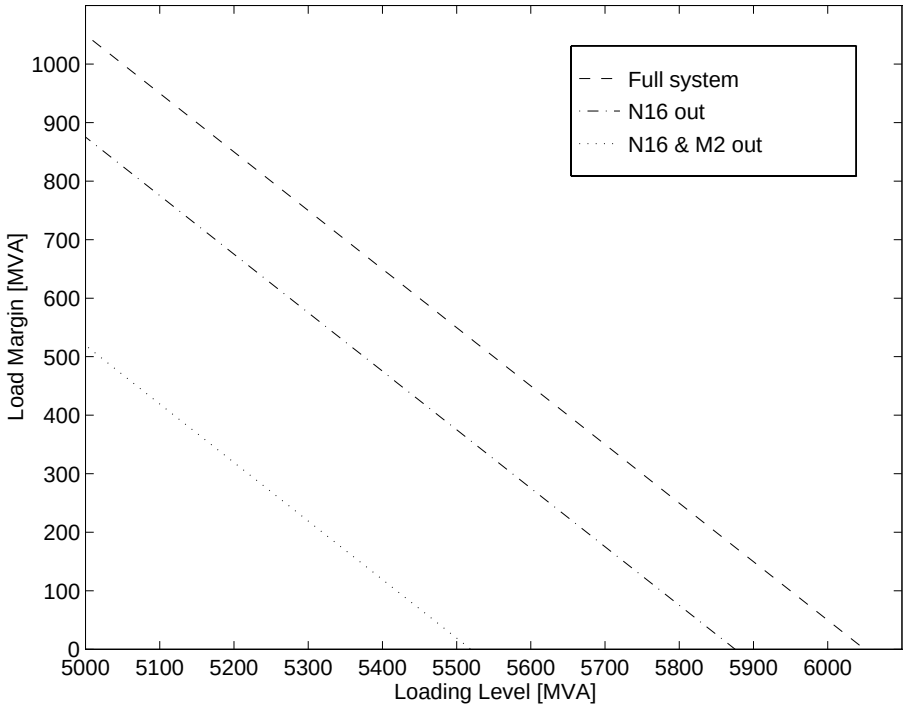

(a)

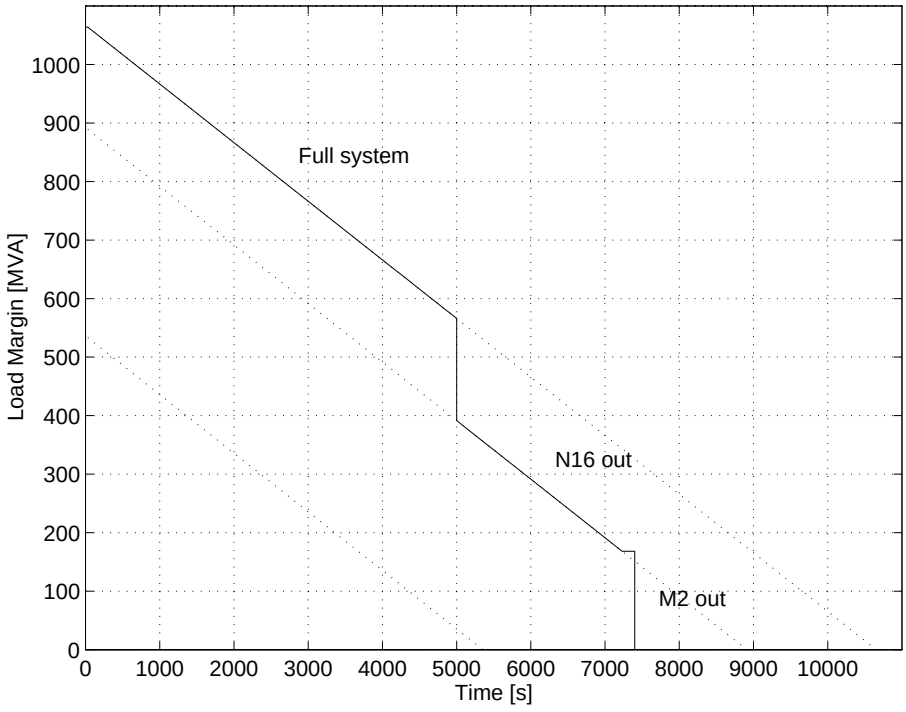

(b)

Figure 4.3-11. (a) Loading margin and its (b) time profile.

4.3.5.2 Continuation Method (Voltage Profiles)

Voltages profiles, also known as QV, PV or nose curves, are currently in use at some utilities for determining proximity to collapse, so that operators can take timely preventive measures to avoid losing the system [41]. Figures 4.3-12 depicts voltage profiles for one of the test system critical buses (N102) and another bus (N8); observe that voltage changes are not a good way of detecting proximity to collapse or detecting the effect of limits or contingencies on system loadability [1, 2], particularly in highly compensated buses or buses that do not belong to the critical area. The latter is clearly shown in Figure 4.3-13, where the time profile of the voltage magnitude in a system bus belonging to the critical area is shown; notice that the voltages remain very much unaffected by the system contingencies. The idea is then to use successive power flow solutions or continuation methods to fully compute the voltage profiles up to the collapse point (the maximum loading point in Figures 4.3-12) to determine the loading margin. Thus, this technique is really used as an alternative to the direct method, as well as for obtaining additional information regarding the voltage behavior in the system buses. The problem with this method is that, although reliable and very informative, its computationally expensive, especially in large systems with multiple limits [33].

Continuation methods overcome certain difficulties of successive power flow solutions methods, as they are not based on a particular system model, and allow the user to trace the complete voltage profile by automatically changing the value of λ, without having to worry about singularities of the system equations. The strategy used in these methods is illustrated in Figure 4.3-14, where a known equilibrium point (z_1, λ_1) is used to compute the direction vector Δz_1 and a change $\Delta\lambda_1$ of the system parameter. This first step is known as the predictor, since it generates an initial guess $(z_1 + \Delta z_1, \lambda_1 + \Delta\lambda_1)$, which is then used in the corrector step to compute a new equilibrium point (z_2, λ_2) on the system profile (bifurcation diagram or manifold). Since the Jacobian $D_z F|_*$ is singular at the collapse (bifurcation) point, a parameterization is sometimes needed in the predictor and/or corrector steps, depending on the techniques used, to guarantee a well behaved numerical solution of the related equations. A detailed description of these techniques follows.

A. Predictor and Parameterization One way of calculating the direction vector Δz_1 at an equilibrium point (z_1, λ_1) on the system profile, is to compute the tangent vector to this trajectory at that point. Hence, since $F(z_1, \lambda_1) = 0$, then

$$\frac{\mathrm{d}F}{\mathrm{d}\lambda}(z_1, \lambda_1) = D_z F(z_1, \lambda_1) \left.\frac{\mathrm{d}z}{\mathrm{d}\lambda}\right|_1 + \left.\frac{\partial F}{\partial \lambda}\right|_1 = 0$$

$$\Rightarrow \quad D_z F|_1 \left.\frac{\mathrm{d}z}{\mathrm{d}\lambda}\right|_1 = - \left.\frac{\partial F}{\partial \lambda}\right|_1 \tag{4.22}$$

Thus, the direction vector and the parameter step come from the normalization of the tangent vector, i.e.,

$$\Delta\lambda_1 \quad = \quad \frac{k}{\| \, \mathrm{d}z/\mathrm{d}\lambda|_1 \, \|} \tag{4.23}$$

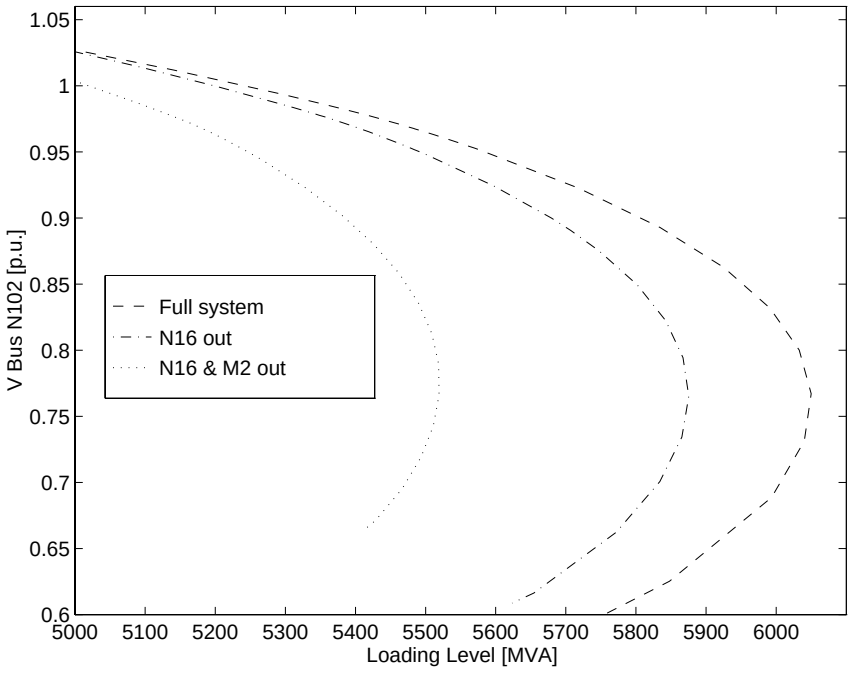

(a)

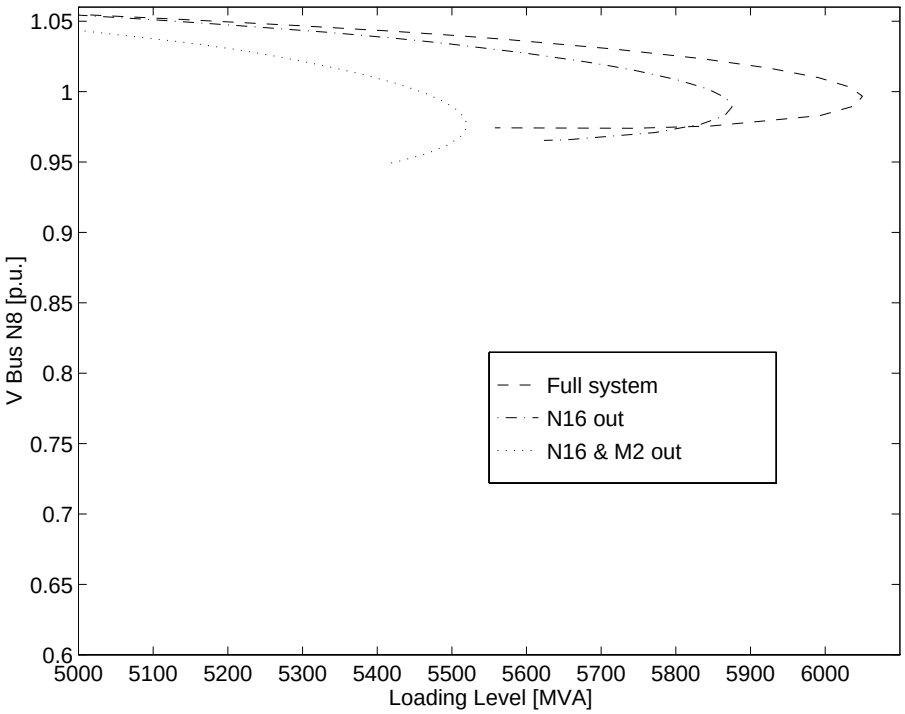

(b)

Figure 4.3-12. Voltage profiles for buses (a) N102 and (b) N8.

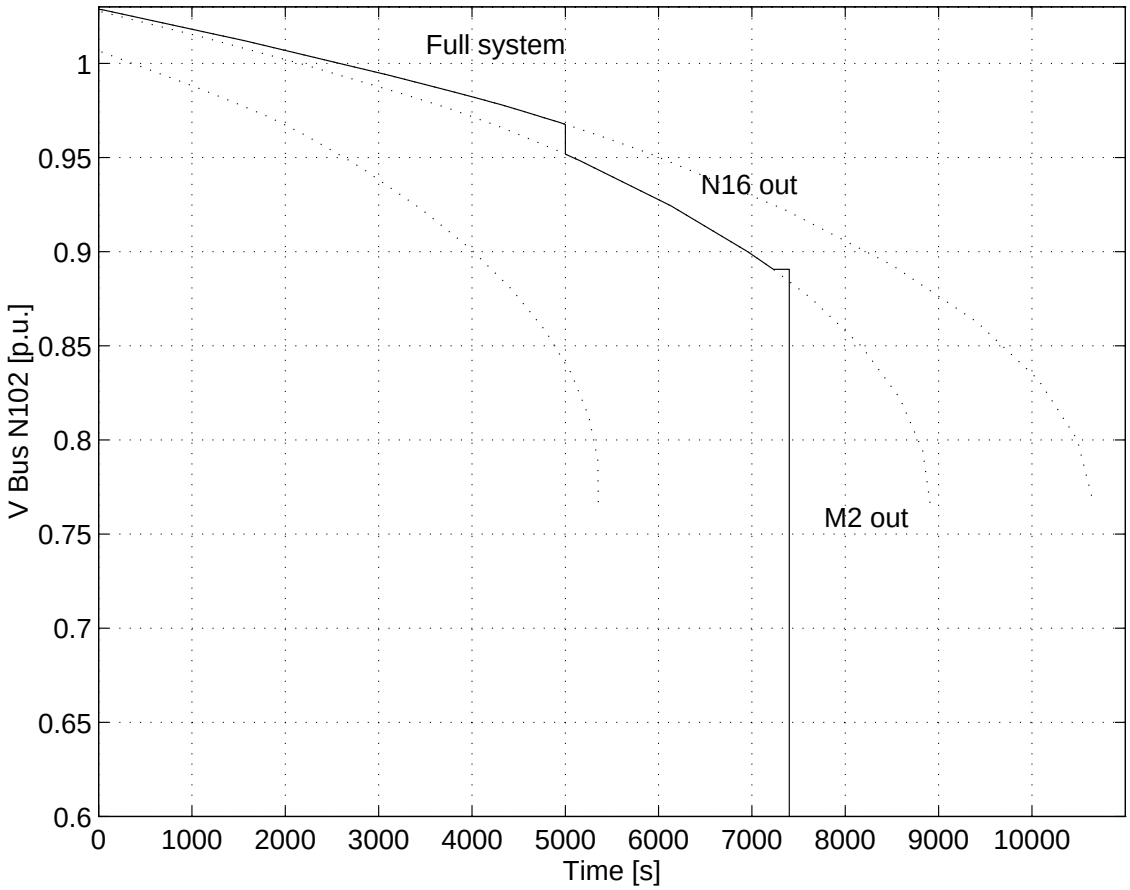

Figure 4.3-13. Voltage profiles on bus N102 versus time.

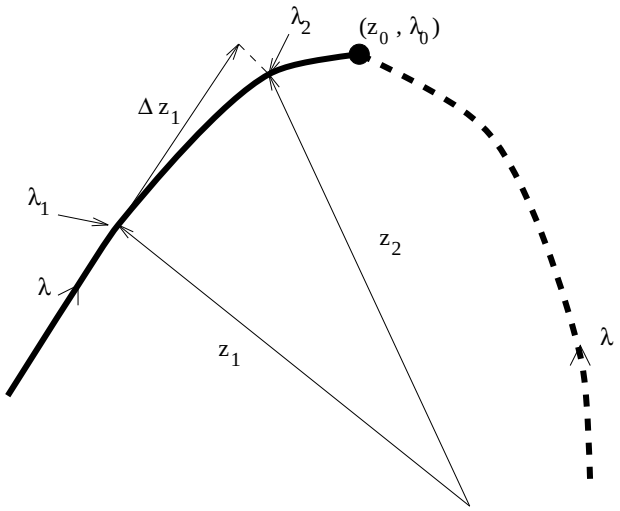

Figure 4.3-14. Continuation method.

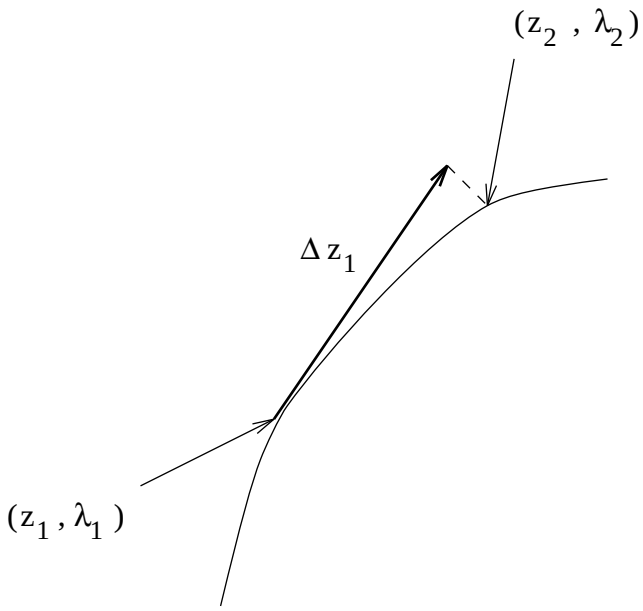

Figure 4.3-15. Standard tangent predictor.

$$\Delta z_1 \;=\; \Delta\lambda_1 \left.\frac{\mathrm{d}z}{\mathrm{d}\lambda}\right|_1$$

where k is a scalar positive constant that controls the size of the predictor step. The normalization in (4.23) results in the reduction of the step size as the system approaches the collapse point, since the magnitude of the tangent vector increases as the system gets closer to this point. If the step is too large, then the initial guess $(z_1 + \Delta z_1, \lambda_1 + \Delta\lambda_1)$ yields convergence problems in the corrector phase, whereas if the step is too small, the method takes too many steps to trace the bifurcation manifold. A technique to determine an "optimal" value of k was proposed in [42], considering the reactive power limits of the generators. Good results were reported in [33] for $k = 1$ in various system sizes, by using step cutting when limits or convergence problems are encountered. A technique to determine an adequate step size based on a tangent vector voltage stability index is proposed in [43, 44] and discussed in more detail in Section 4.3.10.

This predictor technique has the particular advantage of generating an approximation to the "zero" right-eigenvector at the collapse point, since the tangent vector smoothly converges to this eigenvector [3].

Computing the tangent vector in (4.22) does not represent a significant computational cost, since one can use the last factored Jacobian matrix $D_z F(z_1, \lambda_1)$. However, this method has difficulties when the equilibrium point is close to the collapse point, since the system Jacobian becomes ill-conditioned. To avoid this problem, parameterization techniques may be used [31]. A relatively simple technique successfully applied in [33, 42, 45, 46] is local parameterization, which consists in interchanging the parameter λ with the system variable $z_i \in z$ that has the largest normalized entry in the tangent vector, so that λ becomes part of the equations variables, whereas z_i

becomes the new parameter p, i.e.,

$$p = \max_i \left\{ \left| \frac{\Delta z_i}{z_i} \right|, \left| \frac{\Delta \lambda}{\lambda} \right| \right\} \tag{4.24}$$

Nevertheless, when step cutting and perpendicular intersection correctors are used, this local parameterization is not needed in practice [33, 45]; due to the highly nonlinear behavior of the Jacobian eigenvalues, one must be rather close to the collapse point in order to have an ill-conditioned Jacobian matrix.

Another type of predictor with parameterization used to take the system around the singularity of the collapse point is the arclength method [31, 47]. This technique is based on the idea that the system variables and parameter at the equilibrium points can be represented as a function of the arclength s of the system profile, i.e., for $F(z_1(s), \lambda_1(s)) = 0$,

$$D_z F|_1 \left. \frac{\mathrm{d}z}{\mathrm{d}s} \right|_1 + \left. \frac{\partial F}{\partial \lambda} \right|_1 \left. \frac{\mathrm{d}\lambda}{\mathrm{d}s} \right|_1 = 0 \tag{4.25}$$

where the arclength s must satisfy the condition

$$\left. \frac{\mathrm{d}z}{\mathrm{d}s} \right|_1^T \left. \frac{\mathrm{d}z}{\mathrm{d}s} \right|_1 + \left. \frac{\mathrm{d}\lambda}{\mathrm{d}s} \right|_1^2 = 1 \tag{4.26}$$

Therefore, by approximating $\Delta z \approx \mathrm{d}z$, $\Delta \lambda \approx \mathrm{d}\lambda$, and $k = \Delta s \approx \mathrm{d}s$, equations (4.25) and (4.26) become

$$\begin{aligned} D_z F|_1 \Delta z_1 + \left. \frac{\partial F}{\partial \lambda} \right|_1 \Delta \lambda_1 &= 0 \\ \Delta z_1^T \Delta z_1 + \Delta \lambda_1^2 &= k \end{aligned} \tag{4.27}$$

where k is a scalar positive constant that defines the length of the arc, and consequently the size of the predictor step. Equations (4.27) can be used to calculate the predictor step instead of equations (4.22) and (4.23), with a guaranteed nonsingular Jacobian at the collapse point.

Finally, a simpler predictor method that does not require parameterization is the secant method, which was used in power systems collapse analysis in [47]. This technique consists in approximating the tangent vector $\mathrm{d}z/\mathrm{d}\lambda$ using two or more previously determined points on the system profile. Thus, given two points (z_{1_a}, λ_{1_a}) and (z_{1_b}, λ_{1_b}) on the profile, such that $\lambda_{1_b} > \lambda_{1_a}$,

$$\left. \frac{\mathrm{d}z}{\mathrm{d}\lambda} \right|_1 \approx z_{1_b} - z_{1_a}$$

Equations (4.23) can then be used to calculate the direction vector and the parameter step. Notice that the closer these two points are, within reasonable numerical tolerances, the better the approximation of the tangent vector; however, more points have to be computed, taking longer to trace the desired diagram. On the other hand, points too far apart generate inadequate approximations of $\mathrm{d}z/\mathrm{d}\lambda$, yielding initial

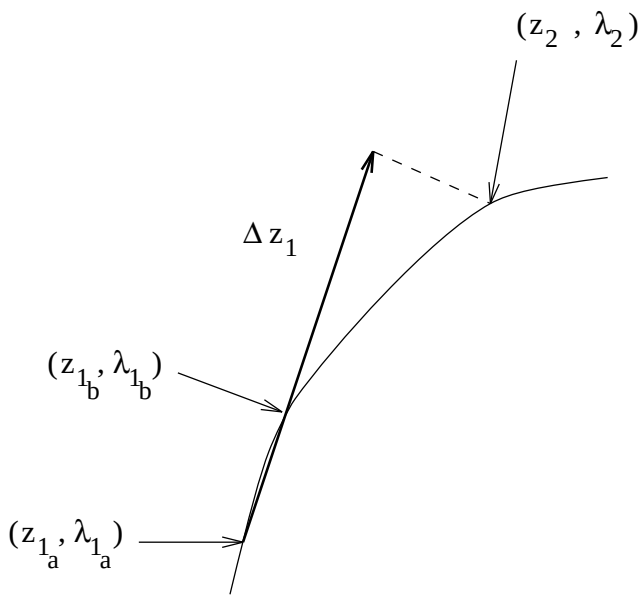

Figure 4.3-16. Secant predictor.

guesses that lead to convergence difficulties during the corrector step. Using more points on the system profile to better predict its curvature, requires greater computational resources, but can be used as an alternative procedure to approximate the tangent vector when the diagram changes direction rapidly, particularly when control limits are encountered. Hence, depending on the curvature of the profile, the secant method presents advantages and disadvantages with respect to the two predictors previously described. A mixed approach is proposed in [31, 47], using the secant predictor when the tangent vector changes slowly on the "flat" part of the diagram, to then switch to tangent vector or arclength predictors when the profile presents larger curvatures. Figure 4.3-16 illustrates the secant predictor procedure, and Figure 4.3-17 depicts the problems with this technique when sharp changes in the system profile are encountered.

B. Corrector Once an initial guess $(z_1 + \Delta z_1, \lambda_1 + \Delta\lambda_1)$ is determined in the predictor step, with or without parameterization, the actual point (z_2, λ_2) on the system profile must be calculated by solving the following set of equations for z and λ [31]:

$$\begin{aligned} F(z,\lambda) &= 0 \\ \rho(z,\lambda) &= 0 \end{aligned} \tag{4.28}$$

The first vector equation in (4.28) corresponds to the steady-state system equations, which have a singular Jacobian $D_z F|_*$ at the collapse point (z_*, λ_*). The second scalar equation represents a phase condition that guarantees non singularity of the corrector

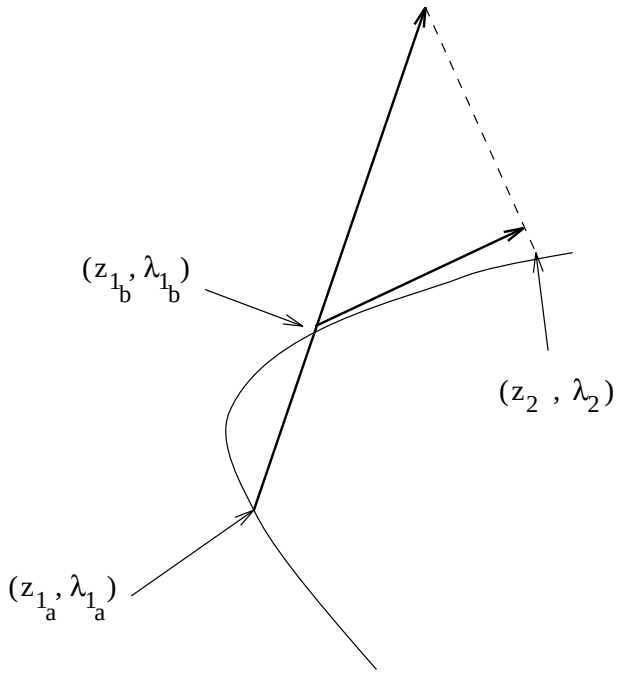

Figure 4.3-17. Secant predictor convergence problems when "sharp corners" are encountered.

equations Jacobian

$$\begin{bmatrix} D_z F & \dfrac{\partial F}{\partial \lambda} \\ D_z \rho & \dfrac{\partial \rho}{\partial \lambda} \end{bmatrix}_{(n+1)\times(n+1)}$$

at all points on the system profile.

Two different phase conditions $\rho(\cdot)$ have been successfully used in collapse studies of power systems. The first condition consists in defining a perpendicular vector to Δz_1, which starts at $(z_1 + \Delta z_1, \lambda_1 + \Delta\lambda_1)$ and intersects the bifurcation manifold at (z, λ), as depicted in Figure 4.3-18. Thus,

$$\rho(z, \lambda) = \Delta z_1^T (z - z_1 - \Delta z_1) + \Delta\lambda_1(\lambda - \lambda_1 - \Delta\lambda_1) \tag{4.29}$$

This was introduced in [48] and successfully applied to various power systems in [33, 45]. This condition does not require any kind of parameterization to guarantee non singularity of equations (4.28) for all system equilibria [3, 49].

A simpler phase condition is used in [46, 47, 50], based on the local parameterization of the system around the collapse point. In this case, a local parameter p (λ or $z_i \in z$), is set to a constant value, i.e.,

$$\rho(z, \lambda) = p - p_1 - \Delta p_1$$

The parameter p is chosen based on parameterization (4.24), guaranteeing a non-singular Jacobian of equations (4.28) [31]. This technique is illustrated in Figure 4.3-19.

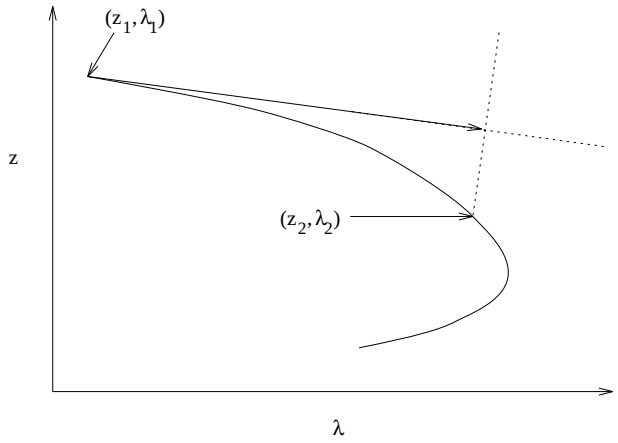

Figure 4.3-18. Perpendicular intersection corrector.

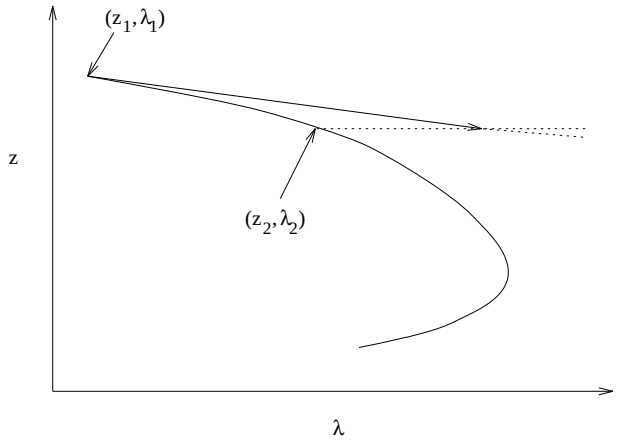

Figure 4.3-19. Fixed parameter corrector.

Of these two corrector techniques, the perpendicular intersection has the advantage of not requiring parameterization. However, it introduces an almost full row in the Jacobian matrix, which must be taken into consideration during the factorization process to avoid sparsity degradation.

It is interesting to highlight the fact that, by restating the collapse problem as an optimization problem as in (4.20), continuation methods can be readily demonstrated to be equivalent to generalized reduced-gradient (GRG) methods [51]. The GRG method is a well-known nonlinear optimization technique [52, 53], that consists in following a solution path using predictor-corrector steps in an "optimal" direction on a given constraint manifold, based on tangent information at a known point on this manifold.

4.3.6 Loading Margin by Multiple Power Flow Solutions

This method calculates an approximation to the closest loadability limit by using a pair of multiple power flow solutions [21]. The closest loadability limit approximated by this method is defined, for a given operating point, as the point on the loadability boundary within the minimum Euclidean distance of the node injection changes. Obtainable information includes load power margins of the total and individual nodes, weak spots of the system, critical voltage profiles, etc. Such information is basically the same as that obtained by direct methods, except that the target critical point is different.

This method utilizes some features of voltage vectors a and b, which are obtained from a pair of multiple power flow solutions, as defined in Section 4.3.4 in equation (4.16). Hence, this technique is based on a particular power flow model of the system. The node injection vector $y(a)$ in (4.17) approximates the closest loadability limit if: (i) the operating point y_s is close to the loadability boundary and (ii) the load flow Jacobian is regarded as symmetrical. Hence, this method utilizes $y(a) = y_s - \tilde{y}(b)$ as a first step estimate, where $\tilde{y}(b)$ is regarded as the loadability margin from y_s to the collapse point $y(a)$. Based on these definitions, an approximation to the closest loadability limit, as proposed in [21], is defined as follows:

$$y_{CLL} = y_s + \alpha \|M\tilde{y}(b)\| \frac{Mw}{\|Mw\|} \tag{4.30}$$

where w is the left eigenvector of the power flow Jacobian at $x = a$, i.e., $J(a)^T\, w = 0$, and is perpendicular to the loadability boundary [28]; and the matrix M is defined as

$$M = diag(\gamma_1 \ldots \gamma_n)$$

$$\gamma_i = \begin{cases} 1 & \text{for P or Q injection for load or generator} \\ 0 & \text{for generator voltage or for junction node} \end{cases}$$

The constant α can be associated with the "curvature" of the loadability boundary at $y(a)$; thus, for $\alpha = 1$, the boundary is assumed to be a sphere, whereas for

$$\alpha = \cos\theta = \frac{-[M\ \tilde{y}(b)]^T\ Mw}{\| - M\tilde{y}(b)\| \|Mw\|} \tag{4.31}$$

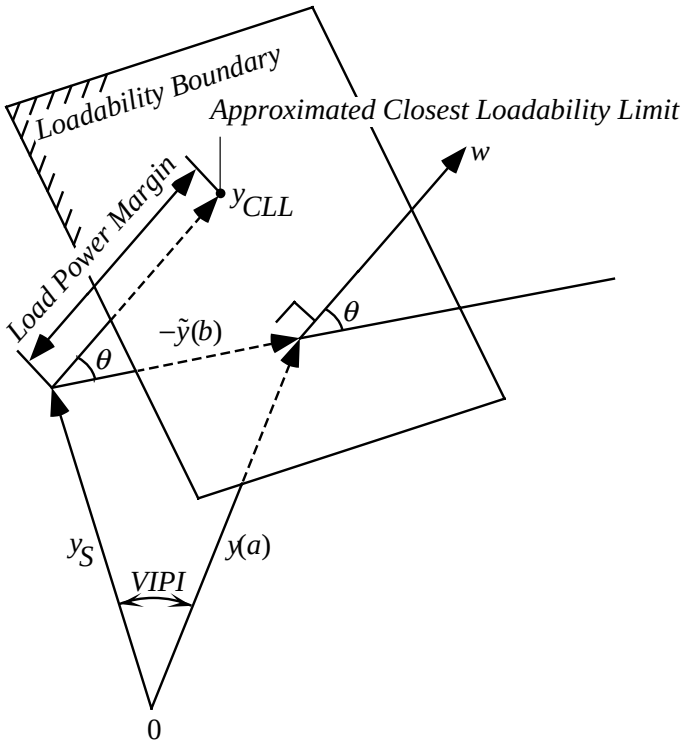

Figure 4.3-20. Approximated Closest Loadability Limit.

the boundary is assumed to be a plane. The limit values $\cos\theta \leq \alpha < 1$ provide the upper and lower bounds of the load power margin y_{CLL} in (4.30). These concepts are depicted in Figure 4.3-20. Observe that for $\theta = 0$, $y(a)$ corresponds to the closest point; therefore, θ may be used as an indicator to estimate the precision of $y(a)$ and y_{CLL}.

The procedure to compute y_{CLL} is as follows:

1. Calculate high voltage solution x_1 and low voltage solution x_2 using a power flow program, and then compute a, b, $y(a)$ and $\tilde{y}(b)$. The VIPI index may be computed optionally at this stage. Notice that the computation of x_2 is a nontrivial problem, and requires some special techniques, as discussed in Section 4.3.4.

2. Solve $J(a)^T\, w = 0$ for w, which is the normal vector to the loadability boundary at $x = a$.

3. Compute $\cos\theta$ from (4.31), and then choose a value of α so that $\cos\theta \leq \alpha < 1$. In [21], a value of $\alpha = 0.95\cos\theta$ is suggested, based on some empirical results.

Figures 4.3-21 and 4.3-22 depict the application of this index to the sample system. The upper and lower bounds in Figure 4.3-21 are the plots for $\alpha = 1$ and $\alpha = 0.95\cos\theta$, respectively, indicating that the actual closest voltage collapse point is expected to exist in the region between the bounds. Various numerical tests have

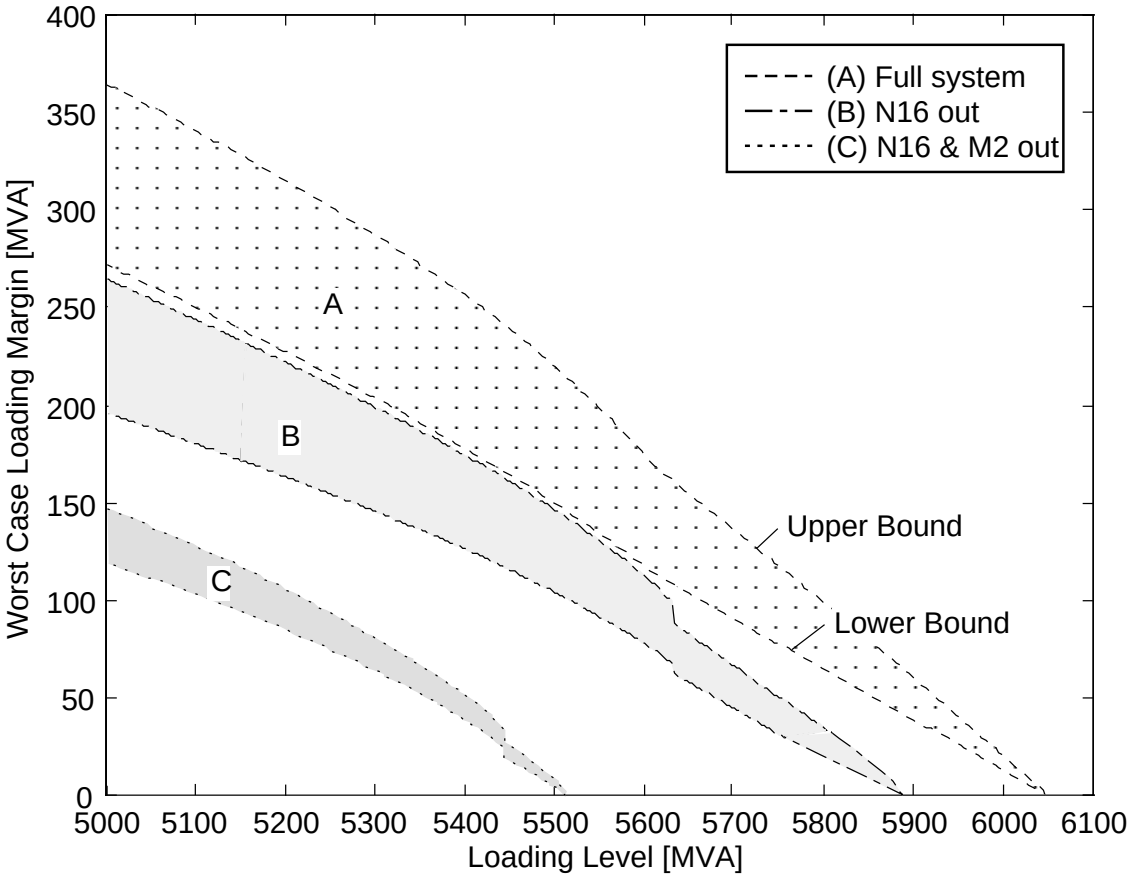

Figure 4.3-21. Worst case loading margin by multiple power flow solutions.

shown that the exact collapse point normally exists quite near to the lower bound; hence, Figure 4.3-22 depicts the lower bound only.

The problems with this technique are:

- As in the case of VIPI index, some care is required in the identification of the target solution x_2.
- In the presence of the singularities of the low voltage solutions, rapid changes in the index appear near these singularities (see Section 4.3.4). Notice that these sudden changes are not large, as shown in Figures 4.3-21 and 4.3-22.
- The method estimates the closest voltage collapse point under the condition that the node specification type, PQ or PV, is unchanged until the system reaches the loadability limit. Therefore, it does not take into account system control limits. However, this problem can be minimized by treating all PV buses as PQ buses during the computation of the low voltage solutions (see Section 4.3.4). In this case, conservative results will be obtained as compared to the actual margin.

Advantages of the index are:

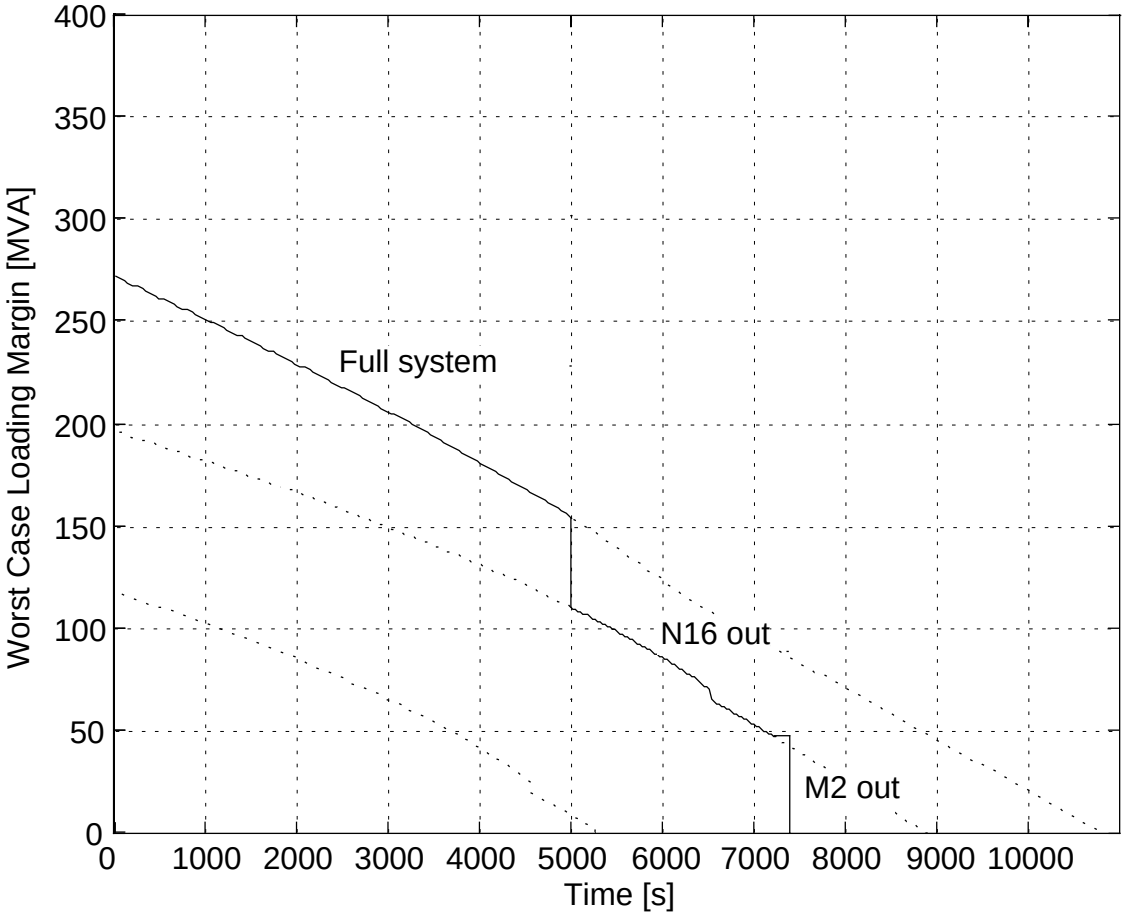

Figure 4.3-22. Worst case loading margin by multiple power flow solutions versus time.

- This method overcomes a weakness of the VIPI index as the original information measured in degrees has been transformed into load power margins measured in MVA/MW/MVAr.

- The closest loadability limit is a unique point, independent of the assumption of a direction of load increase. For example, a comparison of the loading margin results shown in Figures 4.3-21 and 4.3-22 with those depicted in Figure 4.3-11 indicates that, for the worst load pattern given by the vector Mw, only one third of the total load power increase is required to make the system collapse.

- Although the closest loadability limit is in general an effective index for monitoring and controlling voltage stability, its exact computation is time consuming when using the existing methods proposed in [28]. On the other hand, the computation time of (4.30) is quite fast, approximately equivalent to that of one iteration of the power flow (excluding the computation of the power flow solution pair).

- The approximation errors are quite small, normally no more than a few percentage points from light load to heavy load conditions.

4.3.7 Local Load Margins

Indices based on physical quantities are desirable and practical. The index proposed for a power flow system model in [54] satisfies this requirement, and is based on the distance from the initial load (P_{o_i} in MW) to the nose of the PV curve (P_{max_i} in MW) when the load at node i is increased at a fixed power factor, i.e.,

$$P_{Lmg_i} = \frac{P_{max_i} - P_{o_i}}{P_{max_i}} \tag{4.32}$$

The load margin P_{Lmg_i}, which has a value between 1 and 0 (at the collapse point), assumes that the loads at other nodes remain constant, which is somewhat different to the approach previously used in this report to compute load margins. However, (4.32) allows for the computation of a voltage stability margin for each load point. As the voltage may be on a lower solution domain depending on the system conditions, it is convenient to present the value P_{Lmg_i} as a negative number when the system voltage is in this particular state.

As P_{Lmg_i} is defined with respect to a specific node, its computation is relatively easy. However, a voltage stability margin should be evaluated for the entire power system; thus, the index P_{Lmg_i} should be computed for all load nodes, i.e., one needs to calculate as many P_{max}'s as number of load nodes in the system, which is impractical. Therefore, the following method is used that efficiently estimate the P_{max}'s: When a power system model is given, such as that shown in Figure 4.3-23(a), an equivalent system for each node i is formulated, as depicted in Figure 4.3-23(b). Here, "equivalent system" means that the load flow values for both systems are equal. This is the same as determining the phasor values $\tilde{V}_o$, $\tilde{S}_o$, and $\tilde{Y}_o$ of the equivalent network,

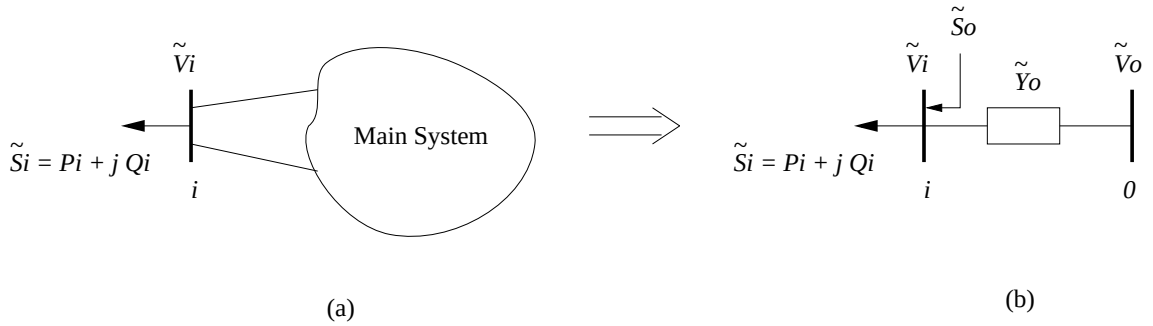

Figure 4.3-23. System reduction: (a) original system; (b) reduced system.

so that the power flow injection $\tilde{S}_i$ and the voltage sensitivity $\partial\tilde{S}_i/\partial\tilde{V}_i$ are equal for both systems.

The voltage sensitivities can be derived from the Jacobian matrix elements of the original network. Thus, the linearized power flow equations in rectangular coordinates ($\tilde{V}_i = e_i + j\ f_i$) can be written as

$$\begin{bmatrix} \Delta e_1 \\ \Delta f_1 \\ \vdots \\ \Delta e_i \\ \Delta f_i \\ \vdots \end{bmatrix} = \underbrace{\begin{bmatrix} \ddots & & & & & & \\ & \ddots & & & & & \\ & & \ddots & & & & \\ & & & K_{11} & K_{12} & & \\ & & & K_{21} & K_{22} & & \\ & & & & & \ddots & \end{bmatrix}}_{K} \begin{bmatrix} \Delta P_1 \\ \Delta Q_1 \\ \vdots \\ \Delta P_i \\ \Delta Q_i \\ \vdots \end{bmatrix} \tag{4.33}$$

where the coefficient matrix K corresponds to the inverse of the Jacobian matrix. Since by definition ΔP_k and ΔQ_k are zero except for $k = i$ in (4.33), the sensitivity $\partial\tilde{S}_i/\partial\tilde{V}_i$ can be determine from

$$\begin{bmatrix} \Delta P_i \\ \Delta Q_i \end{bmatrix} = \begin{bmatrix} K_{11} & K_{12} \\ K_{21} & K_{22} \end{bmatrix}^{-1} \begin{bmatrix} \Delta e_i \\ \Delta f_i \end{bmatrix} \tag{4.34}$$

The phasor values $\tilde{V}_o$, $\tilde{S}_o$, and $\tilde{Y}_o$ of the equivalent network can be determined with the help of the K elements in (4.34).

In order to obtain the block diagonal elements of matrix K on equation (4.33), which is a completely dense matrix, at the least computational costs, the method proposed in [55] can be used. Using this technique, the diagonal elements can be readily computed at approximately the price of one LU factorization of the original Jacobian matrix.

The value of P_{max_i} can then be estimated as follows: Suppose that the load at node i increases by a factor h (typically $h = 1 + \lambda$) of the base load $\tilde{S}_{i_o}$; this produces a phasor voltage change so that $\tilde{V}_i = \tilde{x}\ \tilde{V}_0$. This can be represented by equation

$$\begin{aligned} h\ \tilde{S}_{i_o} &= \tilde{V}_i\ \left[(\tilde{V}_0 - \tilde{V}_i)\ \tilde{Y}_0\right]^* + \tilde{S}_0 \\ &= \tilde{x}\ \tilde{V}_0\ \left[(1-\tilde{x})\tilde{V}_0\tilde{Y}_0\right]^* + \tilde{S}_0 \end{aligned} \tag{4.35}$$

Here, there are only two solutions for $\tilde{x}$, as the equivalent network consists of only one P-Q node; these solutions become one at the nose of the PV curve. Therefore, the problem of obtaining P_{max_i} can be treated as a problem of calculating h for a unique root of $\tilde{x}$ in equation (4.35). Thus, the P_{Lmg_i} index defined in (4.32) can be expressed in terms of h as follows:

$$\begin{aligned} P_{Lmg_i} &= \frac{h\,P_{o_i} - P_{o_i}}{h\,P_{o_i}} \\ &= \frac{h-1}{h} \end{aligned} \tag{4.36}$$

Equations (4.34) through (4.36) are used for all load nodes. Observe that in the computation of h limits are not considered, which leads to dicontinuous index profiles.

Figures 4.3-24 through 4.3-27 were obtained for the sample system using a simulation program from CRIEPI, Japan. This program allows to recreate a given voltage collapse scenario in the time domain by solving a load flow problem every time step, as defined by the user. The program allows to model different load change patterns, generation dispatch, AVRs, taps, compensators, etc., monitoring different system variables and computing P_{Lmg_i} at the same time for each time step. For the test system, a time step of 15 s was chosen for a total simulation time of 150 min (9000 s). All loads were treated as constant impedances with internal taps (no limits) to avoid load flow convergence problems; the internal taps change every time step to keep the load at a given nominal power level, so that the loads can be viewed as constant power loads on the long time range. Loads are assumed to trip off when the corresponding bus voltage magnitudes reach 0.1 p.u.

Figure 4.3-24 depicts the voltage magnitude at one of the main load buses (N207) versus the net load power change at that bus, for the full system and for the system without generators N16 and M2, showing a reduction on the maximum local loading P_{max_i} of about 50 MW. Figure 4.3-25 shows the time profiles of the voltage magnitudes at three main load buses (N201, N204 and N207), as well as the power demand at one of those loads (N201), for the given voltage collapse scenario; observe that the load demand steadily increases by 30 % in two hours (120 min or 7200 s), and that, after tripping generator M2 off at 7400 s (123.3 min), all bus voltages and corresponding power demands collapse with a fall rate defined by the rate of change of the internal ULTCs in the loads. Figure 4.3-26 shows the time profiles of the local load margins P_{Lmg_i} for the same three load buses (N201, N204 and N207), with the margin becoming negative (entering unstable region) after the tripping of generator M2; notice the smooth, quasi-linear profile of the margin for these buses, which is not always the case, allowing for somewhat adequate predictions of proximity to collapse in this case. Finally, Figure 4.3-27 illustrates the use of load shedding as a possible solution to the collapse problem depicted in the previous figures; in this case, the load at bus N207 (bus with smallest value of P_{Lmg_i}) is tripped off at the same time as generator M2, avoiding the collapse of the system, as illustrated by the voltage and local index time profiles.

In [54], the local loading margin index P_{Lmg_i} is applied to a detailed system model with a particular load representation that simulates constant power behavior

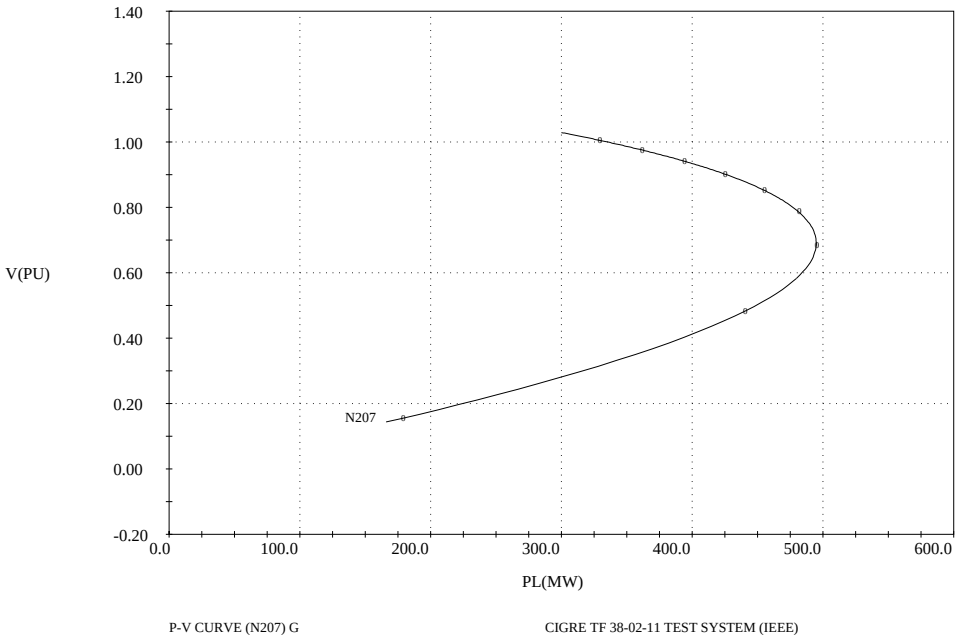

(a)

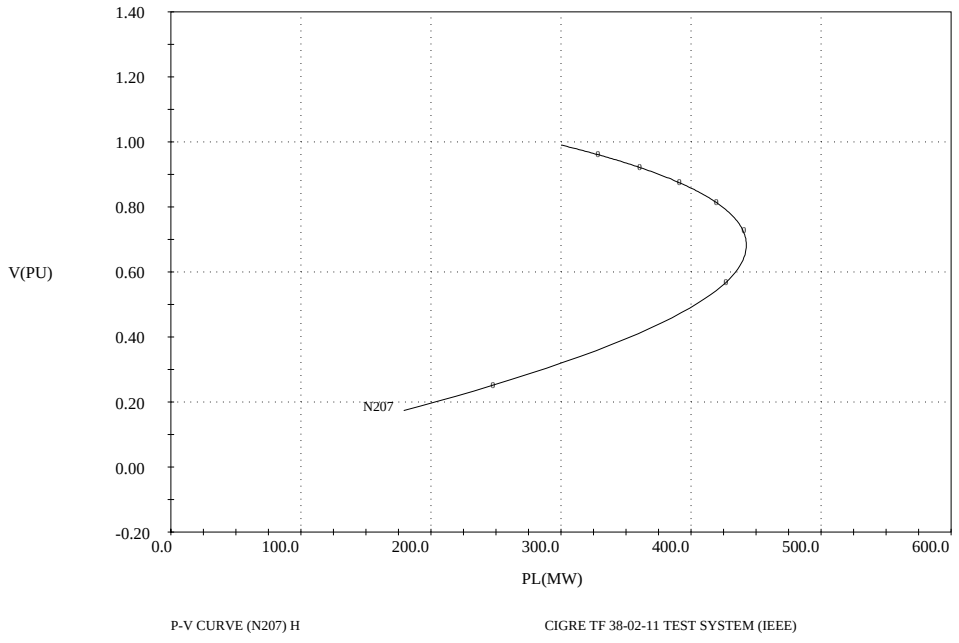

(b)

Figure 4.3-24. Local PV curves at load bus N207 for (a) full system and (b) system with both N16 and M2 tripped off.

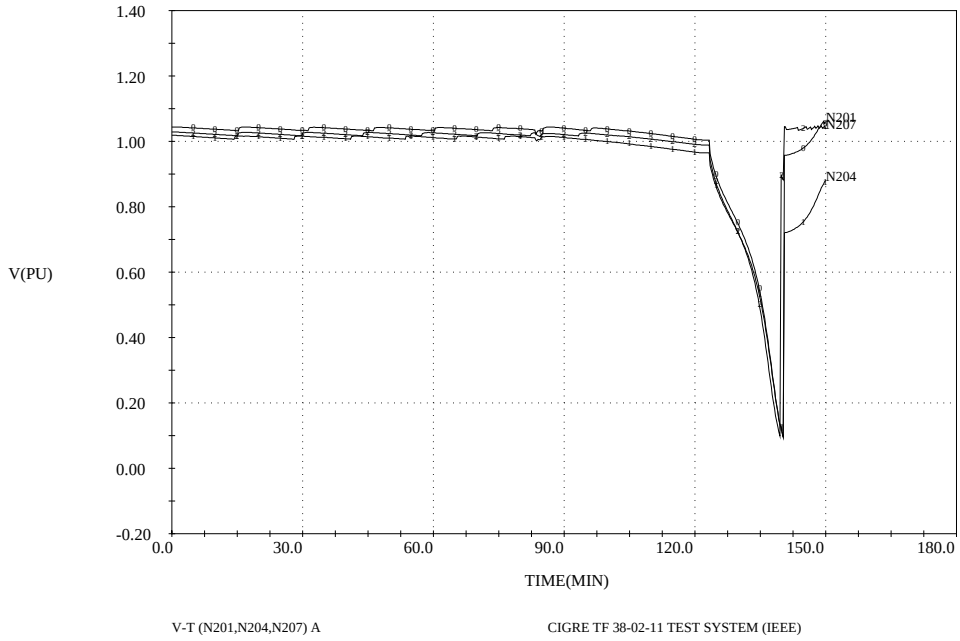

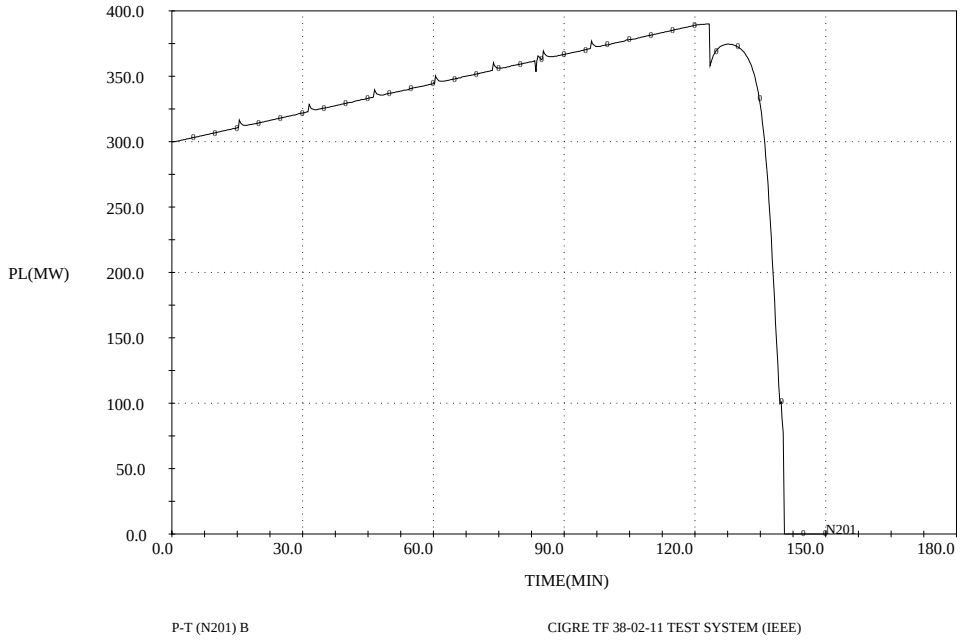

Figure 4.3-25. Voltage time profiles for load buses N201, N204 and N207, and active power demand time profile at load bus N201 for given collapse scenario. Loads are tripped off at a 0.1 p.u. voltage value, after voltage collapses due to M2 tripping off at 123.3 min. (7400 s) .

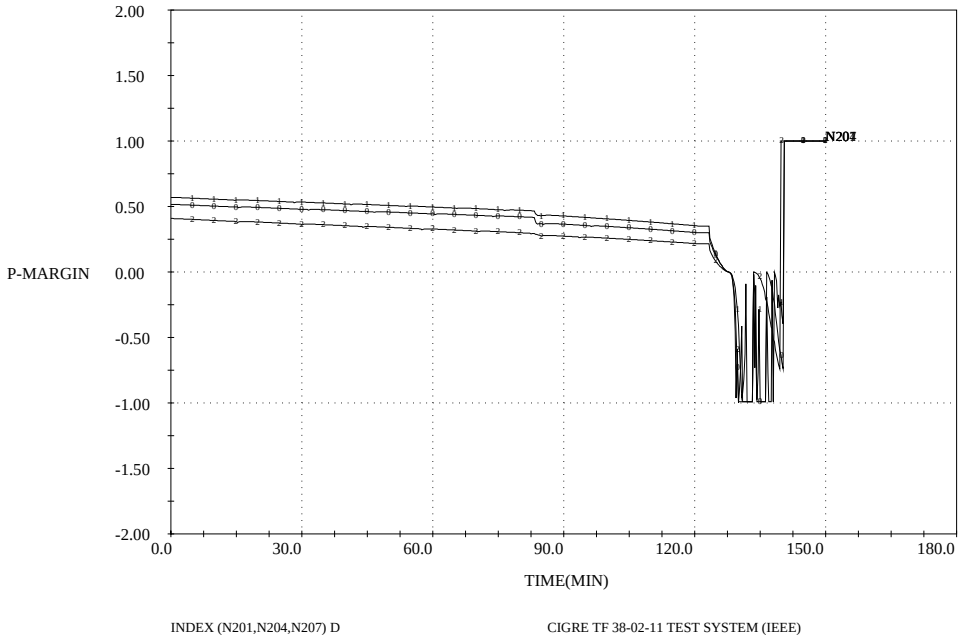

Figure 4.3-26. P_{Lmg_i} time profiles for load buses N201, N204 and N207 for given collapse scenario assuming load tripping at 0.1 p.u. voltage. The index becomes negative after M2 trips off, indicating a system transition into the unstable region.

in the long term, similar to the load model used for the test system in this document. However, this index is strongly based on a power flow model and, hence, more studies are required to determine whether it is suitable for systems with other types of load models. Computational costs could also become a significant issue in large systems, as these local margins have to be computed for all load buses to adequately predict proximity to collapse.

4.3.8 Test Functions

Another voltage stability index independent of the system model has been proposed in [56], based on a family of scalar test functions t_{lk} defined as follows [31]:

$$t_{lk} = |e_l^T J \, J_{lk}^{-1} e_l| \tag{4.37}$$

where J corresponds to the system Jacobian, e_l is the l^{th} unit vector, i.e., a vector with all zero entries except for an entry of 1 in row l, and

$$J_{lk} = (I - e_l e_l^T)J + e_l e_k^T \tag{4.38}$$

Here I represents the identity matrix. Equation (4.38) can be simply interpreted as an operation on the Jacobian matrix J where the l^{th} row is removed and replaced by the row e_k^T. Notice that for the load-flow equations at the voltage collapse point J is singular, but matrix J_{lk} is guaranteed nonsingular if the l^{th} and k^{th} are chosen so that they correspond to non zero entries in the "zero" eigenvectors v and w associated

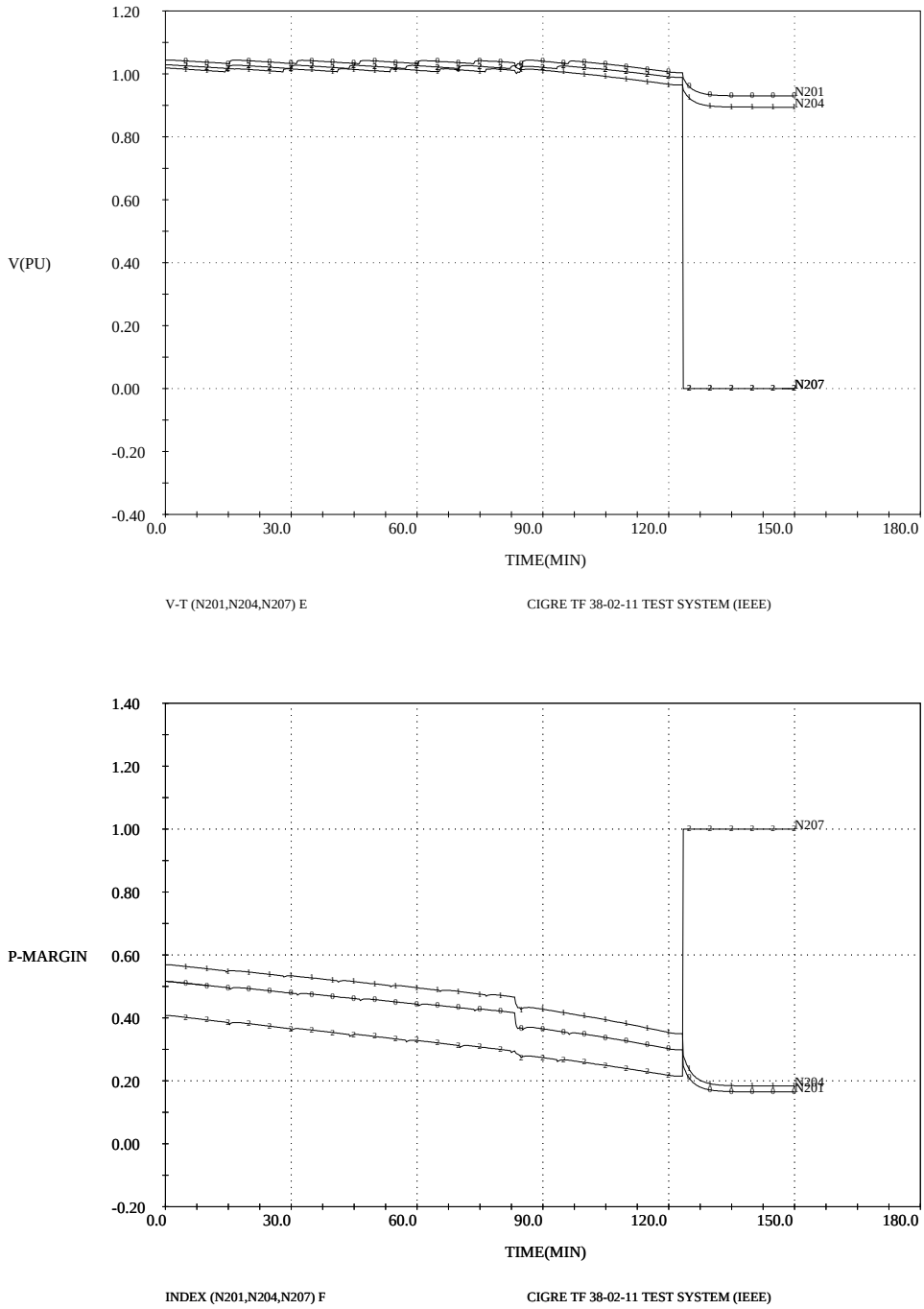

Figure 4.3-27. Voltage and P_{Lmg_i} index time profiles for load buses N201, N204 and N207 assuming that M2 and the load at bus N207 trip off at the same time (123.3 min. or 7400 s) .

with the zero eigenvalue of J. Furthermore, if $l = k = c$, where c corresponds to the maximum or critical entry in v, the test function becomes the "critical" test function

$$t_{cc} = |e_c^T J \, J_{cc}^{-1} e_c| \tag{4.39}$$

The computational procedure required to determine t_{lk} consists of the following steps:

1. Order and factor J_{lk}.
2. Apply a forward and backward substitution (repeat solution) to obtain $r = J_{lk}^{-1} e_l$.
3. Obtain $s = J^T e_l$, i.e., extract row l of J, and compute $t_{lk} = s^T r$ by a vector product.

These steps yield computational costs comparable to an initial iteration of a power flow solution process.

The Jacobian matrices and test function family are functions of the system variables and parameters, i.e., $J = J(z, \lambda)$, $J_{lk} = J_{lk}(z, \lambda)$, and $t_{lk} = t_{lk}(z, \lambda)$. As the parameter λ changes, approaching collapse, the system variables change, with the critical test function t_{cc} displaying a "quadratic" shape as a function of the load margin $\Delta\lambda$ [56, 11]. Thus,

$$\Delta\lambda \approx a \, t_{cc}^2 \tag{4.40}$$

where a is a scalar constant. This allows for the use of t_{cc} to determine system proximity to collapse; in general, test functions t_{ll} for buses that do not belong to the critical area do not display this quadratic shape. On the other hand, device limits alter the shape of t_{cc}, directly affecting the load margin estimates; however, this sharp changes also allow to evaluate the realtive effect of the different limits on the maximum loadability of the system, so that corrective actions can be devised early in the loading process. Although the general profile of t_{cc} is somewhat similar to the profiles previously depicted for the sensitivity factors in Section 4.3.1, the test function index is independent of system size, which is not the case for the sensitivity factors.

The test function profiles for two buses of the test system are depicted in Figure 4.3-28. This index shows a quadratic shape for the bus belonging to the critical area at the collapse point, whereas for the other bus the test function appears rather insensitive to parameter variations. Also, the effect of ULTC limits on system loadability can be observed in the critical bus test function profile, although the changes appear less significant than in the VSF index, which is somewhat to be expected due to the limited voltage control characteristics of ULTC transformers. Figure 4.3-29 depicts the time profile of t_{cc}, as an operator would observe it on console, so that decisions can be made on time, based on the previous observations, to avoid system collapse.

A problem with using t_{cc} is the difficulty of determining the critical buses c. A possible solution is to monitor several buses at the same time, based on the maximum entries in the tangent vector $\mathrm{d}z/\mathrm{d}\lambda$ as defined in (4.22), as critical buses can be

detected this way [43, 44]. However, the computational costs in this case could be significant, depending on the number of buses that have to be monitored in order to be able to make adequate predictions.

4.3.9 Reduced Determinant

This index, as defined in [11], assumes a typical transient stability system model that allows for the related linearized equations to be rewritten at a given load bus l as

$$\left[\begin{array}{c} 0 \\ \hline \Delta P_l \\ \Delta Q_l \end{array}\right] = \left[\begin{array}{c|c} A & B \\ \hline C & D \end{array}\right] \left[\begin{array}{c} \Delta \tilde{z} \\ \hline \Delta \delta_l \\ \Delta V_l \end{array}\right] \tag{4.41}$$

where matrices A, B, C, and D represent the corresponding blocks of the Jacobian matrix J; observe that D is a 2×2 matrix. These equations consider that active and reactive power variations only occur at a load bus l, re-ordering the system equations in such a way that the P and Q mismatches for this bus are the last ones. Hence, equation (4.41) can be reduced to

$$\left[\begin{array}{c} \Delta P_l \\ \Delta Q_l \end{array}\right] = D'_{ll} \left[\begin{array}{c} \Delta \delta_l \\ \Delta V_l \end{array}\right] \tag{4.42}$$

where

$$D'_{ll} = D - CA^{-1}B \tag{4.43}$$

Observe that the matrix D'_{ll} is well defined at all operating points, since A is guaranteed nonsingular even at the collapse point, as long as bus l has non zero entries in the "zero" right eigenvector v of J at that point; this is particularly true for $l = c$ (the critical buses). Thus, the determinant of D'_{ll},

$$\det D'_{ll} = \frac{\det J}{\det A} \tag{4.44}$$

becomes zero only at the collapse point.

Although the definition of D'_{ll} assumes certain loading pattern, results for multiple test systems indicate that monitoring $\det D'_{ll}$ at different operating points for changes in the loading factor λ provides very similar information and behavior than the test function t_{ll}, regardless of the loading pattern [11]. This is especially true for $l = c$, as illustrated for the test system in Figures 4.3-30 and Figure 4.3-31. Hence, the loading margin can also be approximated using $\det D'_{cc}$ instead of t_{cc} in equation (4.40).

Matrix D'_{ll} in (4.43) can be obtained by a partial factorization of the corresponding load-flow Jacobian J, which suggests slightly less computational costs than determining the test function t_{lk} in (4.37), since it does not require repeat solutions and vector products. Based on this procedure, the computational cost of calculating t_{lk} can be estimated as approximately 10% more than what is required for determining D'_{ll}, if efficient ordering and factorization processes are used [57]. Although the improvement is not significant, if several values of the test function or matrix are required, which is typically the case, the difference could amount to significant CPU time savings, particularly for large systems.

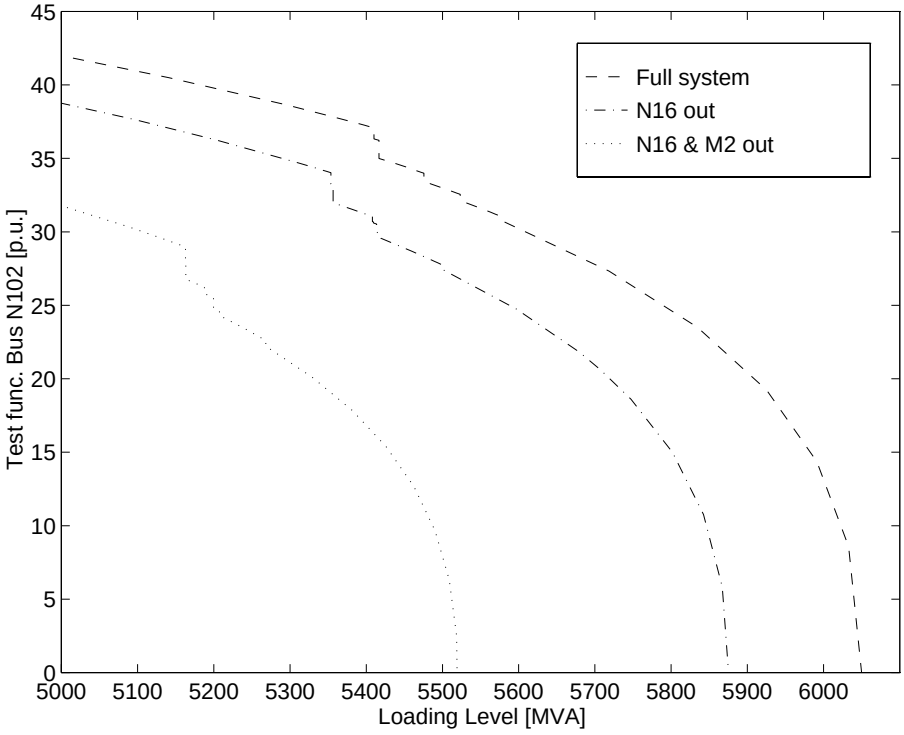

(a)

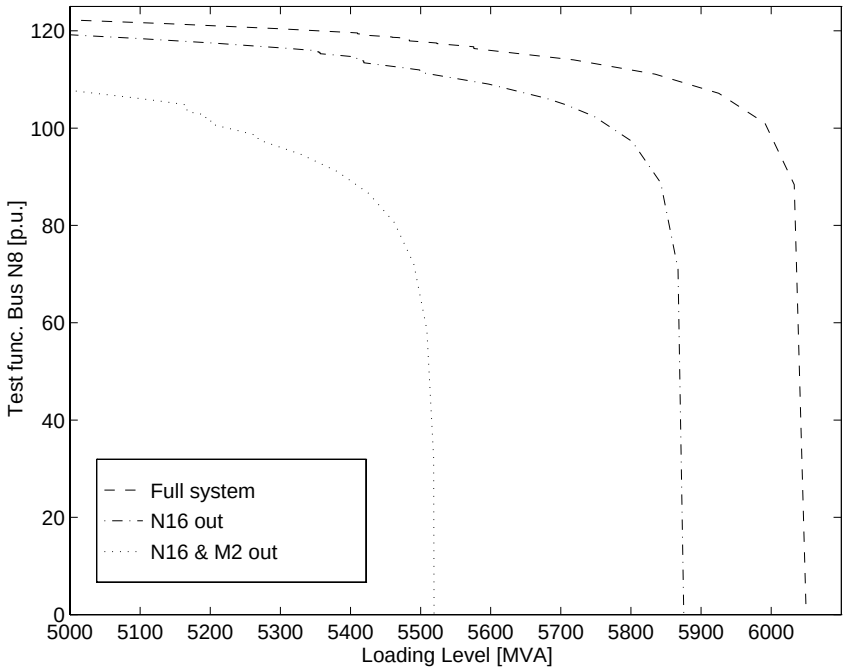

(b)

Figure 4.3-28. Test function for (a) critical bus N102 and (b) bus N8.

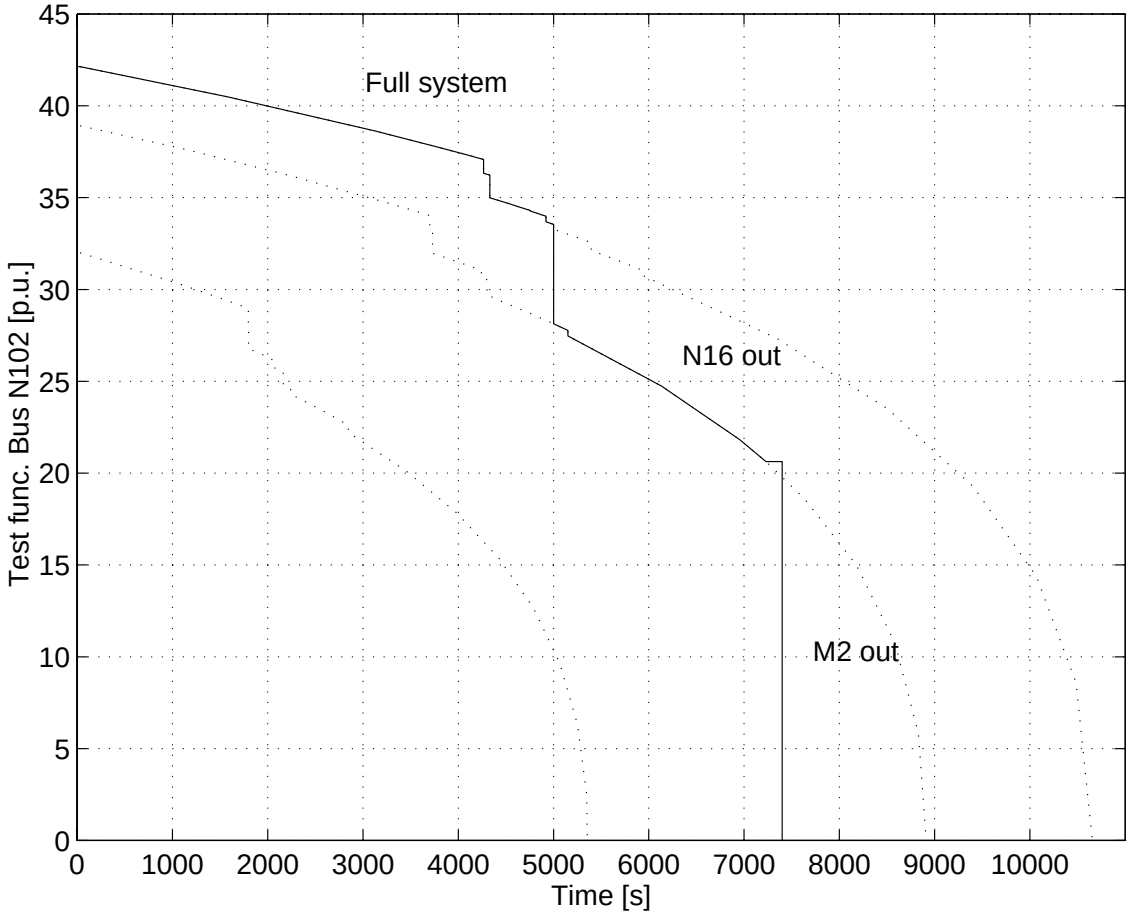

Figure 4.3-29. Critical test function versus time.

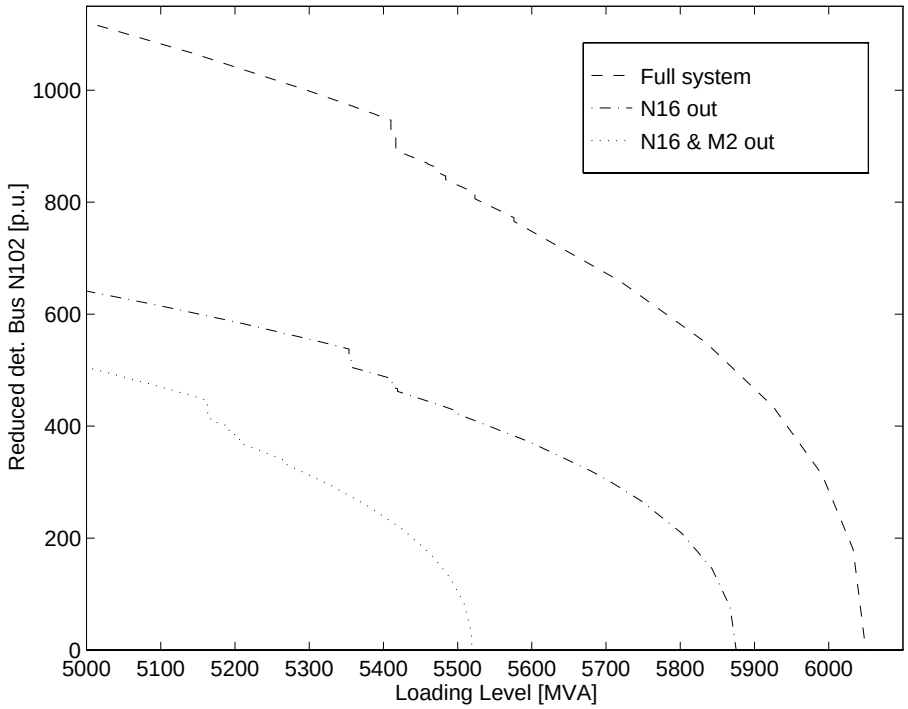

(a)

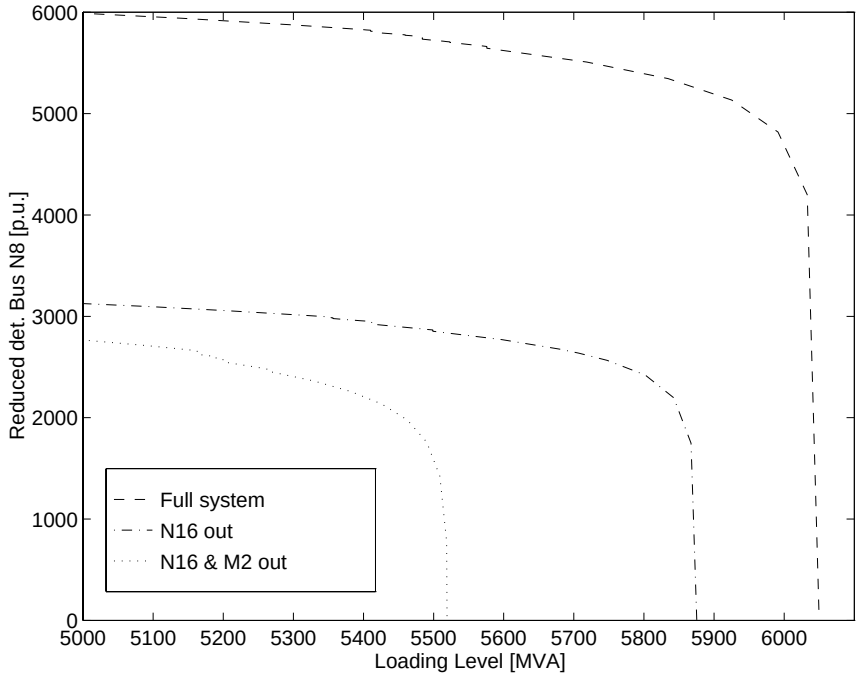

(b)

Figure 4.3-30. Reduced determinant for (a) critical bus N102 and (b) bus N8.

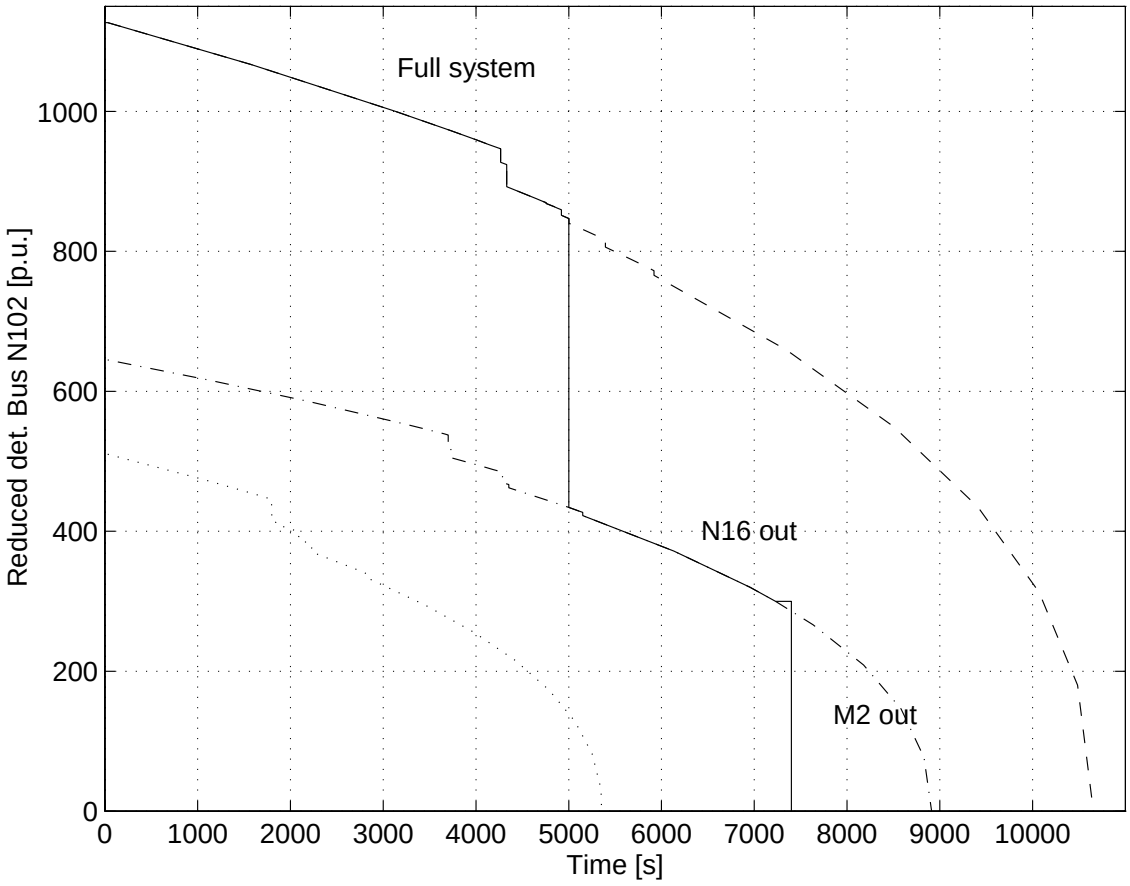

Figure 4.3-31. Critical reduced determinant versus time.

4.3.10 Tangent Vector Index (TVI)

The tangent vector to the system profile represented by $F(z, \lambda) = 0$, i.e., $\mathrm{d}z/\mathrm{d}\lambda$ as defined in (4.22), may be used to define the TVI. This index is also independent of the system model and shows behavior similar to t_{cc} and $\det D_{cc}$ at significantly less computational costs [43, 44].

From (4.22), it is clear that the tangent vector is computationally inexpensive, as it can be computed at a maximum cost of one additional Newton-Raphson iteration. This vector also contains important information regarding how the system variables z are affected by changes on the parameter λ. Furthermore, based on equation (4.22), it can be readily demonstrated that the tangent vector converges to the "zero" right eigenvector v at the collapse point, which pinpoints the critical buses of the system. Hence, this vector has been successfully used for "early" detection of the system critical bus, as demonstrated in [46, 43, 44].

The TVI is defined as

$$TVI_i = \left| \frac{\mathrm{d}V_i}{\mathrm{d}\lambda} \right|^{-1} \tag{4.45}$$

where $\mathrm{d}V_i/\mathrm{d}\lambda$ is the entry in the tangent vector $\mathrm{d}z/\mathrm{d}\lambda$ corresponding to the bus voltage magnitude V_i for a bus i. Observe that this definition is somewhat similar to the VSF index described above. As the collapse point is approached, $\mathrm{d}V_i/\mathrm{d}\lambda \to \infty$ and, hence, $TVI_i \to 0$. This index has a profile rather similar to the test function and reduced determinant indices for the system's critical buses at the collapse point ($i = c$), as depicted in Figures 4.3-32 and 4.3-33.

The quadratic behavior of TVI_c, or t_{cc} and $\det D_{cc}$ for that matter, may be used to modify the predictor step of the continuation method to reduce the number of steps needed to calculate the collapse point [44]. Thus, when two power flow solutions are available, a quadratic equation can be used to approximate the loading margin $\Delta\lambda$ as a function of TVI_i, where i corresponds to the buses with the largest entries in the tangent vector, as follows:

$$\Delta\lambda \approx \min_i \{a\, TVI_i^2\} \tag{4.46}$$

The value of $\Delta\lambda$ is then used to compute Δz_1 in the predictor step of equation (4.23).

$$\Delta z_1 \;=\; \Delta\lambda \left. \frac{\mathrm{d}z}{\mathrm{d}\lambda} \right|_1$$

The TVI continuation algorithm may then be summarized as follows:

1. Using a continuation method based on a tangent predictor, and a corrector with fixed λ and step cutting techniques, compute two operating points on the system profile.

2. Based on the maximum entries in the tangent vector computed at each predictor step, identify the critical clusters in the system at every continuation step and determine the corresponding TVIs.

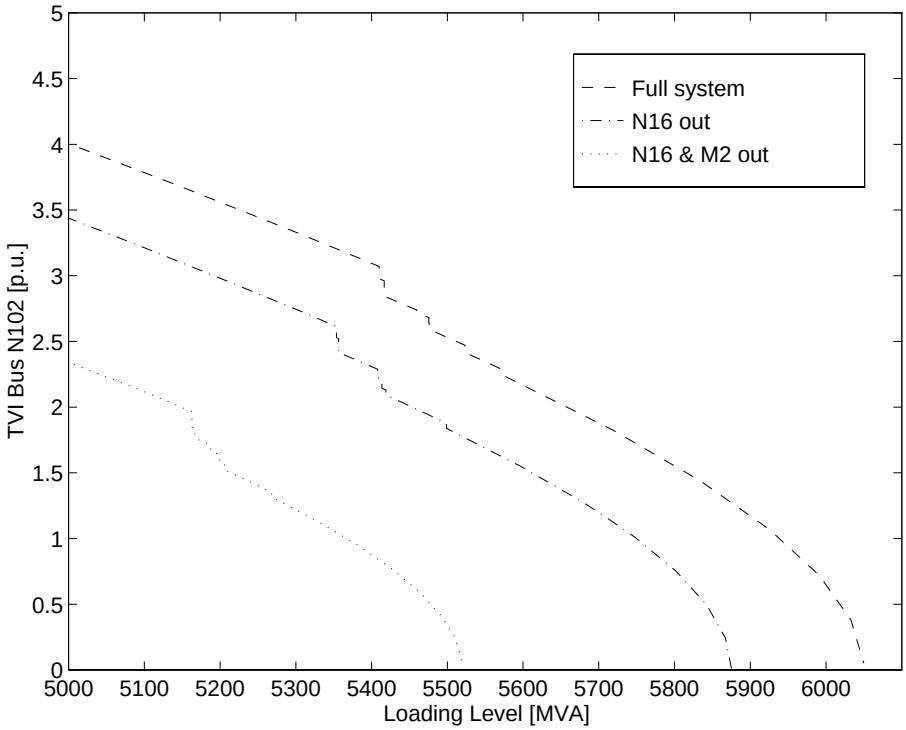

(a)

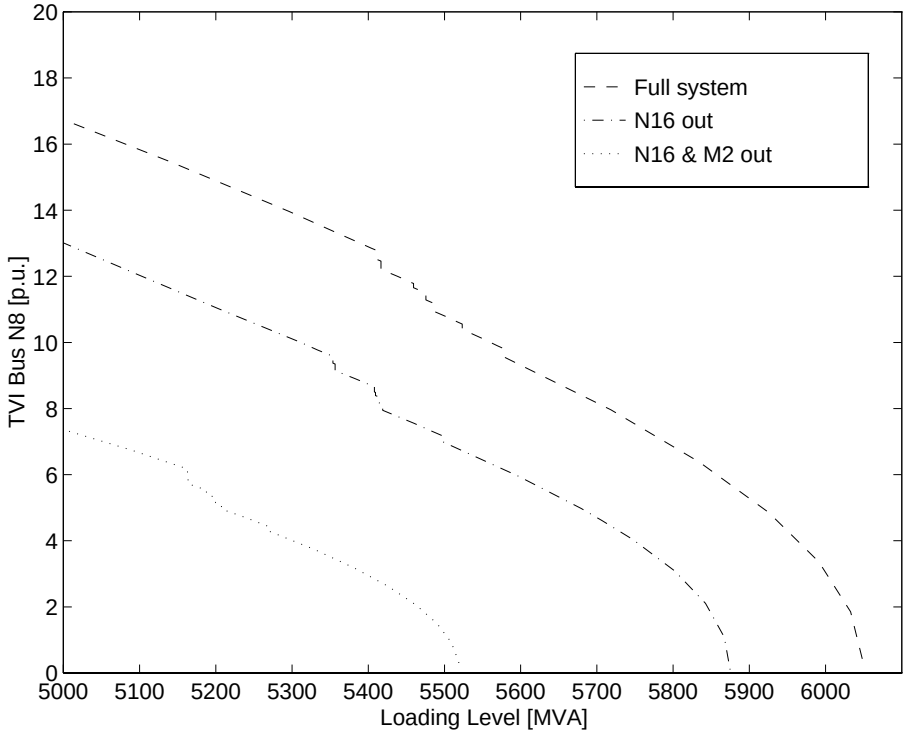

(b)

Figure 4.3-32. TVI for (a) critical bus N102 and (b) bus N8.

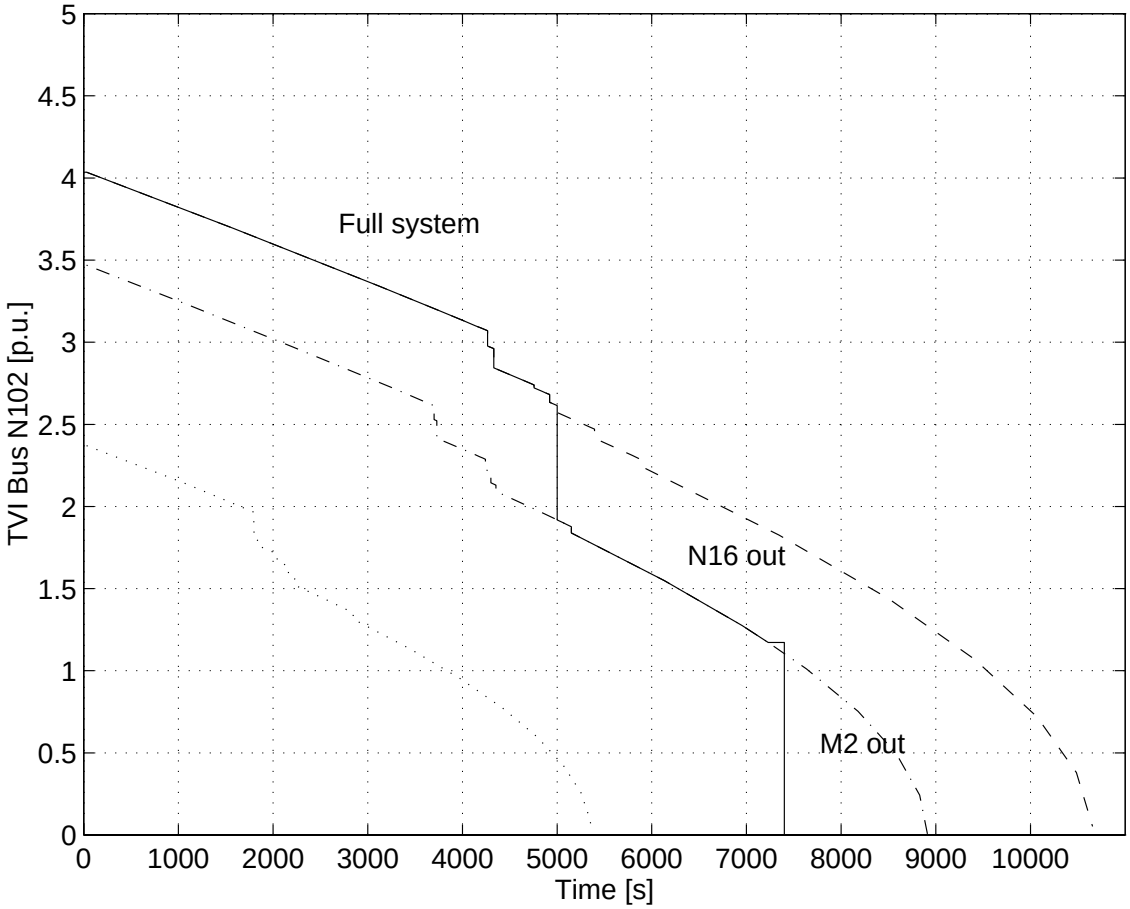

Figure 4.3-33. Critical TVI versus time.

3. After two continuation steps use equation (4.46) in the predictor step, and continue until the collapse point is identified when $TVI_i \leq \epsilon$.

4.4 OTHER INDICES

Several other indices are discussed in this section to give the reader a broad view of what is available in the current literature. Only a brief description is provided here, as the results of applying these indices to the test system were not available.

4.4.1 System Determinant

This is one of the first indices used to detect proximity to collapse. The idea is to detect the collapse point for any system model by monitoring the value of the determinant of the associated Jacobian, which becomes zero at this point (singular point).

The problem with this index is that it yields rather large values, especially in large systems, which makes it numerically impractical. Furthermore, its behavior is highly nonlinear, i.e., it is rather insensitive to system parameter variations, similar to the response observed for the minimum eigenvalues and singular values of the system Jacobian as discussed in Section 4.3.2.

4.4.2 Voltage Controllability Index (VCI)

This index was proposed in [58], and is based on monitoring the largest eigenvalue of a "voltage controllability matrix." This index includes the effect of voltage regulators; however, as the previous determinant index, it is highly nonlinear.

4.4.3 Center Manifold Based Index

In [59], the authors propose the use of the "center manifold" at the collapse (bifurcation) point to define a voltage stability index. For $F(z, \lambda)$ in (4.1), this manifold is locally defined at a saddle bifurcation point (z_*, λ_*) as

$$\frac{1}{2} w^T [D_z^2 F|_* v] v \, z_c^2 + w^T \left. \frac{\partial F}{\partial \lambda} \right|_* \lambda$$

where v and w are the right and left eigenvectors corresponding to the zero eigenvalue of $D_z F|_*$, and z_c is a scalar variable resulting from a linear transformation of z [60].

An index is then proposed based on the locally quadratic shape of this manifold. For certain test systems, this index shows similar quadratic and discontinuous profiles as several of the indices previously discussed in this report. The problem with this index, however, is that the eigenvectors v and w on which it is based tend to change significantly with λ, as mentioned in Section 4.3.2. Also, as compared to other indices with similar characteristics, it is computationally more expensive.

4.4.4 P and Q Angles

As proposed in [61], the angle between the tangent and the gradient vectors of the equilibrium equations $F(z, \lambda) = 0$ may be used as an index of proximity to collapse. This angle may be defined, for a given bus i, as

$$\alpha_i = \cos\left(\frac{\nabla F_i|_o \, \mathrm{d}z/\mathrm{d}\lambda|_o}{||\nabla F_i|o||||\mathrm{d}z/\mathrm{d}\lambda|_o||}\right)$$

where $\mathrm{d}z/\mathrm{d}\lambda|_o$ is the tangent vector of $F(z, \lambda)$ at the equilibrium point (z_o, λ_o), as defined in (4.22), and $\nabla F_i|_o$ is a gradient vector corresponding to the i^{th} row of the system Jacobian $D_z F|_o$.

As the TVI, test function and reduced determinant indices discussed in previous sections, this index is associated with an specific bus i, and presents a quadratic shape for buses belonging to the critical area and discontinuities due to control limits. In terms of computational costs, it is slightly more expensive than the TVI index.

4.4.5 Energy Functions

The Transient Energy Function or TEF, a technique based on Lyapunov stability theory and originally developed for direct stability analysis of power systems [62], has been successfully used as a voltage stability index for collapse studies [63, 64]. The reason for this is that this scalar function can be shown, under certain modeling assumptions, to be directly associated with the area enclosed by the nose curve [65].

A relatively simple way of defining this function was proposed in [66] for the following representation of equations (4.1):

$$F(z, \lambda) = A \, \phi(z, \lambda)$$

where $(A + A^T)$ is a positive semi-definite matrix, and the vector function $\phi(z, \lambda)$ corresponds to

$$\phi(z, \lambda) = \nabla^T \vartheta(z, \lambda)$$

with $\vartheta(z, \lambda)$ representing a Lyapunov function, better known in power systems as the TEF. Hence, the TEF is a scalar function of the state z for a given parameter value λ defined with respect to an equilibrium point z_0 as

$$\vartheta(z, \lambda) = \int_{z_0}^{z} \phi^T(u, \lambda) \, \mathrm{d}u \tag{4.47}$$

For simplified system models, equation (4.47) leads to the following definition of the TEF index, as proposed in [63]:

$$\begin{aligned} TEF \;\; = \;\; & \frac{1}{2}\sum_{k=1}^{n}\sum_{j=1}^{n} B_{kj} V_k^0 V_j^0 \cos(\delta_k^0 - \delta_j^0) \\ & - \frac{1}{2}\sum_{k=1}^{n}\sum_{j=1}^{n} B_{kj} V_k^1 V_j^1 \cos(\delta_k^1 - \delta_j^1) \end{aligned} \tag{4.48}$$

$$
\begin{aligned}
&- \sum_{k=1}^{n} P_k(\lambda_0)(\delta_k^1 - \delta_k^0) - \sum_{k=1}^{n} \int_{V_k^0}^{V_k^1} \frac{Q_k(\nu, \lambda_0)}{\nu}\, \mathrm{d}\nu \\
&+ \sum_{k=1}^{n} \sum_{j=1}^{n} G_{kj} V_k^0 V_j^0 \cos(\delta_k^0 - \delta_j^0)(\delta_k^1 - \delta_k^0) \\
&+ \sum_{k=1}^{n} \sum_{j=1}^{n} G_{kj} V_j^0 \sin(\delta_k^0 - \delta_j^0)(V_k^1 - V_k^0)
\end{aligned}
$$

where $Y_{kj} = G_{kj} + jB_{kj}$ is the kj entry in the Y-bus matrix; $P_k(\lambda)$ and $Q_k(V_k, \lambda)$ are the active and reactive power injections into bus k, respectively; and $V_k^0 \angle \delta_k^0$ and $V_j^0 \angle \delta_j^0$ correspond to the phasor bus voltages at the equilibrium point (z_0, λ_0) for buses k and j. The phasor voltages $V_k^1 \angle \delta_k^1$ and $V_j^1 \angle \delta_j^1$ represent another equilibrium point z_1 for the same parameter value λ_0, which is associated with the "closest" unstable equilibrium point.

The TEF definition in (4.48) provides a measure of the "energy distance" between two equilibrium points. As the system approaches collapse, the two solutions z_0 and z_1 merge into one, i.e., $z_0 = z_1$ at λ_*. Thus, the TEF index has been shown to smoothly and quasi-linearly change as λ changes, even in the presence of device limits, becoming zero at the collapse point; this behavior allows for adequate predictions of system proximity to collapse.

A difficulty with this index is that it cannot be readily modified to include more complex system models. Furthermore, the computation of the second equilibrium point z_1 is not always an easy task, particularly for lightly loaded systems (similarly to what happens with the VIPI discussed in Section 4.3.4).

4.4.6 Reactive Power Margins

On-line monitoring of reactive power and reactive power reserves in the system, including generators or any other reactive power sources such as SVCs, have been proposed as indices for voltage security assessment [67, 68]. The idea is that voltage collapse usually does not occur until current (reactive power) limits are reached, especially in large reactive power sources which may lead to cascading limiting effects at other units. Hence, by monitoring delivered reactive power and its associated reserves throughout the system, operators may be able to determine proximity to voltage collapse and take corrective actions such as load shedding based on areas requiring additional reactive power support. An implementation of these types of indices at the BPA control center is described in [69].

Reactive power margins are used in [70, 71] to evaluate voltage instability problems for coherent bus groups. These margins are based on the reactive reserves on generators, SVCs, and synchronous condensers that exhaust reserves in the process of computing a QV curve at any bus in a coherent group or voltage control area. A detailed description of this technique can be found in Section 3.6.

4.4.7 V/Vo Index

The V/Vo index is rather simple to define and compute. Thus, assuming the bus voltage values (V) to be known from load flow or state estimation studies, new bus voltages (Vo) are obtained by solving a load flow for the system at an identical state but with all loads set to zero. The ratio V/Vo at each node yields a voltage stability map of the system, allowing for immediate detection of weak and effective countermeasure spots.

A problem with this index is that it presents a highly nonlinear profile with respect to changes on the system parameter λ, not allowing for accurate predictions of proximity to collapse [2]. Nevertheless, when used together with operating experience, it has demonstrated in practice to be an effective tool against voltage collapse. Thus, the V/Vo index has been successfully used since 1982 in Belgium for off-line studies, particularly in seasonal operation planning; it was then added in 1995 to the on-line security assessment unit of the new Belgium dispatch center.

4.4.8 Real-time Index for Secondary and Tertiary Voltage Regulation

A real-time dynamic indicator of the proximity to voltage instability at a given operating point is proposed in [72]. Under certain conditions, this index can be computed in a few seconds using a deterministic algorithm, based on actual measurements and control signals. Such indicator has shown to be reliable and to complement other conventional off-line planning and short-term operation stability indices.

A condition for using this real-time index is the presence of automatic secondary and tertiary voltage regulation controls in the system. Secondary voltage regulation yields real-time measurements of pilot node voltages and area reactive power levels that allow for on-line computation of area voltage stability indices. These indices effectively represent instantaneously the proximity of the areas to their voltage stability limits, provided that tertiary voltage regulation is in place, giving the operator real-time information on the current network voltage stability state. These can also be used for timely automatic control actions when facing unexpected network contingencies, as they allow for an effective coordination of the reactive power resources (mainly generators) through a composite control structure that maintains suitable network voltage profiles in spite of continuously changing reactive power demands and grid perturbations.

These indices are currently being tested as part of ENEL's project for secondary and tertiary voltage regulation [73, 74]. The project is based on a hierarchical control structure that provides a network subdivision into areas around certain pilot nodes; these areas are controlled by *reactive power level* signals $q_i(t)$ (one for each area), supplied by Regional Secondary Voltage Regulators (RVRs), to keep the pilot node voltages at desired values. A National Tertiary Voltage Regulator (NVR) coordinates the action of all the RVRs in a closed loop at the national/utility level, determining the *pilot node voltage* pattern $V_i(t)$ based on the actual state of the network and the forecasted optimal voltages and reactive powers, and forcing slow corrections in

order to have a better balance of reactive power generation levels and control margins among the areas.

The proposed indicator of proximity to the voltage stability limit for a given area i, $VSI_i(t)$, is defined as follows

$$VSI_i(t) = q_i(t) + \rho\, \dot{q}_i(t)$$

where $q_i(t)$ represents the instantaneous value of the area's total generator reactive power Q_G level in p.u. with respect to its limits, i.e.

$$q_i(t) = \begin{cases} \sum_{j\in i} Q_{Gj}(t) / \sum_{j\in i} Q_{Gj_{\max}} & \text{for } Q_{Gj}(t) \geq 0 \forall j \\ \\ \sum_{j\in i} Q_{Gj}(t) / \sum_{j\in i} |Q_{Gj_{\min}}| & \text{for } Q_{Gj}(t) < 0 \forall j \end{cases}$$

and ρ is a weight coefficient to effectively account for reactive power level dynamics and, hence, its expected short-term trend. Observe that, $-1 \leq q_i(t) \leq 1 + \varepsilon\, q_i(t)$, where $\varepsilon\, q_i(t)$ is a contribution (usually kept at 0) that may take positive growing values according to the pilot node voltage regulation effort, in case some of the units of area i can be transiently overloaded with respect of their overexcitation limits.

The $VSI_i(t)$ index presents useful real-time information used by the operator to determine critical states of the voltages in area i when predefined thresholds are exceeded. Based on the area alarms, the RVR operates to avoid units operating at their overexcitation limits, since this condition usually anticipates the triggering of a voltage collapse problem. This is achieved by controlling in advance all the available reactive power resources installed in the area (capacitors, reactors, synchronous or static compensators), so that the value of $q_i(t)$ is reduced, reducing the control "effort" of the units.

If all the area reactive power resources have been consumed and reactive power control margins still remain small, the index could reach more critical values, leading the RVR to automatically either modify the voltage set-points of the area ULTCs or completely shut them down to reduce the load seen by the transmission network. At the same time, the RVR sends signals to the regional operator asking for switching of manually operated reactive power sources. If all the area control actions are accomplished with area control units that do not allow excitation overloading, the steady-state difference $1 - VSI_i(t)$ fully represents the distance of area i to its voltage stability limit. When the system recovers from critical operating conditions, the $VSI_i(t)$ value decreases and, hence, the RVR is able to release the area ULTCs and reduce the use of reactive power resources.

Reactive power control margins are strongly reduced during critical network situations, leading to severe network voltage degradation. In this case, tertiary voltage regulation is used to improve the transmission network voltage by progressively renouncing to the optimally planned short-term voltage profiles (defined based on economic reasons). Secondary voltage regulation reaches its limits only when the transmission network voltages are very low, in spite of all the network reactive power resources in operation; in these conditions, the system reaches its real-time voltage stability limit, as operating limits are reached despite the reduced pilot node voltages and reactive power control efforts.

4.5 SUMMARY

Table 4.5-1 summarizes all relevant information regarding the indices discussed in Section 4.3 to allow for a comprehensive comparison of these indices. Observe that all indices have their advantages and disadvantages; hence, it is not practical to recommend a particular index as the only one to use. Some indices seem especially suited for on-line studies, based on their low computational costs as well as base models and additional information provided; however, these indices tend to be poor predictors of proximity to voltage collapse. On the other hand, some indices yield accurate measures of distance to collapse but at higher computational costs, making them more suited for off-line studies. Hence, it appears that the best compromise is to jointly use these indices so that inexpensive but less accurate indices can be used as predictors in the computation of the exact loading margin, as discussed in Section 4.3.10, so that accurate measures of distance to collapse may be obtained together with useful, additional information, such as limit ranking, at reduced computational costs.

4.6 REFERENCES

[1] "Suggested Techniques for Voltage Stability Analysis," technical report 93TH0620-5PWR, IEEE/PES, 1993.

[2] "Indices Predicting Voltage Collapse Including Dynamic Phenomena," technical report TF 38-02-11, CIGRE, 1994.

[3] C. A. Cañizares, "Conditions for Saddle-Node Bifurcations in AC/DC Power Systems," *Int. J. of Electric Power & Energy Systems*, vol. 17, no. 1, February 1995, pp. 61–68.

[4] P. W. Sauer, B. C. Lesieutre, and M. A. Pai, "Dynamic vs. Static Aspects of Voltage Problems," pp. 207–216 in [75].

[5] C. A. Cañizares, "On Bifurcations, Voltage Collapse and Load Modeling," *IEEE Transactions on Power Systems*, vol. 10, no. 1, February 1995, pp. 512–522.

[6] C. A. Cañizares and S. Hranilovic, "Transcritical and Hopf Bifurcations in AC/DC Systems," pp. 105–114 in [76].

[7] C. A. Cañizares et al., "UWPFLOW Program," http://www.power.uwaterloo.ca, 2000.

[8] Working Group on a Common Format, "Common Format for Exchange of Solved Load Flow Data," *IEEE Transactions on Power Apparatus and Systems*, vol. 92, no. 6, November 1973, pp. 1916–1925.

[9] P. W. Sauer and M. A. Pai, "Power System Steady-State Stability and the Load Flow Jacobian," *IEEE Transactions on Power Systems*, vol. 5, no. 4, November 1990, pp. 1374–1383.

Index	Costs	Limit Ranking	Base Models	Profile	Collapse Predictions	Comments
Sensitivity Factors	Low	Yes	Any	Nonlinear Discontinuous	Inadequate	Highly nonlinear.
Singular/ eigenvalues	Medium	Yes	Any	Nonlinear Discontinuous	Inadequate	Information away from collapse point is not very relevant.
Second Order	Medium-High	No	Power Flow	Quasi-linear Discontinuous	Adequate	Tests on larger systems required.
VIPI	Medium-High	No	Power Flow	Quasi-linear Discontinuous	Adequate	Problems with low voltage solutions.
Loading Margin	High	No	Any	Linear Smooth	Exact	Generates additional useful information. Expensive.
Approx. Closest Loadability	Medium	No	Power Flow	Quasi-linear Discontinuous	Adequate	Problems with low voltage solutions and Q-limits. Yields an approximate value of closest collapse point.
Local Load Margins	Medium-High	No	Power Flow	Quasi-linear (for some buses) Discontinuous	Somewhat adequate	Power flow based. Expensive in some cases.
Test Functions	Low	Yes	Any	Quadratic Discontinuous	Somewhat adequate	Knowledge of critical areas is required.
Reduced Determinant	Low	Yes	Any	Quadratic Discontinuous	Somewhat adequate	Knowledge of critical areas is required.
TVI	Very Low	Yes	Any	Quadratic Discontinuous	Somewhat adequate	Knowledge of critical areas is required. Inexpensive.

Table 4.5-1. Comparison of Indices

[10] P. A. Löf, T. Smed, G. Andersson, and D.J. Hill, "Fast Calculation of a Voltage Stability Index," *IEEE Transactions on Power Systems*, vol. 7, no. 1, February 1992, pp. 54–64.

[11] C. A. Cañizares, A. Z. de Souza, and V. H. Quintana, "Comparison of Performance Indices for Detection of Proximity to Voltage Collapse," *IEEE Transactions on Power Systems*, vol. 11, no. 3, August 1996, pp. 1441–1450.

[12] B. Gao, G. K. Morrison, and P. Kundur, "Voltage Stability Evaluation Using Modal Analysis," *IEEE Transactions on Power Systems*, vol. 7, no. 4, November 1992, pp. 1529–1542.

[13] I. Dobson, "Observations on the Geometry of Saddle Node Bifurcations and Voltage Collapse in Electrical Power Systems," *IEEE Transactions on Circuits and Systems—I*, vol. 39, no. 3, March 1992, pp. 240–243.

[14] S. Greene, I. Dobson, and F.L. Alvarado, "Sensitivity of the Loading Margin to Voltage Collapse with respect to Arbitrary Parameters," *IEEE Transactions on Power Systems*, vol. 12, no. 1, February 1997, pp. 262–272.

[15] A. Berizzi, P. Finazzi, D. Dosi, P. Marannino, and S. Corsi, "First and Second Order Methods for Voltage Collapse Assessment and Security Enhancement," IEEE/PES PE-422-PWRS-0-01-1997, Winter Meeting, New York, NY, February 1997.

[16] A. Tiranuchit and R. J. Thomas, "A Posturing Strategy Against Voltage Instability in Electric Power Systems," *IEEE Transactions on Power Systems*, vol. 3, no. 1, February 1988, pp. 87–93.

[17] A. Berizzi, P. Bresesti, P. Marannino, M. Montagna, S. Corsi, and G. Piccini, "Security Enhancement Aspects in the Reactive-Voltage Control," *IEEE Stockholm Power Tech*, vol. Power Systems, June 1995, pp. 674–679.

[18] A. Berizzi, P. Bresesti, P. Marannino, G. P. Granelli, and M. Montagna, "System-Area Operating Margin Assessment and Security Enhancement Against Voltage Collapse," *IEEE Transactions on Power Systems*, vol. 11, no. 3, August 1996, pp. 1451–1462.

[19] Y. Tamura, H. Mori, and S. Iwamoto, "Relationship Between Voltage Instability and Multiple Load Flow Solutions in Electric Power Systems," *IEEE Transactions on Power Apparatus and Systems*, vol. 102, no. 5, May 1983, pp. 1115–1125.

[20] Y. Tamura, K. Sakamoto, and Y. Tayama, "Current Issues in the Analysis of Voltage Instability Phenomena," pp. 5-39–5-53 in [77].

[21] N. Yorino, S. Harada, and H. Cheng, "A Method to Approximate a Closest Loadability Limit Using Multiple Load Flow Solutions," *IEEE Transactions on Power Systems*, vol. 12, no. 1, February 1997, pp. 424–429.

[22] N. Yorino, T. Usui, H. Sasaki, J. Kubokawa, M. Kitagawa, and K. Fujioka, "An Effective Monitoring of Power System Voltage Stability by Means of Voltage Stability Indices," *Trans IEE of Japan*, vol. 111-B, no. 3, March 1991, pp. 267–276.

[23] M. Nanba, Y. Huang, T. Kai, and S. Iwamoto, "Studies on VIPI Based Control Methods for Improving Voltage Stability," *Proc. PSCC*, vol. 2, August 1996, pp. 651–657.

[24] I. Dobson, "The Irrelevance of Load Dynamics for the Loading Margin to Voltage Collapse and its Sensitivities," pp. 509–518 in [76].

[25] S. Greene, I. Dobson, and F.L. Alvarado, "Contingency Ranking for Voltage Collapse via Sensitivities from a Single Nose Curve," IEEE/PES Summer Meeting, Berlin, July 1997.

[26] B. Lee and V. Ajjarapu, "Invariant Subspace Parametric Sensitivity (ISPS) of Structure-Preserving Power Systems Models," *IEEE Transactions on Power Systems*, vol. 11, no. 2, May 1996, pp. 845–850.

[27] B. Long and V. Ajjarapu, "The Sparse Formulation of ISPS and its Application to Voltage Stability Margin Sensitivity and Estimation," *IEEE Transactions on Power Systems*, vol. 14, no. 3, 1999, pp. 944–951.

[28] I. Dobson and L. Lu, "New Methods for Computing a Closest Saddle Node Bifurcation and Worst Case Load Power Margin for Voltage Collapse," *IEEE Transactions on Power Systems*, vol. 8, no. 3, August 1993, pp. 905–913.

[29] F. L. Alvarado, I. Dobson, and Y. Hu, "Computation of Closest Bifurcations in Power Systems," *IEEE Transactions on Power Systems*, vol. 9, no. 2, May 1994, pp. 918–928.

[30] F. L. Alvarado and T. H. Jung, "Direct Detection of Voltage Collapse Conditions," pp. 5.23–5.38 in [77].

[31] R. Seydel, *Practical Bifurcation and Stability Analysis—From Equilibrium to Chaos*. Springer-Verlag, New York, second edition, 1994.

[32] C. A. Cañizares, F. L. Alvarado, C. L. DeMarco, I. Dobson, and W. F. Long, "Point of Collapse Methods Applied to AC/DC Power Systems," *IEEE Transactions on Power Systems*, vol. 7, no. 2, May 1992, pp. 673–683.

[33] C. A. Cañizares and F. L. Alvarado, "Point of Collapse and Continuation Methods for Large AC/DC Systems," *IEEE Transactions on Power Systems*, vol. 8, no. 1, February 1993, pp. 1–8.

[34] V. Ajjarapu, "Identification of Steady State Voltage Stability in Power Systems," *Int. J. of Electric Power & Energy Systems*, vol. 11, 1991, pp. 43–46.

[35] I. Dobson and L. Lu, "Voltage Collapse Precipitated by the Immediate Change in Stability When Generator Reactive Power Limits are Encountered," *IEEE Transactions on Circuits and Systems—I*, vol. 39, no. 9, September 1992, pp. 762–766.

[36] G. K. Morrison, B. Gao, and P. Kundur, "Voltage Stability Analysis Using Static and Dynamic Approaches," *IEEE Transactions on Power Systems*, vol. 8, no. 3, August 1993, pp. 1159–1171.

[37] T. Van Cutsem, "A Method to Compute Reactive Power Margins with Respect to Voltage Collapse," *IEEE Transactions on Power Systems*, vol. 6, no. 1, February 1991, pp. 145–156.

[38] J. Lu, C. W. Liu, and J. S. Thorp, "New Methods for Computing a Saddle-node Bifurcation Point for Voltage Stability Analysis," *IEEE Transactions on Power Systems*, vol. 10, no. 2, May 1995, pp. 978–989.

[39] C. J. Parker, I. F. Morrison, and D. Sutanto, "Application of an Optimization Method for Determining the Reactive Margin from Voltage Collapse in Reactive Power Planning," *IEEE Transactions on Power Systems*, vol. 11, no. 3, August 1996, pp. 1473–1481.

[40] G. D. Irisarri, X. Wang, J. Tong, and S. Moktari, "Maximum Loadability of Power Systems Using Interior Point Non-linear Optimization Method," *IEEE Transactions on Power Systems*, vol. 12, no. 1, February 1997, pp. 162–172.

[41] M. Suzuki, S. Wada, M. Sato, T. Asano, and Y. Kudo, "Newly Developed Voltage Security Monitoring System," *IEEE Transactions on Power Systems*, vol. 7, no. 3, August 1992, pp. 965–973.

[42] V. Ajjarapu, N. Jain, Z. Yu, and S. Battula, "Recent Developments to the Continuation Power Flow," *Proc. NAPS*, Washington, DC, October 1993, pp. 205–214.

[43] A. C. Z. de Souza, C. A. Cañizares, and V. H. Quintana, "Critical Bus and Point of Collapse Determination Using Tangent Vectors," *Proc. NAPS*, M.I.T., November 1996, pp. 329–333.

[44] A. C. Z. de Souza, C. A. Cañizares, and V. H. Quintana, "New Techniques to Speed Up Voltage Collapse Computations Using Tangent Vectors," *IEEE Transactions on Power Systems*, vol. 12, no. 3, August 1997, pp. 1380–1387.

[45] C. A. Cañizares, W. F. Long, F. L. Alvarado, and C. L. DeMarco, "Techniques for Detecting Proximity to Voltage Collapse in AC/DC Systems," *Proc. III SEPOPE*, Belo Horizonte, Brazil, paper IP-18, May 1992.

[46] V. Ajjarapu and C Christy, "The Continuation Power Flow: A Tool for Steady State Voltage Stability Analysis," *IEEE Transactions on Power Systems*, vol. 7, no. 1, February 1992, pp. 416–423.

[47] H. D. Chiang, A. J. Flueck, K. S. Shah, and N. Balu, "CPFLOW: A Practical Tool for Tracing Power System Steady-State Stationary Behavior Due to Load and Generation Variations," *IEEE Transactions on Power Systems*, vol. 10, no. 2, May 1995, pp. 623–634.

[48] K. Iba, H. Suzuki, M. Egawa, and T. Watanabe, "Calculation of Critical Loading Condition with Nose Curve Using Homotopy Continuation Method," *IEEE Transactions on Power Systems*, vol. 6, no. 2, May 1991, pp. 584–593.

[49] C. A. Cañizares, "Saddle-Node Bifurcations in Power Systems," *Proc. JIEE*, Quito, Ecuador, July 1993, pp. 222–229.

[50] H. D. Chiang, W. Ma, R. J. Thomas, and J. S. Thorp, "A Tool for Analyzing Voltage Collapse in Electric Power Systems," *Proc. PSCC*, Graz, Austria, August 1990, pp. 1210–1217.

[51] C. A. Cañizares, "Calculating Optimal System Parameters to Maximize the Distance to Saddle-node Bifurcations," *IEEE Transactions on Circuits and Systems–I*, vol. 40, no. 3, May 1998, pp. 225–237.

[52] R. Fletcher, *Practical Methods of Optimization*. John Wiley & Sons, New York, 1987.

[53] P. E. Gill, W. Murray, and M. H. Wright, *Practical Optimization*. Academic Press, London, 1981.

[54] T. Nagao, K. Tanaka, and K. Takenaka, "Development of Static and Simulation Programs for Voltage Stability Studies of Bulk Power System," *IEEE Transactions on Power Systems*, vol. 12, no. 1, February 1997, pp. 273–281.

[55] K. Takahashi, "Formation of a Sparse Bus Impedance Matrix and its Application to Short Circuit Study," *Proc. PICA*, 1973.

[56] H. D Chiang and R. Jean-Jumeau, "Toward a Practical Performance Index for Predicting Voltage Collapse in Electric Power Systems," *IEEE Transactions on Power Systems*, vol. 10, no. 2, May 1995, pp. 584–592.

[57] I. S. Duff, A. M. Erisman, and J. K. Reid, *Direct Methods for Sparse Matrices*. Oxford Science Publications, New York, 1986.

[58] C. D. Vournas, "Voltage Stability and Controllability Indices for Multimachine Power Systems," *IEEE Transactions on Power Systems*, vol. 10, no. 3, August 1995, pp. 1183–1194.

[59] J. Barquín, T. Gómez, and F. L. Pagola, "Estimating the Loading Limit Margin Taking Into Account Voltage Collapse Areas," *IEEE Transactions on Power Systems*, vol. 10, no. 4, November 1995, pp. 1952–1962.

[60] J. Guckenheimer and P. Holmes, *Nonlinear Oscillations, Dynamical Systems, and Bifurcations of Vector Fields*. Springer-Verlag, New York, 1986.

[61] L. Wang and A. A. Girgis, "On-line Detection of Power System Small Disturbance Voltage Instability," *IEEE Transactions on Power Systems*, vol. 11, no. 3, August 1996, pp. 1304–1313.

[62] M. A. Pai, *Energy Function Analysis for Power System Stability*. Kluwer Academic, 1989.

[63] T. J. Overbye and C. L. DeMarco, "Voltage Security Enhancement Using Energy Based Sensitivities," *IEEE Transactions on Power Systems*, vol. 6, no. 3, August 1991, pp. 1196–1202.

[64] C. L. DeMarco and C. A. Cañizares, "A Vector Energy Function Approach for Security Analysis of AC/DC Systems," *IEEE Transactions on Power Systems*, vol. 7, no. 3, August 1992, pp. 1001–1011.

[65] T. J. Overbye, I. Dobson, and C. L. DeMarco, "Q-V Curve Interpretations of Energy Measures for Voltage Security," *IEEE Transactions on Power Systems*, vol. 9, no. 1, February 1994, pp. 331–340.

[66] C. L. DeMarco, "A New Method of Constructing Lyapunov Functions for Power Systems," *Proc. ISCAS*, 1988, pp. 905–908.

[67] CIGRE WG 39.02 (Control Center Performance), "Possibilities and Expectations for Improved Man Machine Interface in Power System Control," *Proc. CIGRE*, paper 35/39-03, 1992.

[68] L. Sandberg, K. Rouden, and L. Ekstam, "Security Assessment Against Voltage Collapse Based on Real-time Data Including Generator Reactive Power Capacity," *Proc. CIGRE*, paper 39/11-03, 1994.

[69] C. Taylor and R. Ramanathan, "BPA Reactive Power Monitoring and Control Following the August 10, 1996 Power Failure," *Proc. VI SEPOPE*, Salvador, Brazil, May 1998.

[70] R. A. Schlueter, "A Voltage Stability Security Assessment Method," IEEE/PES Summer Meeting, Berlin, July 1997.

[71] R. A. Schlueter and S. Liu, "Intelligent Control for a Power System in a Deregulated Environment," *Proc. NAPS*, M.I.T., November 1996, pp. 81–88.

[72] V. Arcidiacono and S. Corsi, "A Real-Time Voltage Stability Index for Bulk Power Systems with Secondary Voltage Regulation," pp. 197–204 in [76].

[73] V. Arcidiacono, S. Corsi, A. Natale, and C. Raffaelli, "New Developments in the Applications of ENEL Transmission System Automatic Voltage and Reactive Power Control," *Proc. CIGRE*, 1990.

[74] V. Arcidiacono, "Automatic Voltage and Reactive Power Control in Transmission System," *Proc. CIGRE-IFAC*, Survey Paper E, Florence, September 1983.

[75] *Proc. Bulk Power System Voltage Phenomena II—Voltage Stability and Security*, ECC Inc., Fairfax, VA, August 1991.

[76] *Proc. Bulk Power System Voltage Phenomena III—Voltage Stability and Security*, ECC Inc., Davos, Switzerland, August 1994.

[77] *Proc. Bulk Power System Voltage Phenomena—Voltage Stability and Security*, EL-6183, EPRI, January 1989.